MULTIPLE PARAMETERS BASED PULSED EDDY CURRENT NON-DESTRUCTIVE TESTING AND EVALUATION

A thesis submitted for the degree of Doctor of Philosophy

IBUKUN DAPO ADEWALE

School of Electrical and Electronic Engineering, Newcastle University

December 2014

Table of Contents

3

List of Figures

List of Tables

List of Publications

1. I.D. Adewale and G.Y Tian, "Decoupling the influence of permeability and conductivity in pulsed eddy current measurements," *IEEE Transactions on Magnetics,* vol. 49, pp.1119-1127, Mar 2013.

2. G.Y. Tian, Y. He, I. Adewale, and A. Simm, "Research on spectral response of pulsed eddy current and NDE applications," *Sensors and Actuators a-Physical,* vol. 189, pp. 313-320, Jan 15 2013.

3. I.D. Adewale, G.Y. Tian, Song Hua Dong, and Guo Xiaoting, "Separation of lift-off effects and defect features in magnetic-sensor based Pulsed Eddy Current Signals," *Submitted article to Journal of Applied Physics D for review.*

4. I.D. Adewale, H. Zhang, G.Y. Tian and Tom Hope, "Defect mapping of steel substrate under fire protection layer using EM NDE methods," *Nondestructive Evaluation/Testing: New Technology and Application (FENDT),2013 Far East Forum proceedings,* pp. 166-171, June 17-20, 2013.

5. G. Y. Tian, Y. He, I. Adewale, and A. Simms, "Spectral behaviour of pulsed eddy current NDE and applications," presented at the 18th World Conf. on Nondestructive Testing, Durban, South Africa, Apr.16–20, 2012.

List of Acronyms

ACFM	Alternating Current Field Measurement
EC	Eddy Current
EM	Electromagnetic
EMAT	Electromagnetic Acoustic Transducer
ERO	Electrical Runout
ETDR	Electric Time Domain Reflectometry
FEM	Finite Element Modelling
FFT	Fast Fourier Transform
GMR	Giant Magneto Resistive
LO	Lift-off
LOI	Lift-off point of Intersection
MFL	Magnetic Flux Leakage
MIC	Microbial Induced Corrosion
MRO	Mechanical Runout
MST	Magnetostrictive Sensing Technique
NDE	Non-destructive Evaluation
NDT & E	Non-destructive Testing and Evaluation
PEC	Pulsed Eddy Current
PIG	Pipeline Inspection Gauge
PTDF	Petroleum Technology Development Fund
PV	Peak Value
RFEC	Remote Field Eddy Current
RCF	Rolling Contact Fatigue
SCC	Stress Corrosion Cracking
SHM	Structural Health Monitoring

SSTDR   Spread Spectrum Time Domain Reflectometry

UT   Ultrasonic Testing

Acknowledgements

I would like to express my indebtedness to my supervisor and academic mentor Prof. G.Y. Tian for his guidance and constructive suggestions from the conceptualisation of the research work to the completion stage.

My sincere appreciation goes to all my colleagues past and present - Mohammed Alamin, Stuart Crichton, Hong Zhang, Omar Bouzid, Abdul Qubaa, Waleed Amer, Sunny Ali, Kongji Li and everyone in the research group for their valuable and worthwhile discussions throughout the research period. My warm appreciation is also extended to committee of friends in Newcastle upon Tyne especially in the church who through their friendship and love made my stay worthwhile here especially during the writing of this thesis.

I also appreciate all the members of staff in the school for their assistance throughout this programme. Special thanks to all the technicians for assistance with sample fabrication.

Foremost, I am grateful to my parents, Prof. and Mrs A.O. Adewale for their financial, moral and prayer support during the period of writing this thesis. My siblings and in-laws, who were always eager to know the progress of my work, deserve my high commendation.

A special thanks to my darling wife - Banke and my adorable boys (Adeayo and Adedamola – the new addition to the family) for your patience, love, understanding and moral support throughout this journey. Words cannot quantify my deep love and appreciation for being there for me at every stage of this research. I am glad that you are all an integral part of my life.

Thanks to the Petroleum Technology Development Fund (PTDF) for sponsoring this research work through the overseas scholarship scheme.

Finally, my sincere gratitude goes to God Almighty, the source of wisdom and all inspirations, in whom I live, move and have my being.

Abstract

Eddy current sensing technique is widely used primarily because of its high tolerance to harsh environments, low cost, broad bandwidth and ease of automation. And its variant, pulsed eddy current offers richer information of target materials. However, accurate detection and characterisation of defects remains a major challenge in the petro-chemical industry using this technique which leads to spurious detection and false alarm.

A number of parameters are contributory, amongst which is the inhomogeneity of the materials, coupling variation effect and relatively large lift-off effect due to coating layers. These sometimes concurrently affect the response signal. For instance, harsh and dynamic operating conditions cause variation in the electrical conductivity and magnetic permeability of materials. Also, there is the increased need to detect defects and simultaneously measure the coating layer. In practice therefore, multi-sensing modalities are employed for a comprehensive assessment which is often capital intensive. In contrast to this, multiple parameter delineation and estimation from a single transient response which is cost-effective becomes essential. The research concludes that multiple parameter delineation helps in mitigating the effect of a parameter of interest to improve the accuracy of the PEC technique for defect detection and characterisation on the one hand and for multi-parameter estimation on the other.

This research, partly funded by the Petroleum Technology Development Fund (PTDF), proposes use of a novel multiple parameter based pulsed eddy current NDT technique to address the challenges posed by these factors. Numerical modelling and experimental approaches were employed. The study used a 3D finite element model to understand, predict and delineate the effect of varying EM properties of test materials on PEC response; which was experimentally validated. Also, experimental studies have been carried out to demonstrate the capabilities of the proposed to estimate multiple parameters vis-à-vis defect depth (invariant of lift-off effects) and lift-off.

The major contributions of the research can be summarised thus: (1) numerical simulation to understand and separate the effect of material magnetic permeability and electrical conductivity in pulsed eddy current measurements and experimental validation; (2) proposed the lift-off point of intersection (LOI) feature for defect estimation invariant of lift-off effects for ferromagnetic and non-ferromagnetic samples; a feature which is hitherto not apparent in ferromagnetic materials (a primary material used in the oil and gas industry); (3) separation and estimation of defect and the lift-off effects in magnetic sensor based pulsed eddy current response; and (4) application of the LOI feature and demonstration of increased defect sensitivity of the PEC technique with the proposed feature in both ferrous and non-ferrous conductive materials.

15

Chapter 1: Introduction

This chapter gives a brief introduction to non-destructive testing related defects and threats due to corrosion of oil and gas structures in marine environments and an overview of the work undertaken. A synopsis of the aims, objectives and scope of the research work is discussed. Highlights of the major research achievements are presented and the structure of the rest of the thesis is laid out.

1.1. Research Background

Corrosion can occur in many parts of the oil processing and supply infrastructure, from generalised corrosion caused by oxygen rich environments in marine structures, in subsea pipelines under insulation to sulphide stress corrosion in hostile wells. Climate change and the ageing oil and gas pipeline network and structures have accelerated corrosion processes and increased leakages; causing significant environmental damage due to the wide distribution of pipelines and harsh conditions. The majority of petrochemical pipes and structures are usually made of steel and steel alloys.

Pipelines are used in virtually every nation around the globe to transport oil and gas from the fields to the market. While pipes are cheaper than other means of transportation, this cost saving comes with a major price: pipes are subject to cracks, corrosion etc., which in turn can cause leakage and environmental damage. Oil spills, gas leaks and their associated environmental problems has become a serious and major concern in the oil and gas industry; and consequently, this has led to significant losses in revenue, severe disruption of operations, persistent threat to marine life and the ecosystem. This accidental discharge of petroleum products on/offshore has hitherto caused untold and unimaginable environmental hazards and economic loss that requires urgent remedial action and attention.

Petroleum spills acidify the soil, halt cellular respiration, and starve roots of vital oxygen. This destroys crops, aquaculture and marine life through contamination of the ground water and soil. The consumption of dissolved oxygen by bacteria feeding on the spilled hydrocarbons also contributes to the death of fish. In agricultural communities, often a year's supply of food can be destroyed instantaneously.

Statistics show that a great percentage of oil spills the world over can be attributed to the corrosion of pipelines and/or storage tanks [1-3]. For instance in Nigeria(the 6th largest oil exporting country in the world), statistics show that fifty percent (50%) of oil spills is due to corrosion, twenty eight percent (28%) to sabotage and twenty one percent (21%) to oil production operations. One percent (1%) of oil spills is due to engineering drills, inability to effectively control oil wells, failure of machines, and inadequate care in loading and unloading oil vessels [3]. A similar trend is evident in the USA where 40% of spills are due to structural failure; of which 75% of this failure is due to corrosion, 15% due to flawed pipes and 10% to defective welds [4]. Thus, since the bulk of this spillage has been identified to be caused by corrosion, it is pertinent to tackle and mitigate this in order to have a good flow assurance, saving operators huge money and to conserve the ecosystem.

Accurate detection and characterisation of defects due to corrosion is a major challenge in the oil and gas industries. There are a number of factors that contribute to this, amongst which are the inhomogeneity of the materials, lift-off or coupling variation effect and relatively large lift-off effect due to coating or insulation layer. This study therefore seeks to address this challenges using a novel pulsed eddy current technique which has the potential of being incorporated into the design and development of a next generation intelligent PIG that would provide the much needed and urgent solution of minimising the effect of the environmental hazards and pollution caused by oil spills as this device would give adequate and robust pipeline integrity management solution

1.2.   Research Objectives

The research objectives are summarised as follows:
- To explore the potentials of multiple parameter separation and estimation from pulsed eddy current responses.
- To investigate the inhomogeneity effect of test material in pulsed eddy current measurements with a view to understand the influence and behaviour of the electromagnetic properties of the test materials
- To investigate and develop a lift-off independent defect detection and characterisation pulsed eddy current system to mitigate coupling variation

- To undertake case study of ferrous and non-ferrous samples with varying lift-off and defects

1.3. Scope of the Work

An experimental approach is taken to assess the PEC sensing system, with carefully selected samples with known electromagnetic properties, defect geometry and exploiting signal processing and feature extraction techniques to delineate between defects and to establish the repeatable performance of the PEC system.

Samples were prepared to emulate real world conditions. Such samples used in this study include amongst others surface machined slot (to simulate metal loss), surface-breaking machined crack, conductivity and permeability standard samples. They emulate real world problems in terms of sizing that is critical to field scenarios.

As this research seeks to exploit the LOI feature for lift-off invariant defect characterisation of ferromagnetic materials in the main, a numerical and experimental investigation of the influence of the electromagnetic properties of the test sample is carried out. This was to determine distinctive signatures or areas of dominant influence of these properties i.e. magnetic permeability and electrical conductivity in the PEC output response.

Following this initial investigation, an experimental study to investigate the LOI behaviour in ferromagnetic materials and non-ferromagnetic material was carried out to demonstrate the significance of this point and also to underscore its inherent characteristic difference in these two materials. More importantly, to delineate defect depth features in ferrous and non-ferrous materials in the presence of lift-off, as well as the lift-off measurement.

Application and validation of the significance of the LOI point is presented through C-scan sections of the calibrated test pieces to see the contrast between lift-off affected imaging and lift-off compensated imaging using the LOI feature. In addition, it details the behaviour of the LOI with respect to sensor configuration and sample material.

1.4. Main Achievements

- A thorough review of electromagnetic NDE techniques for defect detection and characterisation in petrochemical structures has been carried out. Major benefits and limitations of these techniques and the potential for simultaneous multiple parameter measurement have been assessed.

- Separation of the effects of permeability and conductivity, which is believed to cause measurement errors in PEC systems have been investigated. The investigation revealed that electrical conductivity effect is largely associated with the rising edge and magnetic permeability dominates the stable phase of the transient response. In effect, the delineation of these two EM properties provides a laudable potential for multiple parameter measurement.

  - An experimental validation of the proposed 3-D finite element (numerical) PEC model to separate the influence of magnetic permeability and electrical conductivity in PEC measurements was undertaken and a good agreement within 6% error limit was observed in the numerical and experimental results.

  - This study revealed that the apparent permeability effect in PEC signal response is the recoil or incremental permeability, which can be minimised through normalisation technique.

  - Spectral response of PEC is investigated through numerical studies for samples with different magnetic permeability and electrical conductivity. The spectral response shows that high relative permeability affects the spectral magnitude pattern in a more complex manner than low relative permeability samples.

- The characteristics and behaviour of lift-off point of intersection (LOI) under different test conditions: lift-off, defect and material properties were studied. A novel lift-off invariant method to estimate defects in ferromagnetic materials which preserves the LOI points has been developed. This approach provides a direct means of inspecting ferromagnetic materials without the rigour of covering it with a thin layer of conductive, non-magnetic material. Furthermore, the effect of lift-off and defect were separated. Whilst defect can be characterised by the LOI points, lift-off effects are seen as a second order PEC signal distortion factor.

- This result provided a means for the simultaneous estimation of lift-off (or insulation thickness) and surface material discontinuities (defects), which can be extended for accurate (defect depth estimation) profiling of the geometry of critical and complex structures, like internal pipeline walls.

- A mathematical relationship between the peak values of the normalised differential PEC response [PV (ΔBnorm)], the lift-off (X) and defect depth (d) is developed for both ferromagnetic and non-ferromagnetic material samples. The gradient (m) of this relationship is correlated to defect depths invariant of lift-off variation in the forward process and by an inverse process defect information (d) can be estimated.

- A comparison between the LOI approach and the non-LOI defect estimation approach above shows that the latter is a more involving approach and the relative percentage error (of which the highest value is 7.95%) of the estimated defect sizes is larger relative to those obtained with the LOI approach, which is less involving. Moreover, the LOI approach exhibited lesser defect sizing discrepancy within an approximate relative error value of 4.35% whilst providing the added advantage of estimating lift-off simultaneously.

- The mapping of defects under varying lift-offs was investigated using the LOI time feature:

  - The comparative analysis of the sensitivity to defect of PEC imaging when the LOI time feature were employed to the traditional PEC imaging demonstrated an enhanced sensitivity

  - Also, the study demonstrated more enhancements with improved probe configuration; that is the use of the LOI feature with a ferrite core probe showed improved sensitivity to defect in comparison to the LOI feature in conjunction with an air core probe.

- Publication of research work in peer reviewed journals [5-7] and presentation of work at conferences [8, 9] .

1.5.   Thesis Layout

This thesis consists of seven chapters and a summary of the content of each is given below.

Chapter 1 presents an overview of the research background to underscore the challenges and threats posed by defects due to corrosion on critical structures and components in the oil and gas industry; importance of accurate defect detection and highlights of pertinent challenges of the NDT technique employed. The chapter also outlines the aim and objectives, the scope of the work and the general achievements related to the work.

Chapter 2 presents a survey of literature on the different types of operational defects caused by corrosion and the electromagnetic NDT techniques used in detecting and quantifying it. Electromagnetic NDTs like MFL, ACFM, RFEC, UT and MST (magnetostrictive sensing technique) were reviewed in particular. The merits and demerits of each are discussed. In addition, a review of EC sensing modalities was carried out.

Chapter 3 focuses on the underlying physics of pulsed eddy current (PEC) and related phenomena as this work seeks to tackle the challenges identified in the Literature review, laying a basis for multiple parameter measurement and lift-off invariant pulsed eddy current measurement. This would discuss the electromagnetic induction principles on which pulsed eddy current (PEC) hinges on whilst clearly linking it to Maxwell's unified electromagnetic theories. The remainder of the chapter sets out the research methodology for the thesis.

Chapter 4 and its sub-sections details both numerical and experimental analyses of characterising the electromagnetic properties of the test material in PEC measurements and systems. In-depth investigation into the influence of the electromagnetic properties of the test samples on measurement accuracy and reliability would be presented here. That is, the influence of such parameters like the magnetic permeability and electrical conductivity and their distinct signature are examined.

In chapter 5, the lift-off point of intersection (LOI) behaviour is reported. It presents experimental analyses of the behaviour of LOI point under various test conditions: lift-off, defect and material properties of test specimen with a view to separate lift-off effects from defect features. The investigation showed that whereas the LOI point is not apparent in ferromagnetic materials, it has been demonstrated that with the first order derivative of the normalised PEC transient response, the LOI feature is preserved. The behaviour of the LOI coordinates with changing defect size provides a means for defect characterisation. Also, the

characteristics of the LOI points have been used to delineate and measure varying defect sizes invariant of lift-off effects for both steel and aluminium specimens as those points provide unique coordinates for each defect.

In chapter 6, the application and validation of the significance of the LOI point is presented. In addition, it details the behaviour of the LOI with respect to probe configuration and sample material.

Chapter 7 summarises in the main the research work carried out and outlined in brief the scientific contributions. Also, the possible optimisation of the techniques proffered was discussed whilst emerging and current issues from the work form the outlook for future research directions.

1.6. Chapter Summary

This chapter presents a brief introduction to the research work. The achievements and problems existing in previous research are generalised and depicted as the background to this research, which is followed by the aim and objectives of the research. The contributions of the current work are presented. Finally, the layout of this thesis and content in each chapter are summarised.

Chapter 2: Literature Review

This chapter presents a survey of literature on the different types of defects caused by corrosion and the electromagnetic NDT techniques used in detecting and quantifying it. Electromagnetic NDT like MFL, ACFM, RFEC, UT and Magnetostriction are reviewed in particular. The merits and demerits of each are discussed. In addition, a review of EC sensing modalities was carried out.

2.1. Operational Defects

There are a number of defects that may be encountered in steel pipelines and pipeline coatings. They may be broadly categorised as manufacturing defects (defects that may occur during the manufacturing process), construction defects (those introduced during the construction process), operational defects (defects that initiate and grow after the pipeline has been commissioned) and coating and cathode protection defects (defects that creates the conditions in which external corrosion can develop) [10]. Of these categories of defects, the operational defects are of interest and we would therefore consider a few of them in the subsequent subsections. In general, the defect growth mechanism include but are not limited to external corrosion, internal corrosion, erosion, fatigue, mechanical damage and ground movement[10-12].

2.1.1. Arcing

This is a severe localised metal loss which may show signs of molten materials such as solidified globules. It is often caused by direct shorting from power lines. This kind of flaw may cause a through wall loss in a very short period of time [10].
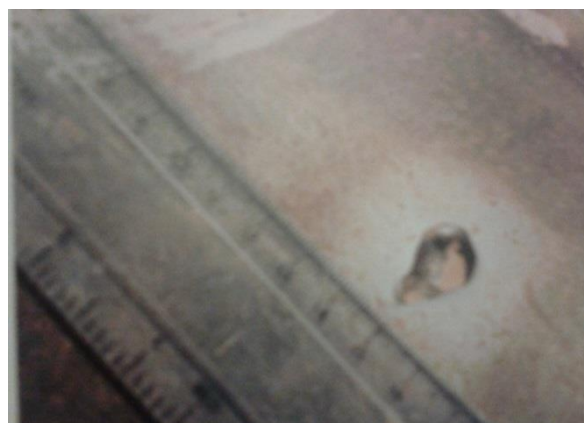
Figure 2.1: Arcing [10]

2.1.2. General Corrosion

General corrosion in assets causes areas of irregular metal loss or pitting to emerge. Disbonded coating or coating damage combined with ineffective cathodic protection usually leads to this. General corrosion may also be caused when soil contamination is entrained beneath a field applied coating [10, 11].

Figure 2.2: General Corrosion [10]

2.1.3. Microbial Induced Corrosion (MIC)

These are typically deep, sharp sided pits. Usually found under disbanded coating or hard accumulations on the pipe surface. The corrosion product within the pit is often soft with no structure and is deep black in colour. This is often caused by the bacterial activity in the anaerobic conditions under the coating or surface deposit. The immediate area of microbial activity may be anodic to the surrounding pipeline [13, 14] .
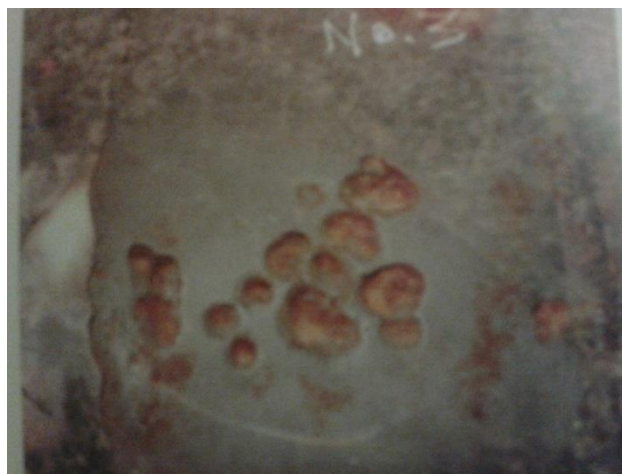
Figure 2.3: Microbial Induced Corrosion [10]

2.1.4. Pitting

These are localised corrosion typically at areas where the coating has suffered impact or damage. Potential causes of this include damage to the coating and ineffective cathodic protection, where for instance the pipe to soil potentials are less negative than -850 mV (with respect to a saturated copper-copper sulphate reference electrode). It may also be caused by MIC, stray current activity and galvanic effects [13-15].

Figure 2.4: Pitting [10]

2.1.5. Stress Corrosion Cracking (SCC)

These are irregular inter-granular cracks that are most commonly aligned axially on the pipe. They are not usually associated with pitting or general corrosion. The initiation and growth of such are caused by a mixture of factors including; high stress, pressure cycling, development of a carbonate-bicarbonate environment, partial shield of the applied cathodic protection and permanent or seasonal wetness in the soil [10-12].
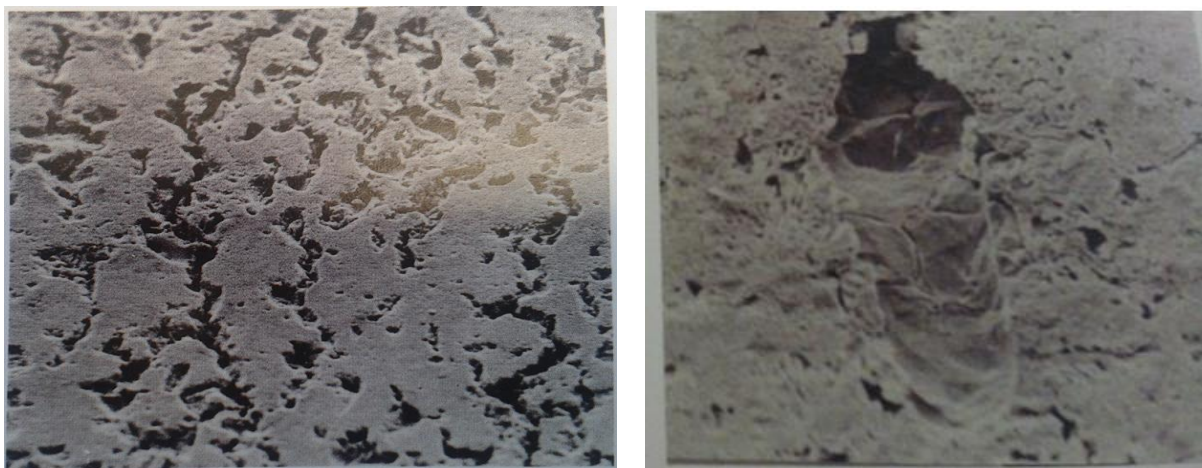
Figure 2.5: Stress Corrosion Cracking [10]

2.1.6. Particulate Erosion

These are kind of metal loss concentrated at the 6 O'clock position in the internal walls of a pipe. When particles of sand or scale are moved by the flow of the product being transported in a rolling or bouncing manner such erosion may occur as impact by such particles may erode the pipe or destroy the protective films and scales to allow erosion and/or corrosion [10, 13].

Figure 2.6: Particulate Erosion [10]

2.2. Electromagnetic NDE Techniques

Non-destructive evaluation (NDE) techniques are widely employed in the industry and science to evaluate the structural integrity and properties of a wide range of materials without causing any damage to them. From the previous section, a number of defects have been identified and discussed. This subsection focuses on the NDE techniques for inspecting and evaluating the severity of these common defects.

2.2.1 Magnetic Flux Leakage (MFL)

As identified in literature, the MFL principle is widely adopted in non-destructive testing and evaluation [16, 17]. This is so because of its simplicity. Basically, this system consists of a magnet yoke, which magnetise pipe wall, and defects in the pipeline causes magnetic flux leakage which is sensed by magnetic field sensor. Figure 2.7 gives a graphical illustration of this principle, while figure 2.8 shows an experimental set up of pulsed magnetic flux leakage (PMFL) for external pipeline defect detection. Wilson *et al.* [18] has used this to demonstrate that PMFL offers better anomaly sizing and sub-surface defect detection in comparison to

traditional MFL technique. However, sensitivity and the accuracy of the magnetic sensor are key factors in this testing method [19]. This is because micro-flaws may cause tremendous risk in the oil and gas industry; hence, it is necessary to detect such defects in pipelines. Since the defects being checked are sometimes very small, the leakage flux induced by them is too weak to be detected by conventional MFL sensors, like the fluxgate, hall element sensor amongst others, there is the need for the development of more sensitive and accurate MFL sensors and or replacements. Haixia et al [19] in their collaborative work have developed the A2PI magnetic field sensor which they demonstrated meets these criteria. It has adopted a differential coil design to reduce noise as in [20]. Where, one coil is placed near the pipe surface to detect the flux signal; invariably this is embedded with certain level of noise. A second coil is placed away from the pipe surface, where noise only is detected. And by subtracting the output of the first coil from the second coil, only the expected flux leakage signal should remain. This is generally achieved by winding one coil clockwise and the other anticlockwise and wiring the coil in series. Most times the noise signals never cancel out completely but give significant noise reduction. Equally, this scheme is optimised by the inclusion of a negative feedback coil and bias magnetic field which in turn makes the output properties of the MFL configuration adjustable by changing the feedback factor [19].

Despite this MFL sensor optimisations, it is stilled plagued with some other deficiencies such as weight and volume due to the need of a magnetic circuit and its associated magnetisation equipment, its inability to detect flaws parallel to the magnetisation direction, pipe end effects and magnetic compression effect [21]. To this end, Sun et al [21] have proposed permanent magnetic perturbation, PMP, testing sensor, which takes care of these aforementioned deficiencies as a clear departure from the flux leakage measurement principle to a direct magnetic interaction in the spatial region where the magnetic perturbation caused by the discontinuities is directly captured. In this method, PMP is proportional to the magnetic fields, meaning that the more the magnetic field, the more the PMP. And since PMP sensors can be made in point mode without additional magnetisation equipment, it has eliminated the problem of volume and weight and can be useful for detection in special locations with narrow operational space e.g. thread and discharge pipes with small radius. Second, the PMP sensor, can detect omni-directional defects including those parallel to the scanning orientation. The PMP has shown no end effect, hence, the non-detection of pipe end problem may be potentially mitigated by the PMP sensor.

Again, Sun et al in [22], has established that magnetic compression effect, MCE, is present in MFL sensors, which has hitherto led to a contact inspection sensor with zero lift-off distance. With this discovery, an emerging drive into the avoidance or minimisation of MCE in MFL sensors could lead to a long range and non-contact inspection MFL sensor.

(a)   (b)
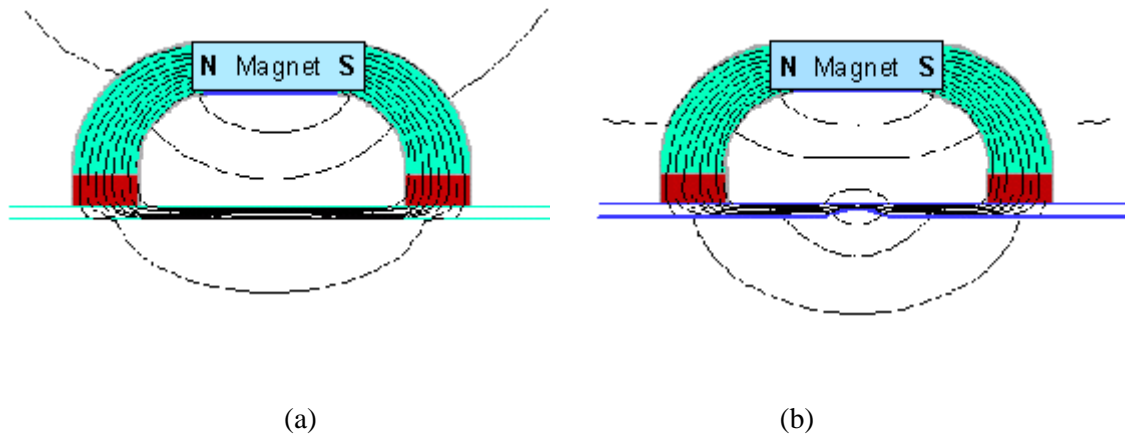
Figure 2.7: MFL principle (a) Pipe without defect - no leakage (b) Pipe with defect – leakage visible [23]

(a)   (b)
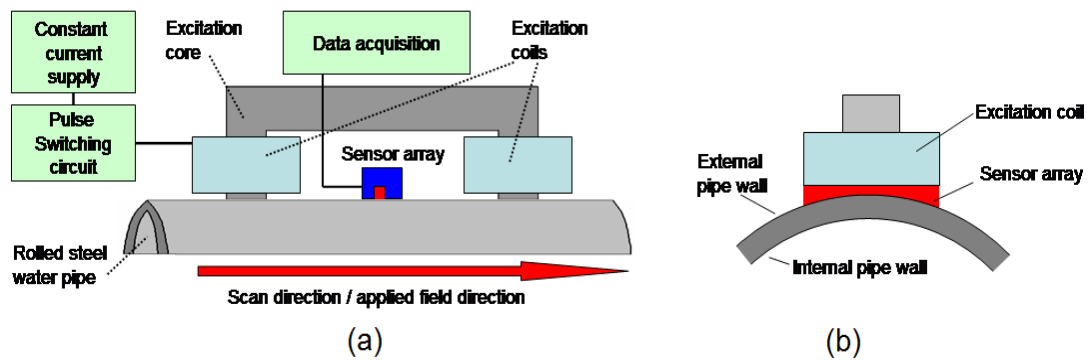
Figure 2.8: Experimental Setup of PMFL testing (a) showing the Longitudinal View and (b) the Cross-sectional view

2.2.2. Alternating Current Field Measurement (ACFM)

This is an electromagnetic non-destructive testing technique which can be used to detect and size surface breaking or near surface defects for both ferromagnetic and non-ferromagnetic materials [24]. In this technique, a solenoid is used to induce uniform alternating current in the target material. If the target is defect-free, a uniform magnetic field is produced above the surface of the target by the induced alternating current. In the presence of a flaw however, the

current distribution is disturbed making it to flow around and beneath the flaw. The associated magnetic field therefore becomes non-uniform and the variations in field are measured by sensors in the ACFM probe [24]. As shown in figure 2.9 [25], the ACFM system measures two field components, that is Bz and Bx. Bz gives information about the defect length while Bx is used to estimate the defect depth. Though originally developed for underwater weld inspection, it has found other useful applications amongst which are railway track inspection [25] , stress measurement [26], inspection of pressure vessels, pipes, drill-pipe threads and risers [24].

This technique has the advantage of having little adverse probe lift-off effect due to the fact that the decay of the uniform input field is less rapid with the distance from the coil; making it attractive to be deployed for coated and rough surfaces [27, 28]. Also, it requires little or no surface preparation before deployment. It has the capability for depth sizing based on theoretical model rather than on calibration employed by other NDT methods [29].

Again, the ACFM technique is relatively insensitive to the electromagnetic property changes of the target material; hence it becomes suitable for both ferrous and non-ferrous metals and ideal for weld inspection [29] . This technique however, is not without its own limitations: as larger coils are used for induction in ACFM, therefore, it has lower sensitivity to shallow flaws at the normal operating frequency of about 5 kHz [30] . Smaller coils and higher frequencies can improve sensitivity but with the trade-off of increased noise [30] . Again, complex or spurious signals can arise from tight geometries, edges and branched defects [29] . The ACFM equipment is less portable and operators require a higher level of training.
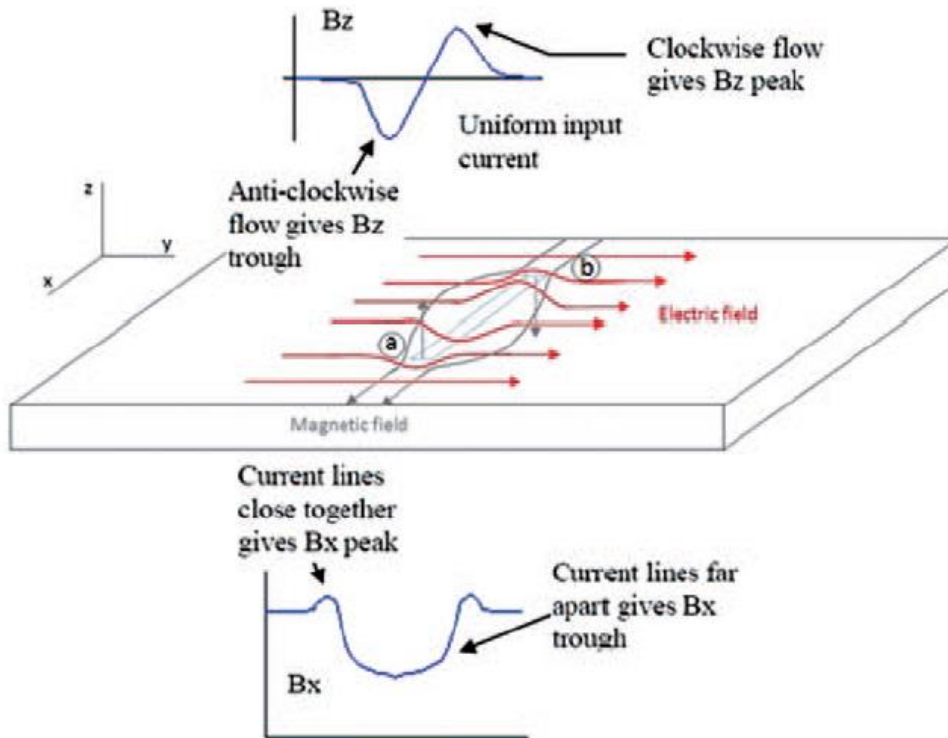
Figure 2.9: Current and Magnetic field distribution in ACFM [24]

2.2.3. Remote Field Eddy Current (RFEC)

This is another electromagnetic non-destructive testing technique. It is quite different from the conventional eddy current method. Sometimes when through penetration of thick pipe walls are necessary, the conventional eddy current technique is limited but the RFEC mitigates this limitation and in addition, it is sensitive to internal and external defects. Whereas this sensitivity to both internal and external defects is an advantage, it makes distinguishing between the two quite difficult [31].

The RFEC probe basically consists of an excitation coil and detector coil(s) placed at about twice the internal diameter of the tube to be inspected. A low frequency alternating current is fed into the excitation coil generating an EM field. The changing magnetic field induces circumferential eddy currents which extend axially and radially in the tube wall. These eddies produce their own field, which opposes the magnetic field from the excitation coil (primary field). Due to the resistance in the wall of the tube and the imperfect inductive coupling, the secondary field does not fully counteract the primary field [31, 32] . However, since the secondary field is more spread out, it extends further along the axis of the tube. The interaction between the fields is fairly complex as shown in figure 2.10, however, the basic

element of this interaction is that the primary field is dominant near the excitation coil and the secondary field becomes dominant at some distance away from the excitation coil. By monitoring the constancy or otherwise of the induced voltage in the detector coil(s) one can detect changes in the test sample. The RFEC is less sensitive to axial defects owing to the fact that this kind of defects only cause a little perturbation in the path of the magnetic field so that the variations in the effect permeability are not significant; but circumferential defects like metal loss due to corrosion can be detected as they perturb the lines of magnetic flux [33]
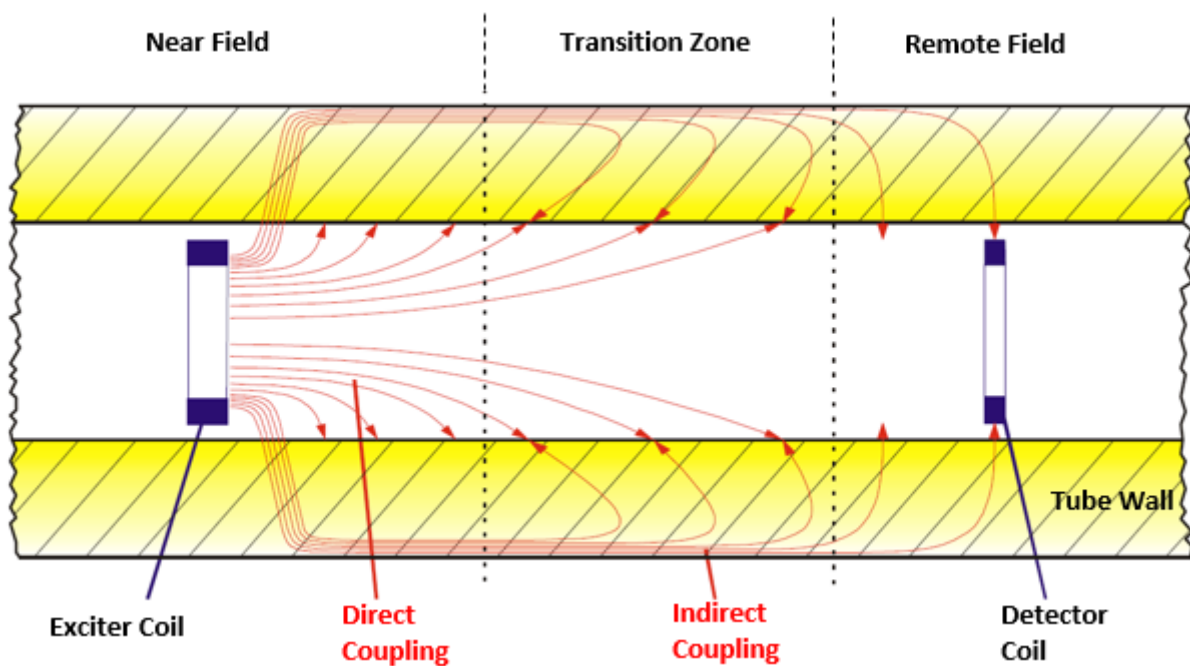
Figure 2.10: Schematic of the RFEC Testing [34]

2.2.4. Electromagnetic Acoustic Transducer (EMAT)

The EMAT is another EM technique that is lending itself in the field of NDT. Advantages of this technique include operation without a coupling fluid, non-contact operation, high temperature operation and the ability to utilise shear horizontal (SH) waves. Equally it is well suited for sending and receiving Rayleigh waves, lamb waves, and SH plate waves [35-37]. It has been mainly used for flaw detection in metallic materials. However the main disadvantage of this technique when compared to piezoelectric transducers is its poor transduction efficiency. The received EMAT signals normally consist of backscattering noise (like back-wall echo, fault echo and reflected ultrasonic waves from specimen) and electronic noise (influence of electronic circuitry). And this has the potential of completely masking the

needed echoes from flaws; hence, they must be suppressed [38]. A number of methods or approaches have been proposed to mitigate this problem, for instance the dual EMAT and PEC non-contact probe by Edwards et al [39]. This exploited the combined ability of an EMAT and PEC sensor to achieve a higher accuracy for sizing and detection of defects. Moreover, a departure from this composite technique where two NDT probes were used in a complimentary manner is the use of a purely EMAT sensor in dual coil configuration [38]. This novel EMAT in dual coil configuration where both coils are transceivers of ultrasonic sounds has been demonstrated to make flaw detection more accurate and noise level can be efficiently suppressed using signal processing algorithm. Figure 2.11 gives a graphical illustration of the EMAT NDE technique.
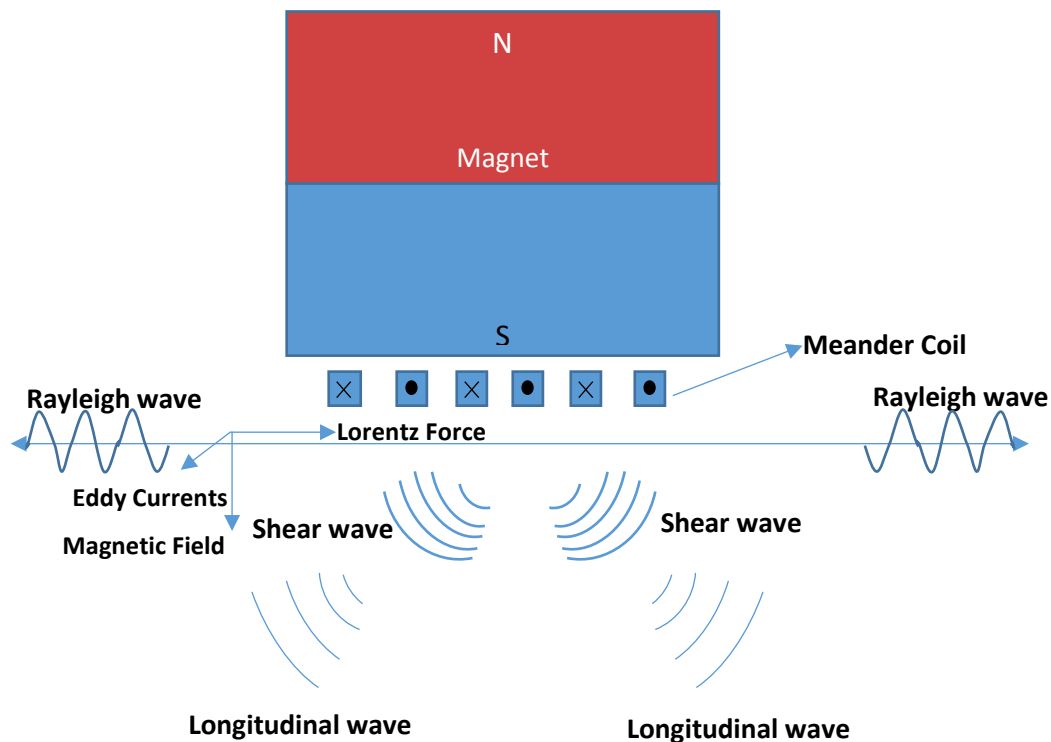
Figure 2.11: EMAT Testing

2.2.5. Magnetostrictive Sensing Technique

Magnetostriction is based on two physical effects; that is, the Joule-Villari effects. The Joule effect on the one hand is a phenomenon whereby ferromagnetic materials are mechanically deformed when placed in a magnetic field while on the other, Villari effect is the inverse phenomenon, where the magnetic induction of the sample changes in the event that the material is mechanically deformed [40]. This bi-directional coupling between the magnetic

and mechanical states of the material provides a transduction capability that can be used in a variety of ways to measure a property of interest [41].

The interplay of these two effects has been used to develop a magnetostrictive sensing technique, which in strict terms is a family of the EMAT: the main difference lie in the generation of the ultrasonic wave, the former proving to be the most cost effective solution [42].

Magnetostrictive probes therefore use the magnetostrictive properties of the target materials to excite elastic waves which can be measured and monitored to characterise the target [40, 41, 43]. An elastic wave may be described as a disturbance or motion in a medium, in which, when a particle is displaced, a force proportional to the displacement acts on the particle to restore them to their original position. Furthermore, if a material has the property of elasticity and the particles in a certain region are set in vibratory motion, an elastic wave will be propagated. For example, gas is an elastic medium; hence sound is transmitted through gas as an elastic wave.

Materials employed in magnetostrictive sensors are majorly transition metals such as iron, cobalt and nickel. The 3d electron shell of these transition metals is not completely filled, hence, allowing the formation of a magnetic moment. It follows that as electron spins rotate by a varying magnetic field, the coupling between the spin and the electron orbit results in energy changes of the electrons. Thus, the crystal of the material strains causing electrons at the surface to relax to states of lower energy [44].

Figure 2.12 gives a vivid illustration of the magnetostrictive principle. The MST in its most basic form consist of a transmitting coil which applies a time varying magnetic field to the target material generating a mechanical wave, a receiving coil which detects changes in the magnetic induction of the material. Bias magnets to saturate the material, necessary to enhance the efficiency of the MST and to make the frequencies of the electrical signal and the mechanical wave same.
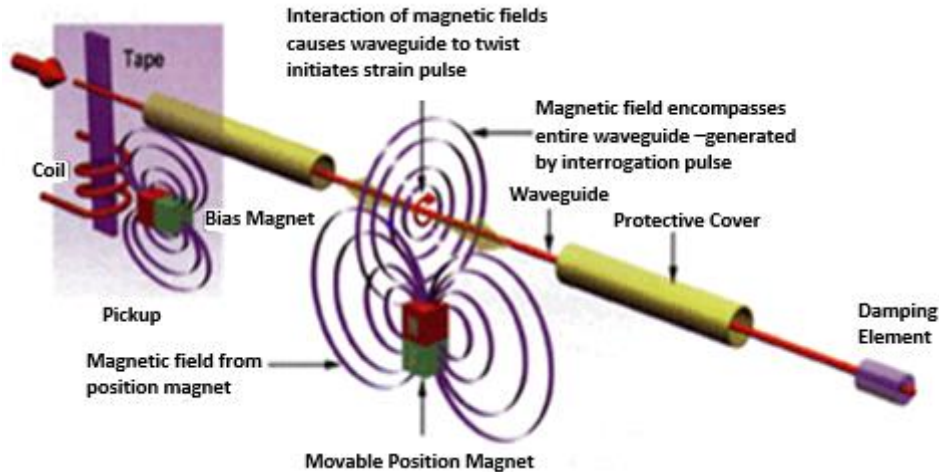
Figure 2.12: Principle of Magnetostriction [45]

2.2.6. Eddy Current Technique

This is arguably the most widely used technique in the field of non-destructive testing and evaluation. The eddy current technique (ECT) depends on the high electrical conductivity of conductor and works commonly due to the decrease of a second magnetic field generated by the distortion of eddy-current in objects with the presence of defects [46]. It has found extensive use in inspecting electrically conductive targets at a very high speed and provides a contactless testing between the probe and the sample [47]. The principle of eddy current NDE hinges upon the interaction between a magnetic field source and the target material. This interaction induces eddy currents in the sample material [47] , which can be used to detect the presence of defects by observing the changes in the eddy current flow [48-50].

Eddy current testing allows defect detection and characterisation for a wide range of conductive materials; ferromagnetic and non-ferromagnetic materials alike, while other NDE techniques are limited to ferromagnetic materials. This method also proffers a non-contact inspection solution which in itself helps extend the service life of the sensor as it is not prone to wear and tear. Again, [51] has demonstrated that for coated pipes, the measurement of non-conductive coating thickness can be carried out. The composition of a material and heat treatment are related to its conductivity, hence, eddy current techniques can be used to discriminate between pure materials and alloys and by extension to know the hardness of test samples after annealing [52].

The main variables of eddy current inspection include amongst others the electrical conductivity and magnetic permeability of the target material, lift-off between the probe and the target piece, skin effect of current distribution in the test piece, SNR, edge effect, and the phase lag.

The principle of operation is explained thus: when the coil or probe is scanned across the material surface, changes in the physical properties of the sample, for example material type, geometry, conductivity, temperature, flaws, amongst other things affects the current flow. This eddy current flow produces a secondary magnetic field (as shown in Figure 2.13), opposite to the direction of the primary field, which can be measured by a magnetic field sensor, or by monitoring the impedance of the inspection coil. Amplitude and phase change can be used to show changes in material properties.
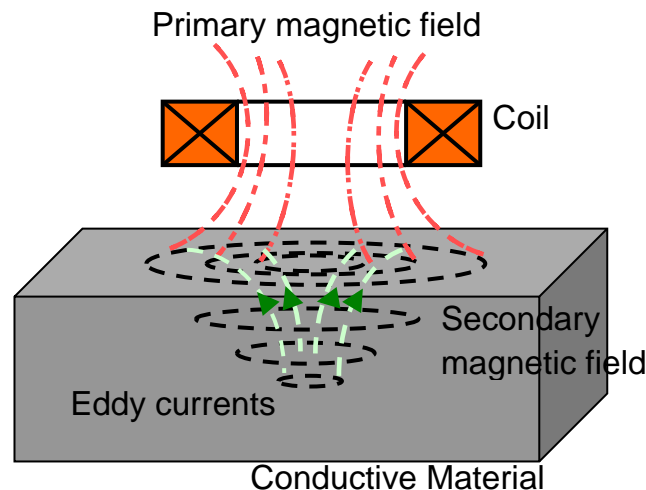
Figure 2.13: Interaction of Eddy current with a Conductive Material Sample

The technique's ability to detect subsurface defects is determined by the skin effect. The majority of the eddy currents induced in the material occur on the surface and decay exponentially with increasing depth, controlled by the depth of penetration (δ):

$$\delta \approx \frac{1}{\sqrt{\pi f \mu \sigma}}$$

The depth of penetration is dependent on the frequency f, the material permeability μ and conductivity, σ. To overcome this limitation, the pulsed eddy current (PEC) technique has been developed where a pulse excitation, containing a range of frequency components, is used to improve penetration depth [53, 54]. Again, these broad spectra of frequencies provide

more information than classical eddy current inspection suitable for defect detection and characterisation of hidden crack [54].

PEC instruments are normally designed with a double function coil or two separate coils. Sensitivity of such instruments is equally increased using magnetic field sensor like GMRs in place of receiver coils [55].

De Haan et al [56, 57] have shown that PEC is not only useful for corrosion detection as they were able to use it to characterise conductivity and magnetic permeability. With a reference measurement of an object with known thickness, they determined the thickness of several types of carbon steel samples, which is proportional to the product of conductivity and magnetic permeability.

Eddy current techniques have a wide variety of applications including steel pipe inspection and coating thickness measurements [58, 59]. The drawback of ECT is that it can only be used on conductive materials.

2.2.6.1. Main Parameters in Eddy Current Testing

There are number of parameters that influence the eddy current testing response. The variation and interplay of these parameters affects the accuracy or otherwise of this NDE technique. The main parameters as identified in literature are herein reviewed in detail.

2.2.6.1.1. Magnetic Permeability and Magnetisation of Ferromagnetic material

Magnetic permeability is an electromagnetic property of ferromagnetic materials. Although ferromagnetic materials do have nominal bulk permeability, large variation in magnetic permeability is an inherent attribute of such materials. This variation strongly affects the distribution of the eddy current in the material, as such; defect detection is flawed when permeability changes in an arbitrary pattern [49, 60]. The inhomogeneity of this material property is a serious problem that has to be dealt with when using (pulsed) eddy current technique.

The main solution that would mitigate this problem and allow for accuracy in measurement is a process that equalises the magnetic permeability. One of such ways is magnetically saturating the material through magnetisation circuits [49, 60]. This brings about a fairly constant magnetic permeability, thereby improving the accuracy of measurement as the

influence of permeability variation is reduced. The equalisation of permeability variation can be understood through the B-H relationship. At the saturation point when the majority of the magnetic domains are aligned, additional magnetisation force will produce slight increase in magnetic flux B resulting in a reasonably constant magnetic permeability [61].This is not without its own associated problems as the magnetisation circuit must produce sufficient field to drive the material to magnetic saturation.

Also, other attempts to solve this problem include the work of Uzal *et al.* who calculated the impedance of an EC probe over a multi-layer sample whose permeability varied continuously as an arbitrary function of depth [62]. Ghanei *et al.* exploited the fact that microstructural changes affect the magnetic property of target samples to demonstrate a reduction in the magnetic permeability effect by increasing the martensite content in dual phase steel [63] but this is not feasible for existing steel structures.

2.2.6.1.2. Electrical Conductivity

Electrical conductivity is an intrinsic material property which measures the ability of a material to conduct electric current. Eddy current testing technique cannot work in non-conductive materials; hence, this material property is an important parameter in this technique. Highly conductive materials therefore generate strong eddy currents and have some advantages over less conductive ones. Amongst such advantages are that defects produces greater signal amplitudes on the impedance plane and the phase lag between lift-off and defects is larger. However, this is with the trade-off that the penetration depth at a fixed operating frequency is lower than in less conductive materials [48]. There are a number of factors that affects this parameter. This includes temperature, the constituents of the alloy residual stress amongst others.

There has equally been a number of conductivity related studies in eddy current technique. For instance, Uzal *et al.* presented numerical and analytical methods for calculating the coil impedance when an arbitrary radial conductivity changes occur in a target material [64]. Also, a method of the conductivity profile reconstruction from eddy current impedance change data has been presented in [65]. Since the eddy current technique is sensitive to conductivity variation, it poses a problem termed electrical runout, ERO. This phenomenon is caused by both electrical and magnetic property variations resulting in apparent displacement of rotating shafts and errors in roundness measurement of tubular structures like pipes [66].

Attempts have been made to mitigate this; amongst such research effort is the development of a coaxial ellipse distribution, CED, pattern that correlates the magnetic field with conductivity variation [67]

2.2.6.1.3. Lift-off

Lift-off may be described as the distance between the probe and the target sample. Its variation adversely affect the EC measurements in many applications [68] it is therefore considered as a noise factor and it is undesirable in discontinuity detection and characterisation as lift-off and defect could be occur in the same direction thereby masking the defect response.

This suggest therefore that a fairly constant displacement between the EC probe and the test piece must be maintained to avoid lift-off effects; this is sometimes difficult in practice as irregular test surfaces, varying coating/lagging thicknesses, operator's movement amongst other things prevent this [69, 70].

To compensate for this lift-off effect Yin *et al.* published a research finding on an analytical model based on multi-frequency excitation and coil design aimed at the reduction of this effect. The finding showed that the phase spectra of such coil designs is essentially lift-off invariant [68, 71]. Shu *et al.* optimised EC coil design in an attempt to reduce lift-off effect [72]. In [73], the use of wavelets to remove probe wobble noise from steam generator tubes has been proposed. A normalisation technique has been proposed by Tian *et al.* to minimise lift-off effect. They demonstrated it could be used in metal thickness measurement under non-conductive coatings and for the measurement of microstructure and stress where the output is susceptible to the lift-off effect [74]. Also, Theodoulidis *et al.* has presented an analytical model of wobble in heat exchanger tube inspection in [75]. Another way of dealing with this effect is by using invariant point features called lift-off point of intersections, which has been successfully used to estimate conductivity of test materials in [69] and for corrosion mapping in gas pipelines [76].

2.2.6.1.4 Edge Effect

When a PEC probe is at the end of a test piece a phenomenon termed edge effect sets in. In such circumstances, the eddy current flow is distorted as current cannot flow at the edge. In order to avoid it being mistaken for flaws, inspection is limited near the edges. Smaller probe may be better suited for inspection near edges [77] . Also, a post-processing subtraction

algorithm has been developed by researchers to compensate for this effect [77]. In addition, Theodoulidis *et al.* equally proposed a model to calculate the quasi-static EM field of a coil probe in the edge of a conductive metal block [78], [79]. This model elicited some analytical field formulations that gave better insight into this phenomenon and could form the basis of a process of solving edge effect associated challenges [49].

2.2.6.1.5 Fill Factor

For encircling eddy current probes the fill factor is a crucial parameter. The fill factor may be conceived as a measure of how well a sample fills the external encircling coil. It can therefore be defined mathematically as the ratio of the square of the diameter of test piece to the square of the diameter of the coil. In other words, it is the ratio of their respective cross-sections. It is desirable that the fill factor is as close to unity as possible. Reason being that for a fill factor close to unity, better response is expected for potential defect detection as the test piece would be closer to the encircling coil [49, 80]. It is therefore paramount that the probe design should be such that the fill factor is close to unity.

2.2.6.1.6. Frequency and Skin Effect

The operating frequency is an important factor in eddy current testing in general. This parameter affects the depth of penetration (which is governed by the skin effect) of the eddy current in a test piece. Studies have revealed that the eddy current flow is not uniformly distributed throughout the volume of the test material. The intensity of the eddy current distribution is strongest at the surface and decays exponentially with material depth. This phenomenon is called the skin effect and for one standard depth of penetration δ the current would have decayed to about 37% of its surface value [56]. From the skin depth equation ($\delta \approx 1/\sqrt{\pi f \mu \sigma}$) one can deduce that at lower operating frequencies the depth of penetration increases and decreases at high frequencies. Hence, lower frequencies would be suitable for sub-surface inspection whilst higher frequencies which would maximise the eddy current flow on the surface of test materials would be best suited for defect inspection in the near-surface area. For instance, in [81] two operating frequencies (200 Hz and 10 KHz) were used to demonstrate the penetration depth of the eddy current in an aluminium test sample and typical values of δ obtained are 5.99mm at 200Hz and 0.85mm at 10 KHz. To avoid the eddy current from passing through the material, the thickness of the test material should be about 2-3δ [48].

2.2.7. Pulsed Eddy Current

As a result of advances in electromagnetic non-destructive evaluation, pulsed eddy current (PEC) technique has become more feasible and preferred in recent years [82, 83]. Where traditional eddy current testing uses a single frequency sinusoid to excite the probe, PEC uses a step function voltage to excite the probe. The unique advantage of this is that a single step function contains a series of frequencies and as penetration depth is frequency dependent, information from a range of depths can be acquired at the same time with just one step function excitation [83].

Conventionally, pulsed eddy current technique uses an inductive coil as its sensor and measurement is based on the rate of change of the magnetic field, however, recent developments in NDE employs solid state magnetic sensor based PEC like Hall sensor, GMR, SQUID amongst others to measure the magnetic field changes directly [84]. For the fact that solid state magnetic sensors are small sized relative to the dimensional characteristics of the received magnetic field, it produces superior spatial resolution to classical coil sensor. In addition, magnetic sensor based PEC allows for the detection of deeper defects in comparison to typical coil sensor based PEC because the former operate well at frequencies much lower than the latter[82, 85, 86].

From the PEC response signal, time and frequency features are often extracted for defect estimation, material characterisation, profile reconstruction and non-destructive evaluation in general. For instance, Bai *et al.*, has developed and demonstrated the potentials of time slices and spectral components of PEC response to linearly reconstruct surface breaking cracks. The research work claimed that the imaginary part of the spectral response provided better estimate of crack profile than the real part of the spectral response. Similarly, the research showed the capabilities of crack profile reconstruction using the transient response between the rise time and the time to peak though it concluded that the linear reconstruction model based on the spectral response showed superior performance for deeper crack reconstruction[87]. He *et al.*[88] has used the peak height and zero-crossing time feature to characterise defect in riveted structures of aging aircraft. Also, in [89] stress in aluminium alloy has been characterised with the peak height of PEC response signal. Lebrun has used the magnitude spectrum and peak time to determine the height and depth of defects respectively [90]. More recently, a NDT method for corrosion distribution in multilayer aluminium structure has been developed which makes use of Rihaczek time-frequency

analysis to convert the received PEC response to a 3-dimension data. After which the maximum variance of principal component analysis, PCA, is extracted and the data classified by K-mean and expectation-maximisation statistical tools [91].

As attractive as this EM NDE technique is, the accuracy of EC and PEC measurements in many applications is however affected by variation in the probe-specimen distance called lift-off [74, 92]. Thus, a number of approaches are currently being explored by researchers to mitigate these effects in pulsed eddy current measurements/techniques. In a broad sense, these approaches may be classified as exploitation of signal processing [93], probe and system design modification [71, 92] and feature extraction [94]. For instance, Tian et al [60] has used a normalisation technique to compensate for unwanted lift-off variation in PEC. Although this normalisation technique was effective for sub-surface defect, it was found to be less effective for surface defects. In [93], Kim et al transformed measured eddy current signal to obtain a zero lift-off equivalent signal by the use of a scaling factor thereby mitigating lift-off effects. Also, in [94] time and frequency features were extracted to reduce the lift-off effect in PEC measurements. Hoshikawa and Koyama [95] have designed an EC probe devoid of lift-off.

The lift-off point of intersection (LOI) feature has been used by a number of authors to obtain lift-off invariant PEC measurements [69, 96-98]. However, all of these have dealt with non-ferrous materials and no LOI feature has been observed in PEC investigation of ferromagnetic materials except for those coated with thin conductive, non-magnetic layers [99, 100]. This approach is limited in application in that not all ferromagnetic materials are coated with conductive layers and the inspection of such could be laborious.

Again, another teething problem that has been identified in practice and in literature with this technique which is a restraining factor in high precision measurements is the issue of material inhomogeneity. This systematic problem is called electrical run-out (ERO) a phenomenon analogous to mechanical run-out (MRO). MRO in displacement measurement may be described as a measure of the displacement due to the contribution of shaft's out-of-centricity and out-of-roundness when PEC technique is used while ERO is the apparent displacement due to variation in the electromagnetic properties of the target material [60, 101].

Researchers have suggested a number of ways of mitigating this problem some of which are application of special coating of sufficient homogeneity on the test material [84], and the use

of a patented device to remove ERO in machine shafts [102]. Here, the apparatus detects inhomogeneity and corrects the crystalline structure and by extension the electromagnetic properties of the material by precise mechanical deformation [102], this presents a great risk of depreciated result moreover it is a delicate and slow process which demands an experienced hand.

In recent years, Tian et al in [58] proposed a redesign of the EC sensor itself with high operational frequencies. This work revealed that in the displacement measurement of ferromagnetic samples, for operating frequencies below 1MHz, sensors with amplitude modulation (AM) converting circuits are less sensitive to ERO in comparison to those with frequency modulation (FM), although the difference in sensitivity at operating frequency above 2MHz between the two becomes negligible, hence, measurements at high operating frequency was suggested. However, for many industrial applications where large measuring range is required this high frequency range would be impracticable.

Also, in [84] attempts were made to mitigate the ERO problem by using multi-resolution decomposition of the measured signal based on discrete wavelet transform. However, the disadvantage of this approach is that it was unable to distinguish between ERO and MRO components. Yating et al also investigated the influence of the sample's electromagnetic properties on the coil impedance showing that the influence of conductivity was simple and regular while that of permeability is complex and irregular [103].

Besides the ERO problem, PEC sensing is affected by the inhomogeneity of test samples which is undesirable for defect measurement and material characterisation leading to spurious signal response [9, 96, 104].

2.3. Comparison of Inspection Techniques

A summary of the literature review of NDE methods for defect detection and characterisation in general and the main parameters influencing their performance is presented in Table 2.1.

The choice and selection of an appropriate NDE technique depends on a number of factors. The applications, accessibility, portability of instrument, the inspection area, target material, type of defect amongst other things are important factors to be considered in the selection process. Whilst some techniques work well for ferromagnetic materials by providing

qualitative and quantitative information, they are less effective or not effective for non-ferromagnetic materials.

Therefore, from the factors enumerated above and the peculiar inspection situation, an informed decision as to which technique to use in order to facilitate repairs/replacement of critical components in the most cost effective manner can be achieved.

Table 2.1: A Comparison of NDE Techniques

Inspection Technique		Merit	Demerit	Target Material	Primary defect	Parameters affecting Performance
EM NDE						
Eddy current	EC	Non-contact, accurate conductivity measurement	Sensitive to coupling variation	Ferromagnetic and non-ferromagnetic	Surface and near surface defect	Lift-off, permeability, conductivity, excitation frequency, skin depth
	PEC	Better depth penetration, multilayer defect detection	Susceptible to material property variation	Ferromagnetic and non-ferromagnetic	General metal loss, pitting and sub-surface flaws	Lift-off, permeability, conductivity, probe geometry
	RFEC	Sensitive to both internal and external defects	Distinguish-ing between internal and external defects can be quite difficult, less sensitive to axial defect	Ferromagnetic tubes	Internal and external wall loss	Material properties
Magnetic Field Measurement	ACFM	Defect sizing without calibration, less affected by probe lift-off effect	Lower sensitivity to shallow defects at normal operating frequency (5 KHz), tight geometries, edges and branched defects are difficult to inspect, Equipment are less portable	Ferromagnetic and non-ferromagnetic	Underwater weld inspection	Coil dimension and geometry, Frequency of operation
	MFL	Versatile and robust for	Unable to detect flaws parallel to the	Ferromagnetic	General wall loss, pitting	Sensitivity and accuracy of the magnetic sensor

		Merit	Demerit	Target Material	Primary Defect	Parameters affecting Performance
Flux Leakage		examining the geometry of metal loss	magnetic field e.g. Axial slots			
	PMFL	Better anomaly sizing and sub-surface defect detection	Limited by large lift-off displacement	Ferromagnetic	General wall loss, pitting	Lift-off, Sensitivity of magnetic sensor
EM Acoustic Wave	EMAT	Non-contact, coupling fluid not required, permits high temperature operation	Poor transduction efficiency, received signal affected by backscattering noise	Ferromagnetic and non-ferromagnetic	General wall loss, SCC, pitting, delamination, sub-surface defects	Material properties, lift-off, transduction efficiency
	MST	No couplant required, permits significant lift-off (up to 1.3cm) and volumetric testing	For long-term installation ferromagnetic materials with low coercivity might lose magnetisation over time, relatively low energy efficiency compared to piezoelectric transducers	Ferromagnetic	General wall loss, SCC, pitting, delamination, sub-surface defects	Material properties, transduction efficiency
Other NDE Techniques		**Merit**	**Demerit**	**Target Material**	**Primary Defect**	**Parameters affecting Performance**
Ultrasonic Wave	UT	Sensitive to both surface and sub-surface defects, good penetration depth	Requires a couplant fluid, surface must be accessible, rough and irregular shaped materials are difficult to inspect	Metals in general & composite	General wall loss, SCC, delamination	Attenuation coefficient and metallurgical characteristics of the test material
	Laser UT	Non-contact & faster inspection time, independent of couplant, can be used in curved complex surfaces	Lower sensitivity than PZT UT, relatively more expensive system	Metals in general & composite	General wall loss, SCC, delamination	Surface roughness, optical phase variation

Radiography	X-ray	Capable of detecting both surface and subsurface defects, provides a permanent record of inspection	delamination and planar cracks are difficult to detect, material must have two-side accessibility	Virtually for all materials	Surface and sub-surface defects, crystallographic structure of materials	Attenuation coefficient, Exposure time, spectrum of radiation generated, material thickness and constituent
	Gamma Ray	Greater penetration power, less scatter, no electrical or water supplies needed	Higher energy level requirement, poorer quality radiographs, longer exposure time	Virtually for all materials	Surface and sub-surface defects, crystallographic structure of materials	Exposure time, source-film distance, spectrum of radiation generated, material thickness and constituent
Visual/ Optical Testing	Thermo-graphy	Fast and cost effective technique for thermal analysis over relatively large area	Sensitive to material emissivity, affected by probe-sample proximity	Metals in general & composite	Delaminat-ion, Disbond, voids and inclusions	Emissivity, thermal conductivity, electrical conductivity and magnetic permeability
	Shearogra-phy	Non-contact, relatively large inspection area & requires no reference beam	Limited by tolerance to rigid body movement which reduces flaw detectability	Metals in general & composite	Disbond, voids and inclusions	Rigid-body movement
	Dye Penetrant Technique	Low cost and sensitive to small size defect	Surface roughness can heavily influence the inspection sensitivity. Limited to surface breaking defects	All non-porous materials; i.e. Metals, plastics or ceramics	Surface breaking cracks and pinholes non-visible to the naked eye	Surface roughness
Electrical Signal Reflection Measurement	ETDR	Low cost, capability for distributed sensing and a reliable technique	Low defect sensitivity and high noise, Limited by the minimum system rise time	Conductive metals, composites	Subsurface delaminat-ion in composites discontinuities in cables	Impedance variation, material properties, sensor geometry, dielectrostrict-

		for SHM				ion
	SSTDR	precise fault location, robust for high noise environment	Requires high data rate signals, affected by blind zone due to impedance mismatch	Conductive metals, composites	discontinui ties in cables	Attenuation and dispersion coefficients, propagation speed

2.4. Problems and Challenges

In general, from this survey it is apparent that the complex nature of natural occurring defects due to corrosion mechanism and other operational mechanisms plus the complex geometry of structures pose a challenge to employed EM NDE techniques. Also, harsh and dynamic operating environment constitute another cause of concern for the choice of technique to be adopted. In order to mitigate these challenges, multiple physics leading to multi-sensing modalities are often employed. This in itself is sometimes intricate and capital intensive. Therefore, the extraction of multiple parameters from a single NDE response signal, which is cost effective, becomes attractive. The sensitivity of PEC technique to a broad variety of parameter variations set it apart for this multiple parameter based NDT&E.

However, one of the greatest challenges in pulsed eddy current NDE technique is that of lift-off which is as a result of many field realities identified in this survey.

A review of extant literature has shown that lift-off tend to mask useful information thereby affecting the accuracy and reliability of PEC measurements; hence, a number of approaches has been researched to solve this problem. An attractive approach to mitigate this problem is the use of the lift-off point of intersection (LOI) feature. However, this LOI feature is not apparent in ferromagnetic materials (which is widely used in the petro-chemical industry) except for a case where a non-magnetic but conductive layer of coating has been applied to the ferromagnetic material.

Fundamental to this approach of a thin-layer conductive non-magnetic material coating of a magnetic material is to drastically reduce the apparent magnetic permeability effects so that the LOI feature can be used for defect characterisation. To circumvent this limitation

therefore, there is a need to have adequate understanding of how the magnetic permeability influences the PEC output response. This understanding would present a means to mitigate this effect and in turn be able to characterise defect using the LOI feature in ferromagnetic materials without the use of conductive coating layers.

2.5. Chapter Summary

This chapter has presented in the main a review of some operational defects, common electromagnetic NDE techniques, a comparison of these techniques and the inherent problems and challenges with them often leading to multi-sensing modalities which could be capital intensive. This present an opportunity to explore multiple parameter delineation and estimation for a comprehensive assessment of target materials from a single PEC response signal which is less capital intensive. Based on this therefore, the theoretical background to PEC is presented in the next chapter, followed by a study of the influence of the material properties on the PEC response signal in chapter 4. Consequent upon this understanding a novel and direct LOI based PEC inspection of ferromagnetic materials without the use of a conductive layer coating is presented in chapter 5. Thereafter, useful application and validation of the proposed method is demonstrated in chapter 6.

Chapter 3: Research Methodology for Multiple Parameters PEC NDT & E

This chapter focuses on the underlying physics of pulsed eddy current (PEC) and related phenomena as this work seeks to tackle the challenges identified in the Literature review, laying a basis for multiple parameter estimation and lift-off invariant pulsed eddy current measurement. This will discuss the electromagnetic induction principles on which pulsed eddy current (PEC) hinges on whilst clearly linking it to Maxwell's unified electromagnetic theories. The remainder of the chapter sets out the proposed research methodology and outlines the research investigations carried out.

3.1. Theoretical Background to PEC

Electromagnetic NDE employs the interaction between electric and magnetic fields in its applications, thus, they are governed by the fundamental principles of electromagnetism, which are based on Maxwell's unified electromagnetic theory [80, 105]. These are a set of four coherent physical laws namely Ampere-Maxwell's law, Faraday's law, Gauss' laws for electric and magnetic fields. For a time-changing field therefore, and with the assumption that materials within the system of consideration are homogenous and linear the point form of Maxwell's equations are given below [80]:

$$\nabla \times \bar{H} = \bar{J} + \frac{\partial \bar{D}}{\partial t} \qquad (3.1)$$

$$\nabla \times \bar{E} = -\frac{\partial \bar{B}}{\partial t} \qquad (3.2)$$

$$\nabla \cdot \bar{D} = \rho \qquad (3.3)$$

$$\nabla \cdot \bar{B} = 0 \qquad (3.4)$$

where $\bar{H}$ and $\bar{B}$ represent the magnetic field intensity and magnetic flux density respectively; $\bar{E}$ denotes the electric field intensity; $\bar{J}$ and $\bar{D}$ are the current density and displacement current density respectively; while ρ and t stands for electric charge density and time respectively.

If we take the divergence of equation (3.1) and use Gauss law of equation (3.3) in (3.1) we obtain the relation below

$$\nabla \cdot \bar{J} = -\frac{\partial \rho}{\partial t} \qquad (3.5)$$

Equation (3.5) above is the conservation of charge. This implies that the current through an enclosed surface is equal to the time rate of charge within the surface.

For a macroscopic investigation of the electromagnetic phenomena in a closed system, the Maxwell's equations are solved with the appropriate boundary conditions and constitutive relationships representing the properties of the material as mathematically expressed below:

$$\bar{D} = \varepsilon_0 \bar{E} + \bar{P} \qquad (3.6)$$

$$\bar{B} = \mu_0 (\bar{H} + \bar{M}) \qquad (3.7)$$

$$\mathrm{J} = \sigma \bar{E} \qquad (3.8)$$

Where $\bar{P}$ stands for electric polarisation vector; $\bar{M}$ the magnetisation vector; ε_0 and μ_0 denote permittivity and permeability of free space respectively; and σ denotes electrical conductivity.

For most electromagnetic NDE problems, the displacement current density $\bar{D}$ vanishes since the wavelength of the EM wave is much larger than the dimensions of the structure under investigation when frequencies of less than 10 MHz are employed, hence equations (3.1) and (3.5) simplifies to [80, 105] :

$$\nabla \times \bar{H} = \bar{J} \qquad (3.9)$$

$$\nabla \cdot \bar{J} = 0 \qquad (3.10)$$

3.1.1. Eddy Currents and Magnetic Diffusion

In a time-varying electromagnetic field, wave propagation is a distinctive feature in free space and/or dielectric media, however, in an electrically conductive material, time-dependent magnetic fields exhibit a diffusive characteristic. Moon [106] has shown that using the quasi-static form of equation (3.1) and the constitutive equations for $\bar{B}$ and $\bar{J}$ assuming a linear isotropic ferromagnetic material one can obtain the general equation for a moving conductive material as

$$\frac{1}{\mu\sigma}\nabla^2\bar{B} + \nabla \times (\bar{v} \times \bar{B}) = \frac{\partial \bar{B}}{\partial t} \qquad (3.11)$$

If we consider a case where the material is stationary with respect to the observer and the field is one dimensional, that is, the magnetic quantity $\boldsymbol{B} =(0, B(x, t),0)$ then equation (3.11) reduces to

$$\frac{1}{\mu\sigma}\frac{\partial^2 \overline{B}}{\partial x^2} = \frac{\partial \overline{B}}{\partial t} \tag{3.12}$$

Equation (3.12) is the classic diffusion equation, which is analogous to that found in heat energy transfer into a solid. Being a second order homogenous equation, the general solution to this is

$$\overline{B} = C_1 e^{(1+j)x/\delta} + C_2 e^{-(1+j)x/\delta} \tag{3.13}$$

Where $\delta^2 = 2/\omega\mu\sigma$. From a physical point of view therefore, the first term C_1 must be zero. Otherwise this term would go to infinity as x approaches infinity. If the magnetic flux density at the surface is defined as $\overline{B}(0) = \overline{B}_0$, then equation (3.13) expresses the field inside the material as:

$$\overline{B} = \overline{B}_0 e^{-x/\delta} e^{-jx/\delta} \tag{3.14}$$

Thus, the first term shows that the magnitude of the magnetic flux density decreases exponentially to a value $\overline{B}_0/e$ in a characteristic distance δ called the skin depth; whilst the second exponential term has a magnitude of one and describes the phase shift of the magnetic flux density. At a depth $x= \delta$, the flux density lags the surface flux density by one radian. The skin depth which is dependent on the electromagnetic properties of the material (σ and μ) and the frequency is an important parameter in eddy current analysis. Similarly, the current density can be obtained from the flux density. From Ampere's law, [107] has shown that the current density can be expressed as in equation (3.15), where J_o is the surface current density.

$$J = J_0 e^{-(1+j)x/\delta} \tag{3.15}$$

3.1.2. Pulsed Eddy Current and Diffusion

If we consider a semi-infinite material of conductivity, σ_2, and permeability, μ_2 occupying the half-space $x \geq 0$ as shown in figure 3.1 below. And the applied field is parallel to the conducting surface of incidence, it follows therefore that the current density $\overline{J}$ has a z

component as illustrated in figure 3.1b; hence, we can rewrite equation 3.12 in the scalar form as

$$\frac{1}{\mu\sigma}\frac{\partial^2 By}{\partial x^2} = \frac{\partial By}{\partial t}$$

$$\frac{1}{\mu\sigma}\frac{\partial^2 Jz}{\partial x^2} = \frac{\partial Jz}{\partial t}$$

(3.16)

(a)   (b)
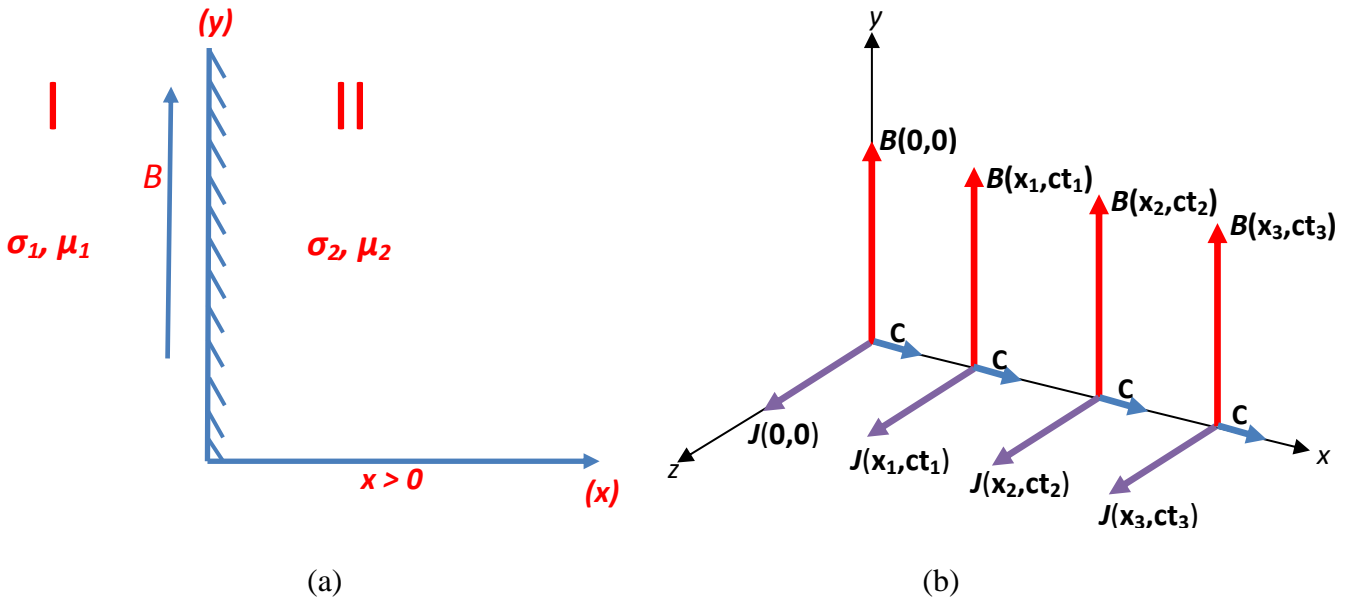
Figure 3.1: (a) Semi-infinite Material occupying the half-space x>0 (b) Direction of the J component and the variation of both B and J in the x-direction

For pulsed or transient fields however, the solution of equation (3.16) if $B_0(t)$ is known at $x = 0$ according to [106] is

$$B(x,t) = \frac{2}{\sqrt{\pi}} \int_{\eta}^{\infty} B_0(t - \frac{\mu\sigma x^2}{\lambda^2})e^{-\lambda^2}\,d\lambda \,,$$

(3.17)

where $\eta = x/2(\mu\sigma/t)^{1/2}$. It follows that if $B_0(t)$ is step increase from zero to $B_0(t=0)$, then

$$B = B_0 erfc(\eta) \,,$$

(3.18)

where *erfc* is the complementary error function. From equation (3.18) above one can give an approximate interpretation of the magnetic diffusion in the material by making use of the series expansion

$$erfc(\eta) = 1 - \frac{2}{\pi^{1/2}} \exp(-\eta^2)\left(\eta + \frac{2\eta^3}{1.3} + \frac{4\eta^5}{1.3.5} + ... \right), \qquad (3.19)$$

which is uniformly and absolutely convergent everywhere. We can limit the second member of the above series expansion to the first two terms for small values of η, therefore,

$$erfc\left[\frac{x}{2}\left(\frac{\mu\sigma}{t} \right)^{\frac{1}{2}} \right] \approx 1 - \frac{2}{\pi^{\frac{1}{2}}}\left[\frac{x}{2}\left(\frac{\mu\sigma}{t} \right)^{\frac{1}{2}} \right] \exp\left[-\frac{x^2}{4}\left(\frac{\mu\sigma}{t} \right) \right] \qquad (3.20)$$

Substituting (3.20) into equation (3.18) the magnetic field diffusion into the material can be expressed as equation (3.21) and illustrated in figure 3.2 below

$$B = B_0\left[1 - x\left(\frac{\mu\sigma}{\pi t} \right)^{\frac{1}{2}} e^{-\frac{\mu\sigma x^2}{4t}} \right] \qquad (3.21)$$

Finding the partial derivative of the magnetic flux density with respect to x then the induced current may be expressed as

$$\mu_0 J = \frac{\partial B}{\partial x} \approx -B_0\left(\frac{\mu\sigma}{\pi t} \right)^{\frac{1}{2}} e^{-\frac{\mu\sigma x^2}{4t}} \qquad (3.22)$$

In the above transient consideration one can define a time dependent depth of penetration as

$$\delta_p = \left(\frac{2t}{\mu\sigma} \right)^{1/2} \qquad (3.23)$$

From equation (3.23) one can deduce that the penetration depth grows in time to a peak value. In a practical sense, for a conducting material of finite thickness D, one can estimate diffusion time (t_0) of the magnetic field through the material after an abrupt change in the field as $t_0 = \frac{1}{2}\mu\sigma D^2$.
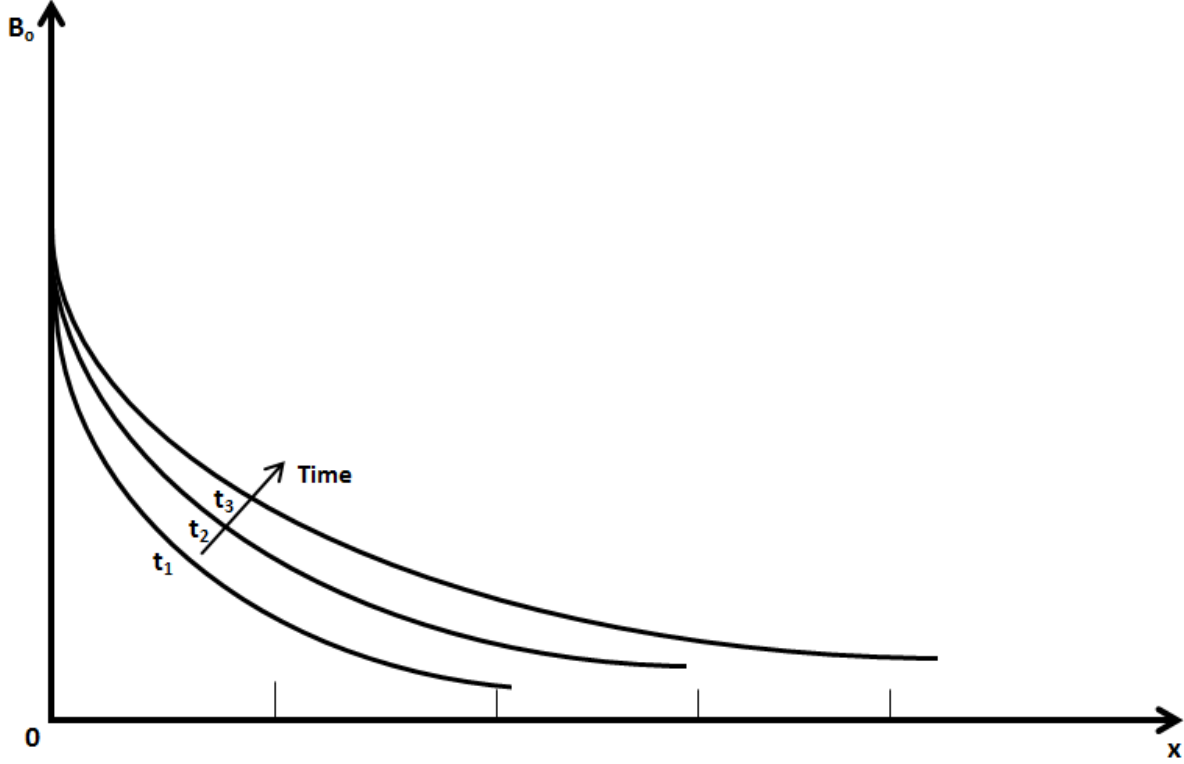
Figure 3.2: Magnetic Field Diffusion in a Conductive Material - inspired by [106]

Similarly, to investigate the diffusion of pulsed eddy currents and estimate its corresponding depth of penetration, Vallese in [108] gave a generalised current density distribution expression in complex form using the scenario described in figure 3.1 as

$$J(x,s) = s^{\frac{(n-1)}{2}} e^{\left[-\frac{x(s)^{1/2}}{\kappa}\right]} \frac{I(s)}{\kappa} s^{\frac{(2-n)}{2}}, \qquad (3.24)$$

where $\kappa = \dfrac{1}{(\mu\sigma)^{\frac{1}{2}}}$.

If one considers particular cases of using a square wave excitation and an exponentially damped square wave where the associated currents are of the form $i(t) = I_0[U(t) - U(t - T_0)]$ and $i(t) = I_0 e^{-\alpha t}[U(t) - U(t - T_0)]$, then the current distribution is expressed in equations (3.25) and (3.26) respectively [108] as

$$J(x,t) \approx \frac{I_0}{k(\pi t)^{\frac{1}{2}}} e^{-\left(\frac{x^2}{4k^2 t}\right)}, \qquad (3.25)$$

$$J(x,t) \approx \frac{I_0}{k(\pi t)^{\frac{1}{2}}} (1 - 2\alpha t) e^{-\left(\frac{x^2}{4k^2 t}\right)}. \qquad (3.26)$$

And the equivalent penetration depth for the first case of pulsed excitation at $t=T_o$ may be defined as

$$x = k(2T_0)^{\frac{1}{2}} \qquad (3.27)$$

Where T_0 satisfies the partial derivative of equation (3.25) equated to zero $\{$i.e. $\partial J(x,t)/\partial t = 0\}$. At time $t= T_0$ a peak value of $J(x, t)$ is reached at the depth described by equation (3.27). However, for $t>T_0$ the peak value of $J(x, t)$ falls rapidly past the depth x defined in equation (3.27). For the second case of pulsed excitation (exponentially damped), equating the partial derivative of equation (3.26) to zero and for simplicity $u=x/2k$, one can write

$$t - 2u^2 = -2\alpha t^2 - 4\alpha u^2 t \qquad (3.28)$$

At $t=T_o$ (3.28), we solve for u^2 and insert the definition of u^2 to find the equivalent penetration depth expressed as

$$x = k(2T_0)^{\frac{1}{2}} \left(\frac{1+2\alpha T_0}{1-2\alpha T_0} \right)^{\frac{1}{2}} \qquad (3.29)$$

And one can approximate this for small values of α to be

$$x = k(2T_0)^{\frac{1}{2}} (1 + 2\alpha T_0) \qquad (3.30)$$

3.1.3. Multiple Influences on PEC Response

Pulsed eddy current response is affected by a number of parameters which may be classified into two broad categories; those related to the material under test and those related to the PEC probe. Parameters that fall within the first category include the magnetic permeability, electrical conductivity and defect (e.g. crack) whilst those attributed to the latter category include the probe lift-off, frequency, and coil geometry amongst others. These multiple parameters of influence can be functionally depicted in a typical PEC signal as

$$P = f(\sigma, \mu, \ell, v, \xi, \theta) \qquad (3.31)$$

where, σ and μ is the electrical conductivity and magnetic permeability of the test material, ℓ represents the probe lift-off, v and θ represent the frequency and type of excitation and ξ symbolise the probe geometry. The simultaneous variation of two or more of these parameters

makes the PEC response quite complicated to interpret. For instance, in an anisotropic material where there is macroscopic variation of conductivity and permeability, which may lead to inaccurate interpretation, there is a need for multiple parameter delineation in order to mitigate the individual effects of these parameters in PEC response. Traditionally, to alleviate the effect of permeability variation in PEC response, the test material is driven to magnetic saturation [49, 60] which brings about a fairly constant magnetic permeability.

3.1.4. Effect of Defect on PEC response

The presence of defects (e.g. crack, discontinuities) has a significant effect on the output PEC signal. The shape of the magnetic field pulse contains information that characterises the defect being tested. From the magnetic diffusion phenomenon associated with pulsed eddy current, it takes a finite time for the field to propagate to a defect and then back, as such, shallow defects would exhibit shorter arrival time back to the surface. And the deeper defects would exhibit longer arrival time. Consequent upon this, the influence of deeper defects affects the transient response later in time while that of shallow defects is apparent at earlier time in the transient response [109-113].

3.1.5. Lift-off Effect and Lift-off point of Intersection (LOI)

The varying probe-specimen distance called lift-off as identified in literature may mask defect information, hence, in such instances, it becomes an undesirable parameter in pulsed eddy current measurement. To understand this effect, a transformer equivalent circuit model of the eddy current system depicted in figure 3.3 is examined.
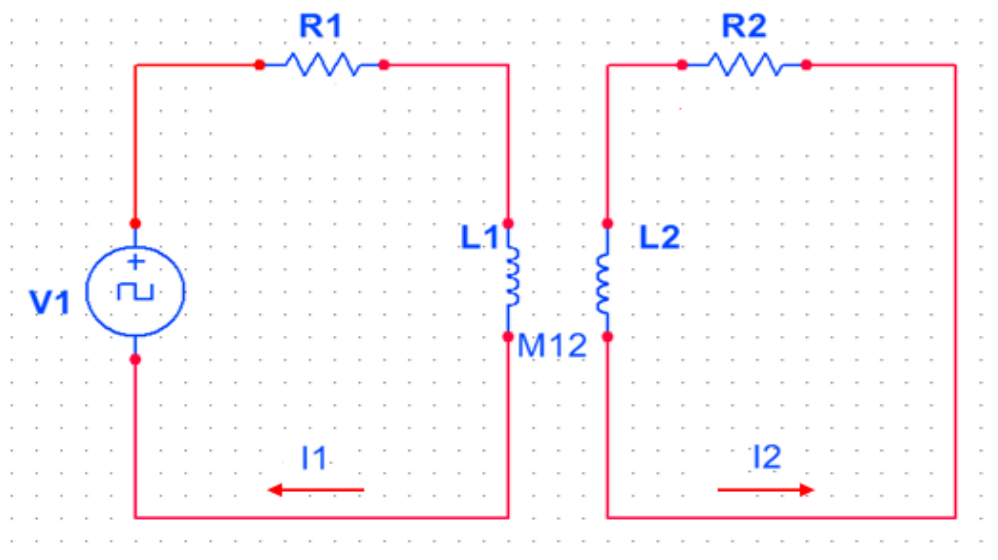
Figure 3.3: Transformer Equivalent Circuit of Pulsed Eddy Current

From the equivalent circuit of figure 3.3, R_1 and L_1 symbolise the resistance and inductance of the probe's coil, while R_2 and L_2 are the equivalent resistance and inductance of the sample under test. I_1 is time varying current flowing in the exciter coil and I_2 is the induced eddy current in the sample. M_{12} defines the mutual inductance which is the coupling factor between the induced eddy current in the sample and the change in coil's current which produced it. This is deduced from the fact that the generated emf, E_2, in the sample may be expressed as $(E_2 = -M_{12} \, \Delta I_1 / \Delta t)$ Faraday's law. The mutual inductance is very important (in NDT) as it varies with the lift-off [72]. M_{12} increases with decreasing lift-off and vice-versa. However, it has been observed that there is an instant in time (lift-off point of intersection) when the instantaneous value of the induced current I_2 is independent of M_{12} [96-98, 114]. An attempt has been made to theoretically define [97] this unique instant in time (t_{LOI}) when the LOI occurs.

If a pulsed excitation signal $f(t)$ with amplitude Vo is considered as a unique combination of a number of sinusoids, containing the fundamental frequency, ω_o, and its harmonics such that every frequency is an integral multiple of ω_o. Then one can synthesize or reconstruct the pulsed excitation signal $f(t)$ according to equation (3.32) [97, 115]

$$f(t) = \frac{4V_o}{\pi} \sum_{n=1,3,5...}^{\infty} \frac{1}{n} \sin n\omega_o t$$

(3.32)

By extension therefore, since the pulsed eddy current technique obeys the diffusion phenomenon of equation (3.16) its solution can be superimposed. Hence, one can safely assume that the output response can also be reconstructed from the output harmonics, which has been verified in [97] by the superposition of multiple single frequency sinusoidal signals shown graphically in figure 3.4.
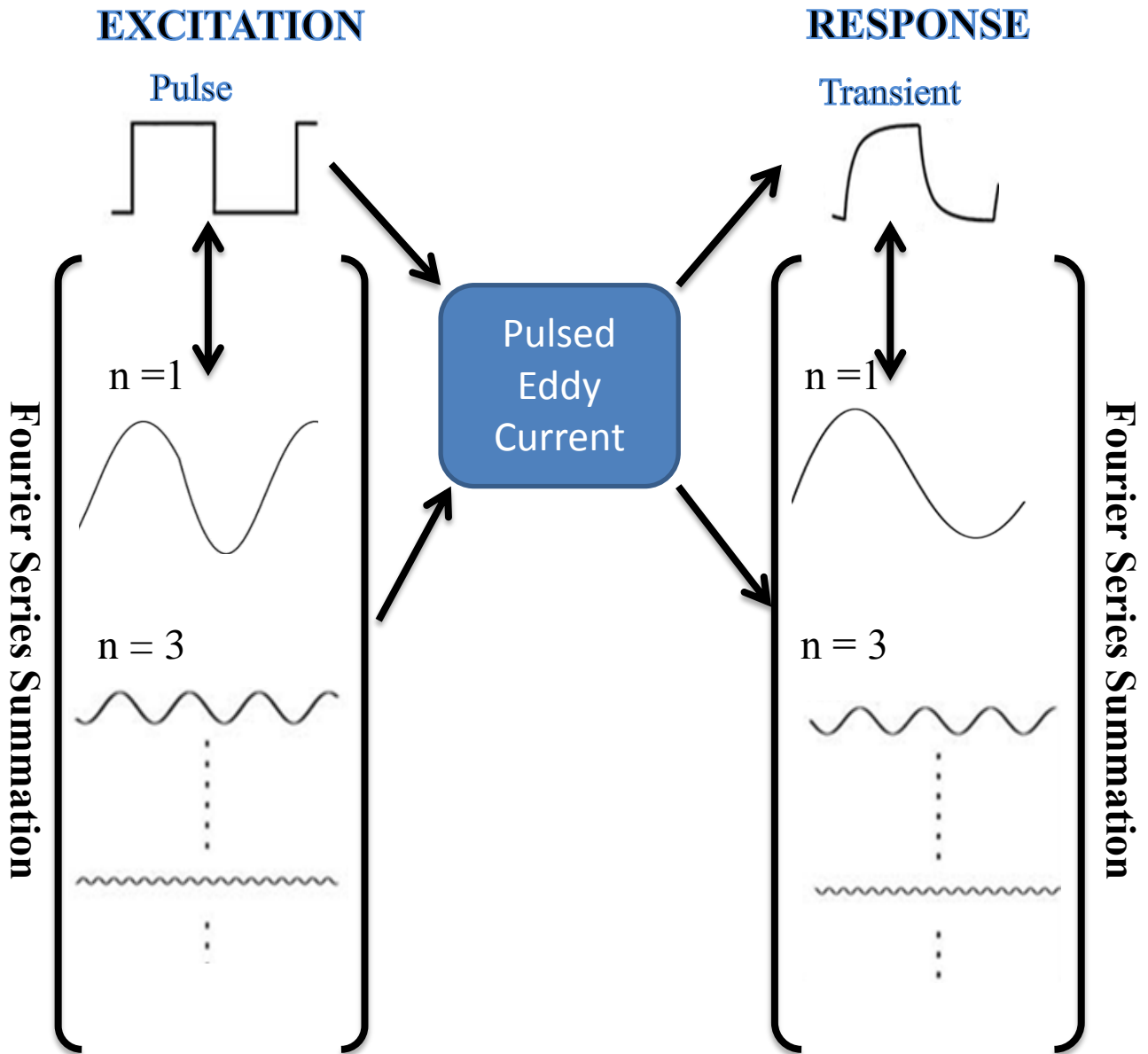
Figure 3.4: Schematic of the excitation and output response of a PEC system and its frequency components - inspired by [97]

In this illustration, the input pulsed excitation is represented as a synthesis of multiple single frequency sinusoids on the left-hand side of the PEC system whilst the transient response depicts the reconstruction of the multi-single frequency sinusoids. An amplitude and phase change occurs when the excitation sinusoids passes through the eddy current system but their frequency remains constant, thereby the synthesis/reconstruction of the transient response is possible in line with equation (3.32). Due to the fact that the combined variation in the amplitude and phase with lift-off leads to the occurrence of the LOI point; the time of occurrence of this invariant feature t_{LOI} can be defined as the point where $g_1(t) = g_2(t)$ is satisfied. Where $g_1(t)$ and $g_2(t)$ are any two sinusoidal output responses at different lift-off

values. It follows therefore that if the amplitudes and phase shifts of the defined output functions are V_1, V_2, and θ_1, θ_2 then one can write

$$V_1 \sin(n\omega t_{LOI} - \theta_1) = V_2 \sin(n\omega t_{LOI} - \theta_2) \tag{3.33}$$

Thus, the solution of equation (3.32) above gives a theoretical definition of the t_{LOI}

$$t_{LOI} = \frac{1}{n\omega} \tan^{-1}\left[\frac{V_1 \sin\theta_1 - V_2 \sin\theta_2}{V_1 \cos\theta_1 - V_2 \cos\theta_2}\right] \tag{3.34}$$

3.2. Numerical Simulation Model for PEC

Simulation and/or modelling in general are of immense importance in engineering. Amongst other things; it helps to show the relationship between design and performance parameters, it has become a veritable tool to mirror systems as it attempts to emulate real scenarios, and it is a powerful means for evaluating options by assessing varied scenarios, it helps identify problem areas and provides a cost effective way of applying and testing design modifications [116, 117].

Numerical methods like finite element method (FEM) in particular are useful in solving boundary-value problems by sub-dividing an entire continuous domain into a number of sub-domains, where the unknown function is represented by interpolation functions with unknown coefficients [118] . That is, the solution of the entire system is approximated by a finite number of unknown coefficients. In general therefore, FEM analyses of boundary-value problems include these essential steps: subdivision of the domain, selection of the interpolation functions, formulation of the system of equations and finally the solution of the system of equations [107, 118].

There are a number of commercially available FEM simulation software packages some of which include COMSOL, Magnet by Infolytica etc. For COMSOL Multiphysics [119] used in this research work, the magnetic vector potential, A, formulation which is a derivative of Maxwell's equations and relevant constitutive relations is used in its domain equations to solve eddy current problems. The magnetic vector potential is based on the conservation of flux defined in equation (3.4) and obeys the mathematical relation expressed below for harmonic fields as derived in [119]:

$$\sigma j\omega \bar{A} + \nabla \times (\mu^{-1}\nabla \times \bar{A}) - \sigma \bar{v} \times (\nabla \times \bar{A}) = \bar{J}_s \qquad (3.34)$$

where, $\sigma j\omega \bar{A} = \bar{J}_e$ is the eddy current density; $\bar{J}_s$ represents the source current density; μ is the material permeability, $\bar{v}$ is the media velocity and $\bar{A}$ is the magnetic vector potential.

To mathematically define the vector potential, A, we consider the Maxwell-Gauss law. Since the divergence of B is zero everywhere, then it is possible to express the flux density as the curl of some vector. Thus, from equation (3.4) we can write

$$\bar{B} = \nabla \times \bar{A} \qquad (3.35)$$

If we define the divergence of A as zero ($\nabla \cdot \bar{A} = 0$: Coulomb's gauge), then using equation (3.35) in Maxwell-Ampere's law (3.1) along with the Coulomb's gauge, the following relation results for a linear ferromagnetic material:

$$\nabla^2 \bar{A} = -\mu \bar{J} \qquad (3.36)$$

Equation (3.36) presents a relation in the form of Poisson's equation whose solution as derived in [120] is

$$\bar{A} = \frac{\mu}{4\pi} \int_v \frac{\bar{J}}{r} dv \qquad (3.37)$$

According to equation (3.37) therefore, the magnetic vector potential, A, at a point as a result of a current distribution may be defined as the ratio $\frac{\bar{J}}{r}$ integrated over the volume occupied by the current distribution, where $\bar{J}$ is the current density at each elemental volume dv and r is the distance from each elemental volume to the point where A is being measured.

This formulation has been used as a forward model to understand and delineate the effects of varying magnetic permeability and electrical conductivity in PEC response signals, which is presented in chapter 4. An analytical model is also a plausible approach with the advantage of providing exact or closed form solutions to eddy current NDE problems. However, this approach is limited to canonical problems which hinder its extension to more complex geometries.

3.3. Experimental System and Sample Description

The overall experimental system for this research is shown in figure 3.5. The PEC probe consists of an excitation coil with a ferrite core and a Hall sensor as the pickup sensor. The PEC acquisition scheme uses the QinetiQ TRESCAN® system. A unit period of a digital excitation waveform is created in Matlab, which is then converted to an analogue voltage signal by the analogue output subsystem of the NI PCI-6255 DAQ board. This voltage signal is converted into an excitation current by the signal-conditioning TRESCAN box. This operates in current mode with an exponentially damped rectangular wave that has a 50% duty cycle, time constant 100μs, and repetitive frequency of 200Hz. The excitation is fed into the probe's excitation coil and a Hall sensor measures the PEC response, which is low-pass filtered (10-kHz cut-off) and amplified by TRESCAN. This is then digitized by the DAQ board and the acquired digital waveform is post-processed in Matlab [5].

This is low-pass filtered at 10 kHz cut-off because although the Hall sensor used produces an output voltage proportional to the magnetic field perpendicular to the device averaged over the area of the sensor for frequency range DC to 100 kHz. Nevertheless, the operational amplifier of the QinetiQ signal conditioner limits the frequency range produced in the first place because it has a low bandwidth. Precisely, the TL072ACP op-amp embedded in the system has a gain bandwidth product of 3MHz and voltage gain of 100 producing a bandwidth of 30 kHz. Hence, the response from DC to 10 kHz is deemed suitable for this investigation as the higher frequency components do not penetrate deep into the material according to the skin depth phenomenon $(\delta^2 = 2/\omega\mu\sigma)$. For instance, if we consider two frequencies; 200 Hz and 10 kHz, the penetration depths (δ) of the eddy current in an aluminium test sample could be estimated. The typical values of δ obtained are 5.99mm at 200Hz and 0.85mm at 10 kHz which substantiate the fact that lower frequency components penetrates deeper into the material under test whilst higher frequency components have lower penetration depths.

The Hall sensor's response to a wide range of frequencies allows the capture of detailed transient data sets. Most commonly used coil sensors respond to the rate of change of the magnetic field and therefore has a frequency-dependent response that reduces to zero at DC. The good response at low frequencies is the main reason for adopting the Hall-effect sensor as it is the low frequencies that penetrate deep into specimen. In addition, Hall sensors used as a field detector rather than coils improve the spatial resolution and the detectability of deep defects [121].
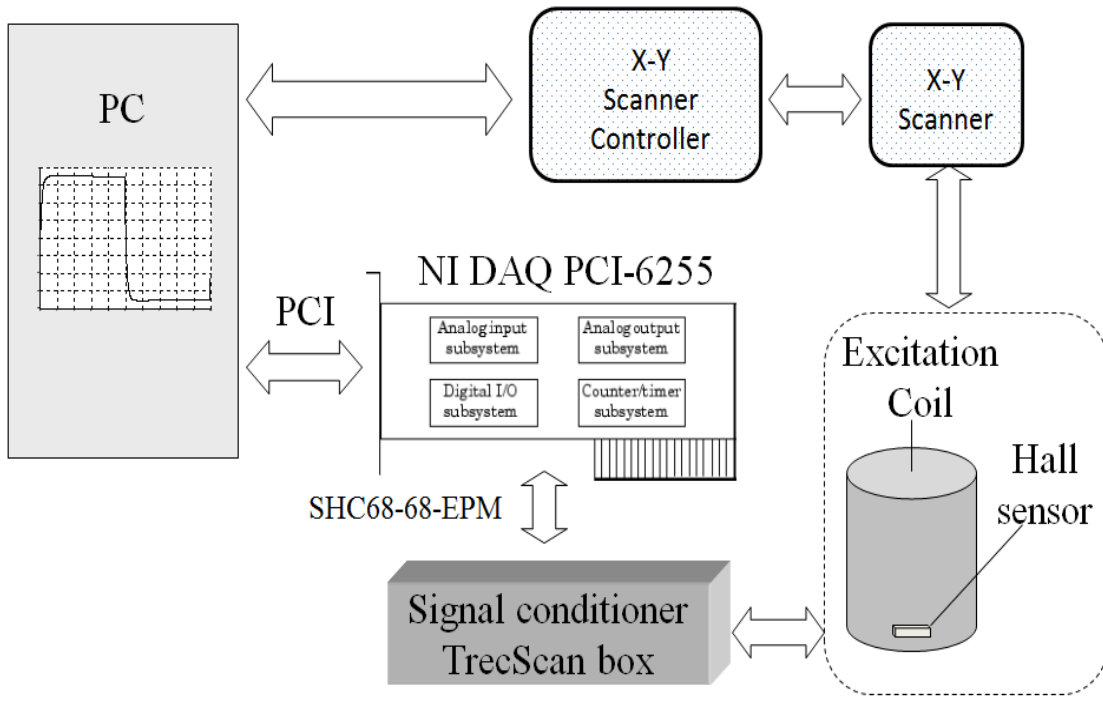
(a)
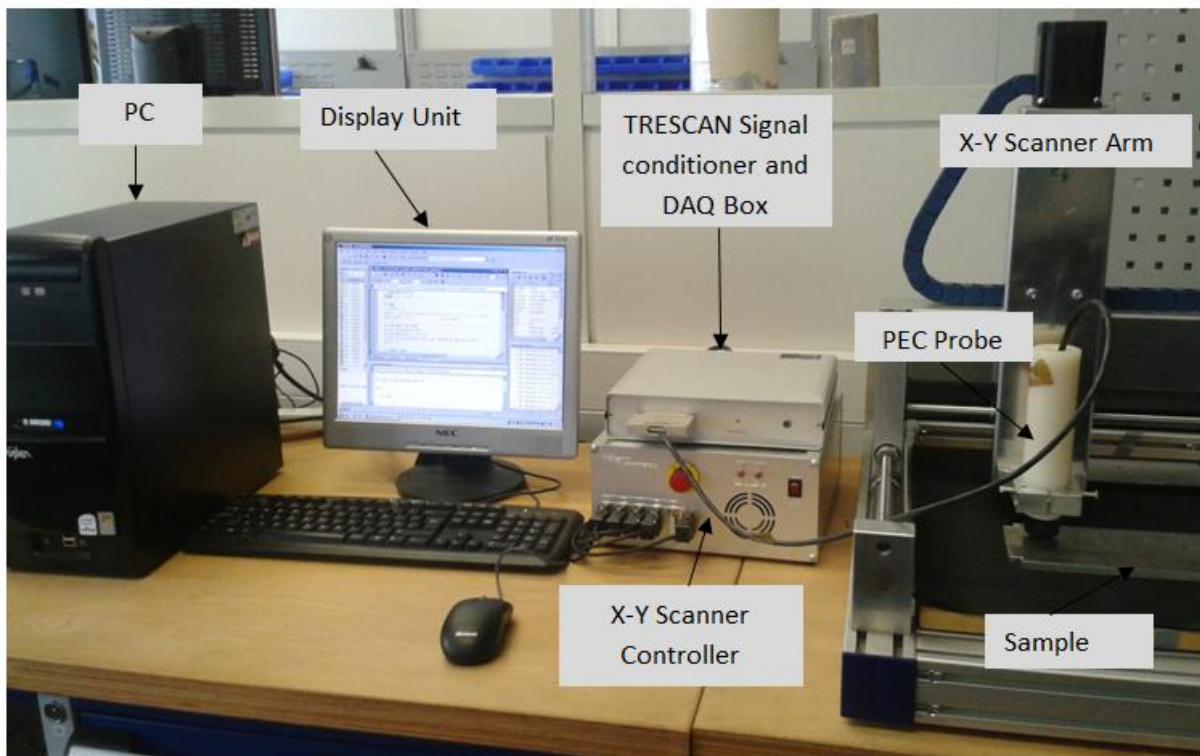
(b)

Figure 3.5: Schematic and Photograph of the PEC System

For accuracy of result, the experimental system employs an X-Y scanner (CNC High-Z S-720) to control the PEC probe over the areas of interest of test samples. The scanner comprises of four ST5918 series stepping motors; one for the y and z axes respectively and two for the x-axis. The movement of which are controlled by a written Matlab algorithm. The Matlab algorithm also provides the excitation current for the probe via the QinetiQ Trecscan signal conditioner and stores the Hall sensor received signals, which are post-processed for parameter information of interest.

For the proposed multiple parameter separation and estimation from PEC response signals for different types of defects and materials; five samples were prepared for investigation. Table 3.1 provides a summary of sample information. Detailed information is given in the individual chapters where they are reported.

Table 3.1 Sample and Defect Description

Sample	Sample Dimension (mm)	Defect Information	Photograph
Machined Slot (Steel)	210x76x12	Defect depth of 1-4mm with constant width	
Machined Slot (Aluminium)	218x97x12	Defect depth of 1-4mm with constant width	
Surface Breaking Crack (Steel)	253x50x10	Defect depth of 6-7mm with constant width	
Surface Breaking Crack (Aluminium)	253x50x10	Defect depth of 7 & 9mm with constant width	

Sample	Sample Dimension (mm)	Defect Information	Photograph
Natural Crack: SCC (Steel)	Cross-section of Steel pipe with internal diameter of 211mm and wall thickness of 5mm	Irregular and complex shaped defect	

3.4. Research Methodology

This research work involves both numerical and experimental investigation of the pulsed eddy current technique for multiple parameter delineation and estimation; a proposed method flow diagram of this is illustrated in figure 3.6 giving an outline of the work.

Foremost, a PEC numerical model is designed and developed to separate the influence of material electromagnetic properties from PEC responses which is experimentally verified. Post-processing algorithm developed to extract useful information. Thereafter a lift-off independent defect detection and characterisation PEC system was developed to mitigate coupling variation. The separation and multiple parameter estimation from PEC responses were explored and demonstrated. Finally case studies of ferromagnetic and non-ferromagnetic samples were carried out for different defects and lift-off values. A synopsis of this is given in subsequent sub-sections and detailed in the succeeding chapters.
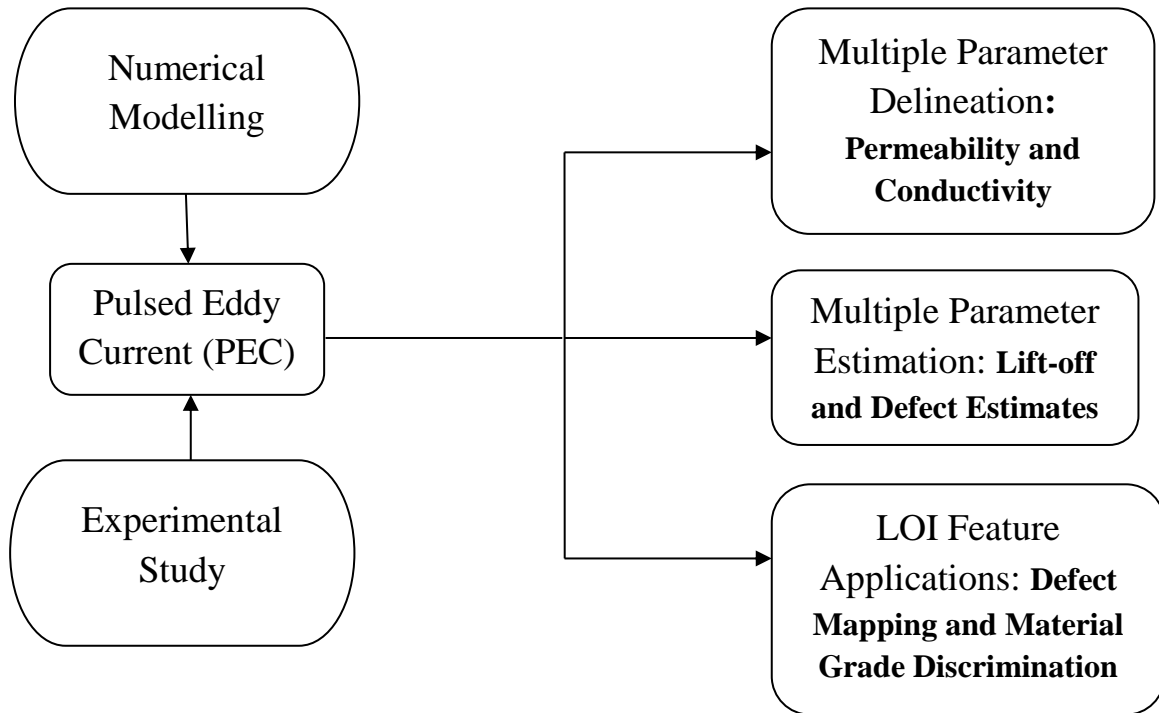
Figure 3.6: Research Flow Diagram

3.4.1. Study 1: Numerical model for material parameter separation

Pulsed eddy current diffusion in a material is a 3-dimensional problem since the induced currents propagates through the material volume, as such; a 3-D pulsed eddy current numerical model was developed to simulate and investigate the influence of material electromagnetic properties (magnetic permeability and electrical conductivity) in PEC measurement with a view to separate the influence of these parameters. First, a simultaneous variation of the conductivity and permeability values at a controlled lift-off is simulated to have a PEC signature for this scenario and then the magnetic permeability and lift-off values are controlled and conductivity varied. Thirdly, the magnetic permeability is varied and the electrical conductivity and the lift-off are controlled to get a specific PEC signature for this scenario as well. With these three distinct signatures the area of influence of these material parameters on the PEC response signal is delineated using both time and frequency domain analyses viz-a-viz transient response, differential normalised transient response, magnitude spectrum and normalised magnitude spectrum.

3.4.2. Study 2: Experiment for material parameter separation

Here, an experimental validation of the proposed PEC numerical model is carried out using carefully designed samples from National Physical Laboratory (NPL). The samples are reference standards with known conductivity and permeability values; details of their values are given in chapter 4. It should be noted that these reference standard samples were selected because they exhibited the conductivity and permeability properties of the modelled samples to facilitate a direct correlation. The results from this experimental study using the same analytic tools are correlated for proof of concept and to validate the numerical model set-up in study 1.

3.4.3. Study 3: Defect detection and characterisation independent of lift-off

This experimental study exploited the use of the lift-off point of intersection feature to estimate and characterise defect invariant of lift-off. Furthermore, it made use of signal processing algorithm to separate the lift-off effect from defect in the PEC system developed. Two carefully designed case studies of both ferromagnetic and non-ferromagnetic material samples with surface slot defects (depicting metal loss) of similar dimensions were examined to compare the LOI behaviour in these two materials.

The main assessment criteria involved in this study are:

- Defect detection and differentiation; experiments are carried out to demonstrate the ability of the developed PEC system to distinguish between different defects independent of the lift-off effect. The LOI features were used to estimate varying defect depths through calibration
- Lift-off and Defect Separation; the lift-off and defect features in the PEC response are separated with the aid of appropriate signal processing techniques for two material samples (ferromagnetic and non-ferromagnetic). The study is aimed at obtaining two unique derivatives from the PEC response signal which are measures of these two parameters (lift-off and defect) from which estimates of each can be derived.

3.4.4. Study 4: Development of defect depth estimation

This study made use of the slope of the curve of the normalised differential PEC signal versus lift-off for defect depth estimation using the same set of material samples as in study 3. Two sets of equations, one each for the ferrous and non-ferrous material sample, were developed which made defect depth estimation feasible without the influence of the lift-off effect.

3.4.5. Study 5: Application: Defect Mapping and Material Grade Discrimination with the LOI feature

Here, the scanned pulsed eddy current images with and without the LOI time feature are examined for comparison to demonstrate that scanned images obtained with the LOI feature are more sensitive to defect than their counterparts. In addition, the potentials of material grade discrimination with the LOI featured are explored.

3.5. Chapter Summary

This chapter has provided a theoretical background to pulsed eddy current and electromagnetic NDE. In particular, the (pulsed) eddy current and magnetic diffusion behaviour in the presence of conductive substrate and their associated effects have been presented and discussed. Also, the lift-off effect and the importance of lift-off invariant point phenomenon have been elicited. The research methodology is equally underscored in the subsections of this chapter.

Subsequent chapters of this thesis will report the numerical and experimental studies carried out and the mitigating ideas advanced to overcome the identified issues with the PEC technique. The analysis of the results obtained and critical discussion are presented.

Chapter 4: Decoupling Permeability and Conductivity Effects in Pulsed Eddy Current Measurements

Following on from the theoretical background to pulsed eddy current and the research methodology in chapter 3, this chapter and its sub-sections presents both a numerical simulation and an experimental validation of the model to delineate the electromagnetic properties of the test material in PEC measurements and systems. As identified in literature PEC sensing technique are susceptible to measurement errors due to the intrinsic inhomogeneity of the test material. The main thrust of this chapter is to investigate therefore the contributions of the electromagnetic properties (permeability and conductivity) of the sample to the PEC signal response with a view to separate the influence of these two properties. Both time domain and frequency domain analyses are carried out in this investigation viz-a-viz: transient response, differential normalized response, magnitude spectrum and normalized magnitude spectrum.

4.1. Multiple Influence and Transient Response

Pulsed eddy current sensing work on electromagnetic induction principles consisting mainly of an excitation coil and a sensing coil or a magnetic field sensor. When a time varying current in the excitation coil creates an alternating magnetic field commonly called the primary magnetic field in literature, eddy currents are induced in the conductive sample. The eddy currents simultaneously generate a secondary magnetic field, which resists the variation of primary magnetic field, the net field is measured and analysed to evaluate the integrity of various target samples [122]. There are a number of factors that affects the interaction between the primary magnetic field and the secondary magnetic field amongst which are probe-sample gap called lift-off (l), excitation frequency (f), the electromagnetic properties of the sample(σ and μ) and probe geometry(ξ) [49]. The relationship between these factors that influences PEC responses have been expressed mathematically in [101]; consider a PEC system with a target of dimensions a × b and thickness δ, then the absolute value of the complex magnetic flux amplitude, Φ ,of the magnetic flux density, B, is given as

$$\Phi = \Phi_O \frac{\sqrt{2}}{k\delta} \sqrt{\frac{\cosh(k\delta) - \cos(k\delta)}{\cosh(k\delta) + \cos(k\delta)}} \qquad (4.1)$$

Where Φ_o is the initial flux amplitude and

$$k = \sqrt{\frac{\omega\sigma\mu}{2}}$$ (4.2)

.

Equations (4.1) and (4.2) above describe the response of a simplified PEC model, showing that Φ is not just a function of geometry but also of the EM properties of the test sample in addition to the angular frequency, ω, which is defined as $2\pi f$.

Figure 4.1 shows a typical PEC response where time is normalized to the repetitive period T of the excitation. In Figure 4.1(a) BREF is the reference signal obtained in air or defect-free sample [82] whilst B is the transient response of the detected area. However, in order to increase the signal resolution, the balance or differential signal (ΔB) is quantified [9, 123] as illustrated in (4.3).

$$\Delta B = B - B_{REF}$$ (4.3)
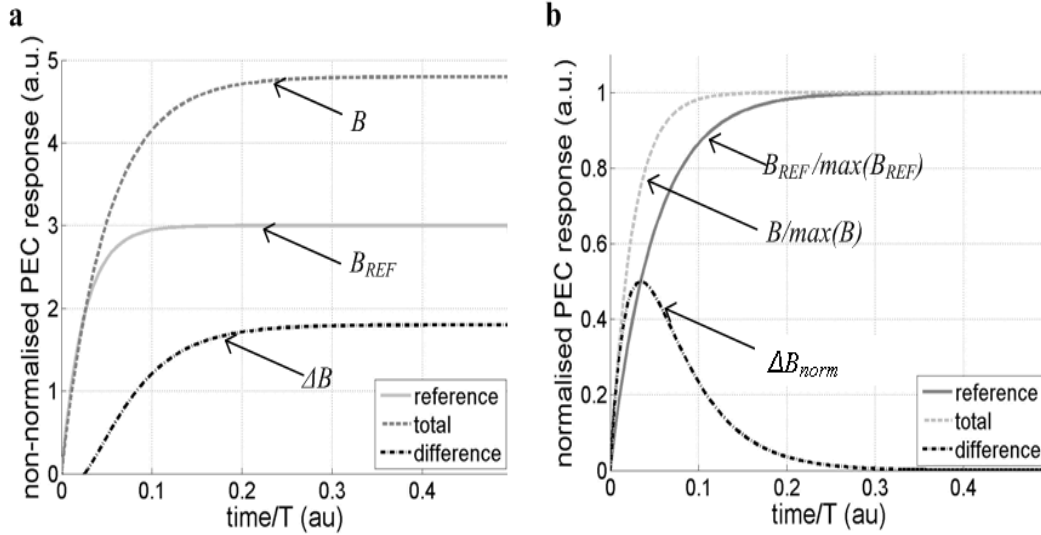
Figure 4.1: PEC Transient Response

In PEC analysis illustrated in Figure 4.1b, it is common to use differential normalized response [89] to characterise test materials which (4.4) describes below.

$$\Delta Bnorm = B/\max(B) - B_{REF}/\max(B_{REF})$$

(4.4)

Where B/max(B) is the normalised response and B_{REF}/max(B_{REF}) is the normalised reference signal. In this work however, the spectral behaviour of $\Delta Bnorm$ shall be investigated in order to decouple the influence of conductivity and permeability in PEC responses. The transient response of an anisotropic material is obtained using (4.3) and (4.4) and thereafter the magnitude spectrum of the transient response is investigated by taking the Fast Fourier Transform (FFT) of (4.4) as expressed in (4.5).

$$mag(\Delta Bnorm) = amp\left[F\left\{ \frac{B}{\max(B)} - \frac{B_{REF}}{\max(B_{REF})} \right\} \right]$$

(4.5)

4.1.1. Sources of Uncertainty in PEC Measurements

Ferrous materials often exhibit inhomogeneity which leads to an undesirable mal-distribution of material properties causing uncertainty in measurement. This could be as a result of mechanical and heat treatment during fabrication [103] and sometimes due to the metallurgical properties of the material itself [101]. Heat treatment or annealing alters the microstructure of a material causing material property changes. When a ferrous material is heated below its curie temperature but to a high enough temperature; which allows substantial short-range atomic mobility, the magnetic domain structures changes leading to structural inhomogeneity [124]. Also, mechanical treatment like rolling effect can cause a reorientation of the material crystalline structure leading to an anisotropic material with varying electromagnetic properties [101] . Furthermore, a third source of structural inhomogeneity is the metallurgy of the material itself. This consists of a number of things amongst which are, the crystalline structure, anisotropic structure, crystal lattice orientation and so on. All these, in part or has a whole lead to the random variation of permeability and conductivity of the ferrous material [125, 126].

4.2. Finite Element Model

From the above sections, since it has been established that the effect of the EM properties of test materials are an integral part of PEC response signals, it is necessary to delineate the individual influences of these EM parameters. To wit, a numerical model is exploited foremost to understand the areas of dominance of these influences in the PEC response signal as a forward model and then to verify this through experimental study as an inverse process. The understanding and delineation of the EM parameters becomes invaluable in multiple parameter estimation in subsequent chapters.

To understand this electromagnetic (EM) variation therefore, a 3D numerical model is designed as illustrated in Figure 4.2 using the AC/DC module of Comsol Multiphysics 3.4[119]. To simplify the model, a quarter of the geometry is used since it is axisymmetric. The specimen is considered to be an inhomogeneous material with varying conductivity and permeability at the macro level, whose EM properties varies as shown in Table 4.1. The conductivity and permeability values in Table 4.1 typify reference standards obtainable from the National Physical Laboratory, NPL [127-129]. With a repetitive period of 0.005s and sampling time of 1e-5s, time domain analysis and spectral behaviour were investigated. It should be noted however that throughout this work only half the period is considered as we are largely interested in the transient response.
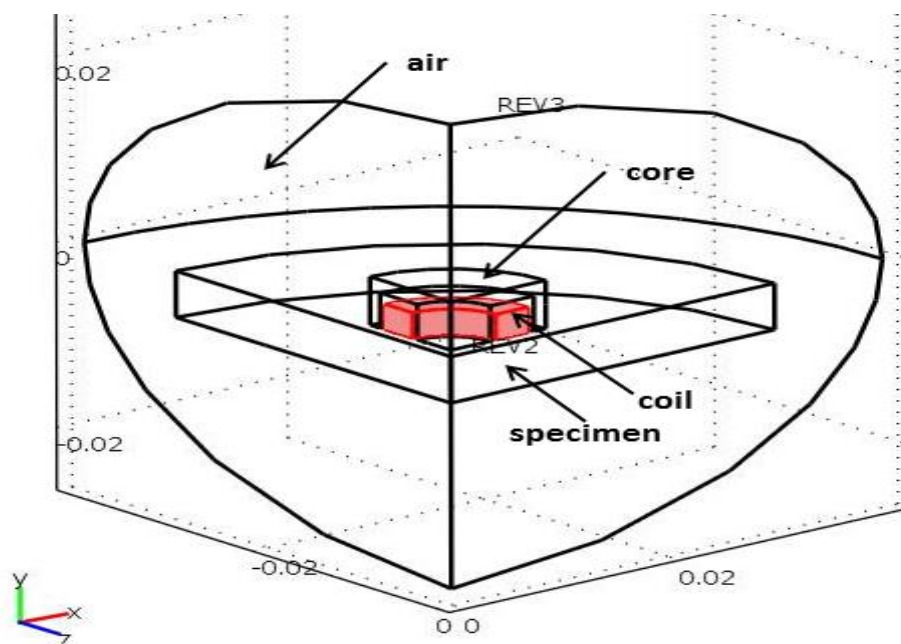
Figure 4.2: 3D FEM Model

TABLE 4.1: EM PROPERTIES VARIATION

Conductivity (Standard)	C179	R179	A179	W179
σ (MS/m)	14.33	22.45	36.02	59.47
Relative Permeability μ	1.00	1.10	1.27	1.63
Reference	NPL[127,128]	NPL[127,128]	NPL[127,128]	NPL[127,128]

4.2.1. Numerical Simulation Results

Results from the numerical simulation described above are herein presented. The combined influence of the EM properties and the individual influences of these parameters on the PEC signal response are delineated.

4.2.1.1. Combined Influence of Conductivity and Permeability

Based on the simulation set-up described above, figure 4.3(a) shows the non-normalised PEC response of an anisotropic test material. It is observed from figure 4.3(a) that B increases as the value of EM properties of the target material increases in the stable phase of the PEC response while the reverse is observed in the transient or rising edge of the PEC response. It is of interest therefore to determine which of these EM properties is actually responsible for these two observations.

Furthermore, in figure 4.3(b) the resultant differential normalised response shows a consistent decrease as the EM properties increased.

(a)   (b)
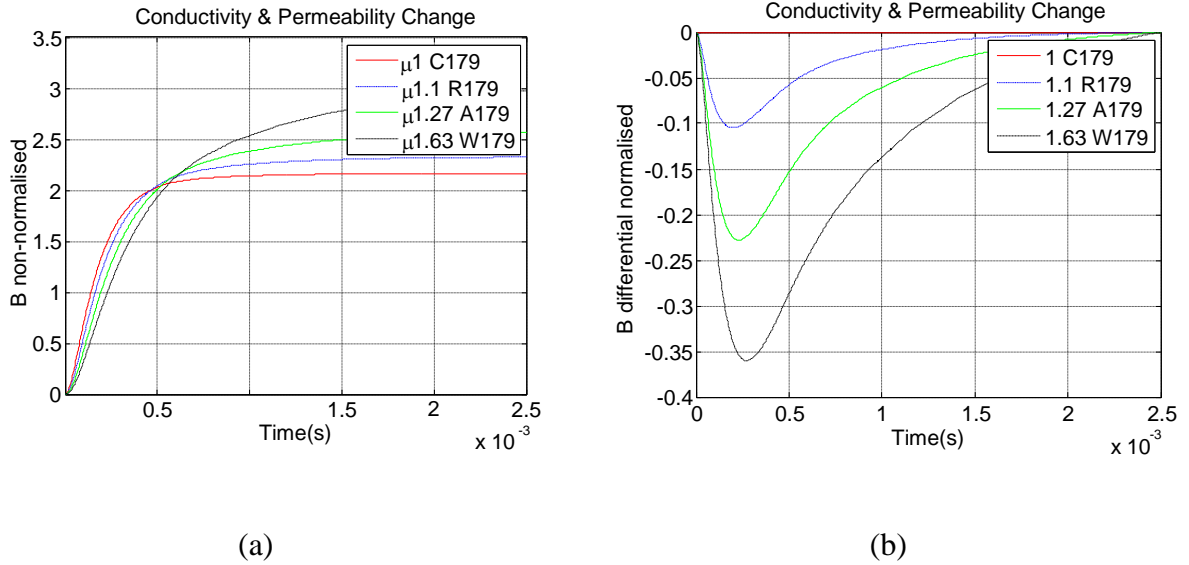
Figure 4.3: (a) Non-normalised response. (b) Differential normalised response.

Figures 4.4(a) and (b) show the spectral pattern observed for the inhomogeneous test sample. A non-linear pattern is obvious from these results. Normalising the magnitude spectrum did not remove the effect of this combined variation of the EM property components. At the 200Hz mark in figure 4.4(b) after normalising the magnitude spectrum the nonlinearity remains and the normalised magnitude change is approximately 0.16. In real life application this means that it will be difficult to distinguish between the conductivity effects and the influence of permeability.

(a)   (b)
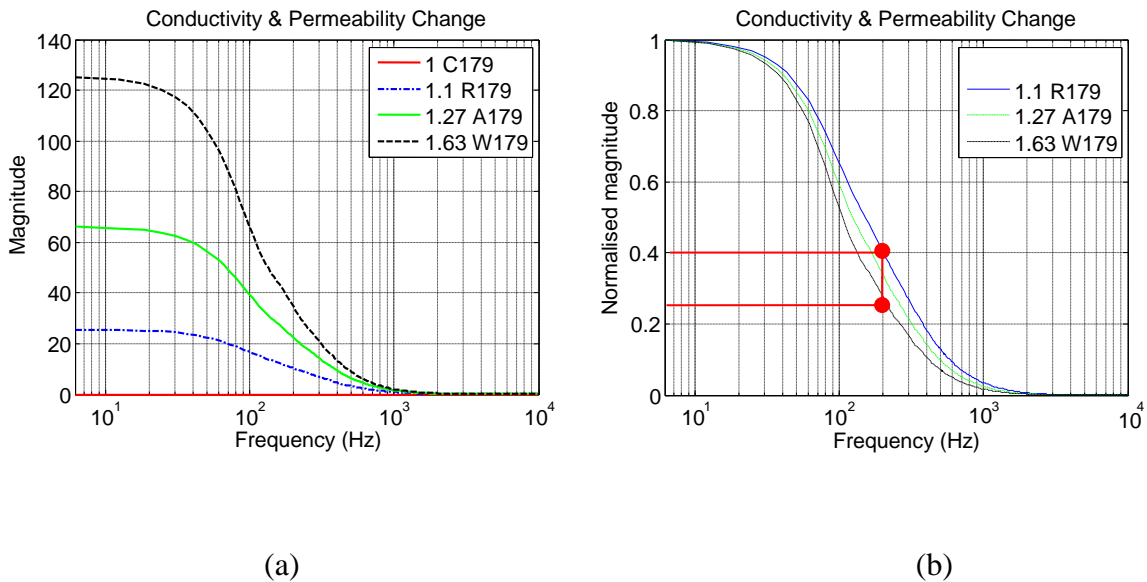
Figure 4.4: Magnitude spectrum pattern for combined parameter change: (a) non-normalised; and (b) normalised.

4.2.1.2. Decoupled Influence of Conductivity

Following the results obtained in section 4.3.1.1 above; it is of interest to delineate these parameters in order to investigate their singular influences and contributions to PEC signal response. Using the same finite element model of figure 4.2, lift-off and relative permeability are kept constant at 0.5mm and 1.27 respectively whilst conductivity is varied using standard values from 14.33 to 59.47 MS/m as shown in Table 4.1 above.

Figure 4.5a shows the non-normalised transient response and here it is observed that the influence of conductivity is prominent in the rising edge such that the magnetic flux density decreases as the conductivity variation increases. From Lenz's law, it is clear that electrical intensity (or emf.) is directly proportional to magnetic flux [$E = -N(\partial \phi_B / \partial t)$, where N is the number of turns, ϕ_B is the magnetic flux, and t is time] but conductivity, σ, is inversely proportional to emf. from the fact that $\sigma = I / EA$ (where I is current, E = emf, and A is the cross-sectional area), hence, this explains the inverse relation between conductivity and magnetic induction, B, in figure 4.5a. A consistent decrease in ΔBnorm with increased conductivity is shown in figure 4.5b.

Moreover, the magnitude spectrum pattern of conductivity is presented in figure 4.6. It is observed that after normalisation process the effect of conductivity is not eliminated and quantitatively the normalised magnitude change is 0.13 at 200Hz which accounts for about 81% of the change observed in figure 4.4(b) when the combined influences of conductivity and permeability were considered. This may be attributed to the fact that in time domain for the ΔBnorm produced as a result of the rising edge of the pulsed excitation current, the time constant, T_c, of B decreases more than that of B_{REF} consistent with decreasing conductivity in consonant with $T_c = L/R$ [89, 130]; where L and R are the inductance and resistance of the PEC system. Hence, it becomes clear that the influence of conductivity on PEC response is more than an amplitude change.

(a)   (b)

Figure 4.5.: (a) Non-normalised PEC response. (b) Differential normalised PEC response.

(a)   (b)
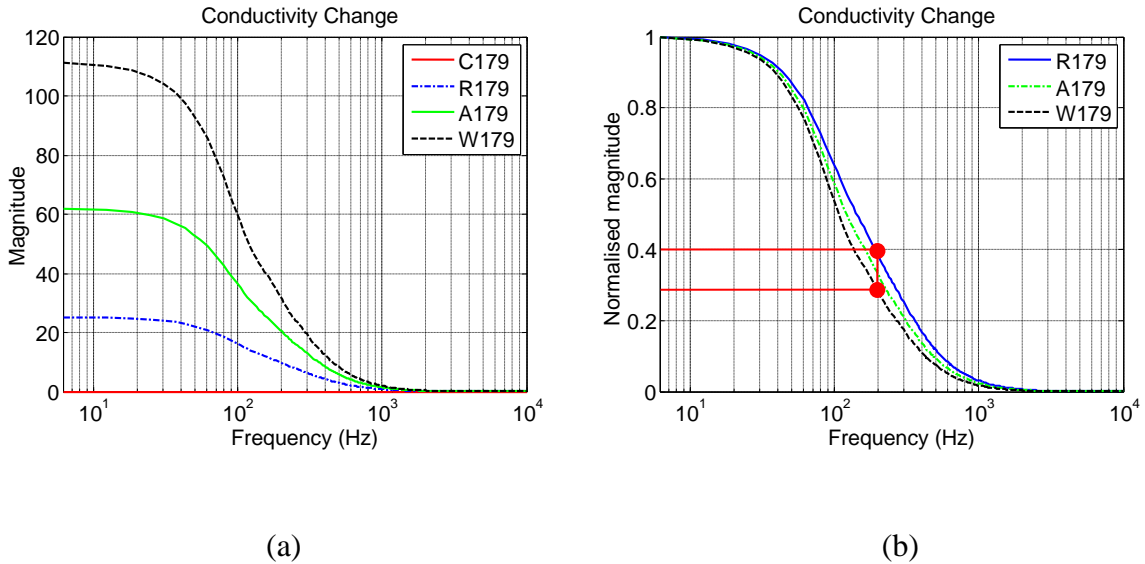
Figure 4.6.: Magnitude spectrum pattern for conductivity: (a) non-normalised; and (b) normalised.

4.2.1.3. Decoupled Influence of Permeability

Again, to investigate the singular influence of permeability, all parameters were kept constant in the finite element model while permeability was varied from 1 to 1.63 as shown in Table 4.1. Lift-off set to 0.5mm and conductivity set as 36.02 MS/m.

It can be clearly seen in figure 4.7(a) that the influence of permeability is prominent in the stable phase of the transient response. As permeability increases, the values of non-normalised B increases as well showing no significant change in the rising edge of the PEC response. An analogous pattern is observed in the differential normalised PEC response also. Furthermore, figure. 4.8 reveal that after normalisation the influence of permeability on PEC

response is significantly suppressed. Only a 0.03 change in normalised magnitude is observed at the 200Hz mark in figure 4.8(b); accounting for only 19% of the total change when the combined influences of the EM properties were considered in section 4.2.1.1. It is an important result in that the normalisation process can actually reduce significantly the effects of permeability, thus, reducing measurement error or false alarm when using PEC system in practice.
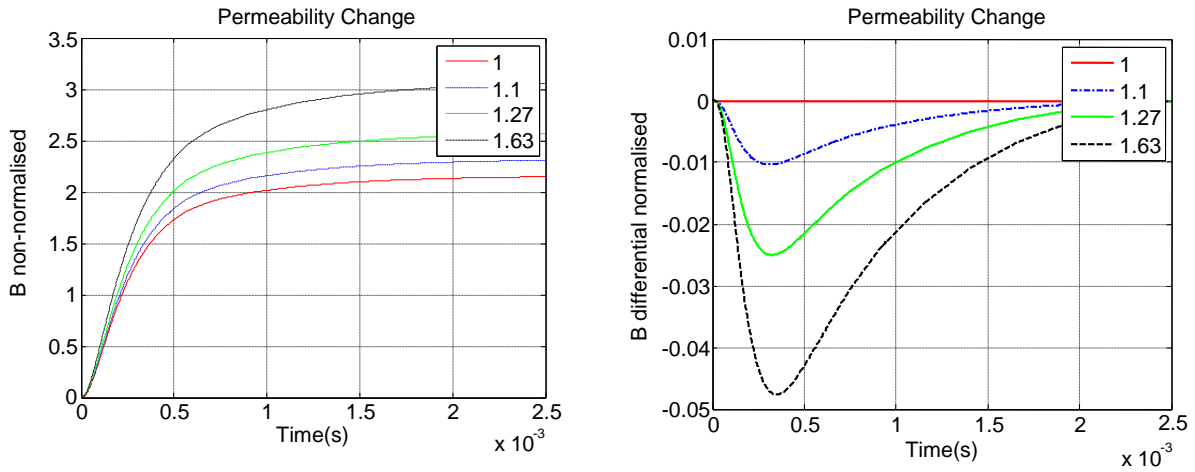
(a)   (b)

Figure 4.7.: (a) Non-normalised PEC response. (b) Differential normalised PEC response.
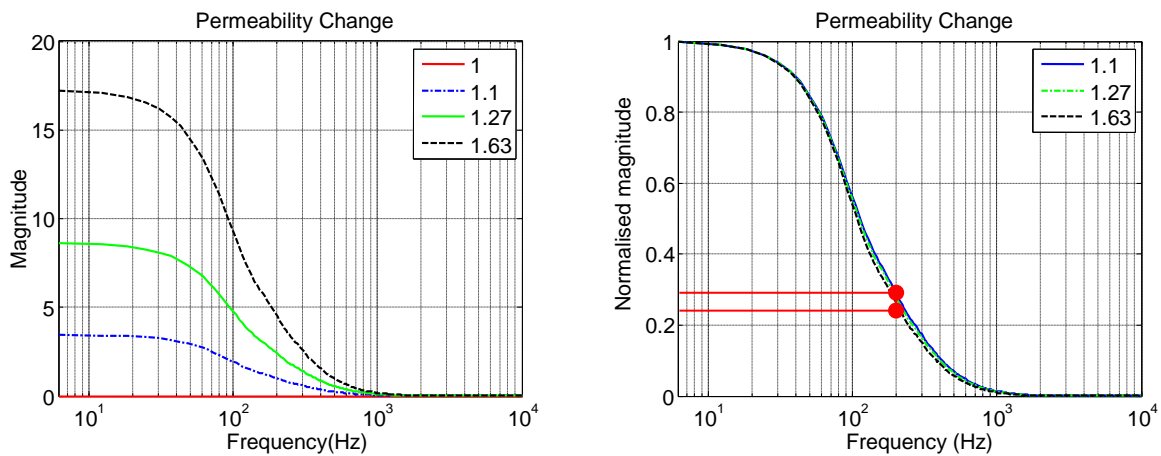
(a)   (b)

Figure 4.8.: Magnitude spectrum pattern for permeability: (a) non-normalised; and (b) normalised.

Furthermore, it is of interest to consider larger variations in the magnetic permeability. Therefore in the simulation model we vary the permeability from 5% to 160% of the initial relative permeability value of 60. Throughout the simulation a probe lift-off of 0.5mm and material conductivity of 4.68 MS/m is maintained [9]. The numerical simulation predicted magnitude and normalised magnitude spectra are shown in figure 4.9 below. It is seen from the figure 4.9(b) that normalisation is not removing the effect of permeability in this case and the magnitude pattern changes non-linearly. However, in practice the applied field from a typical PEC probe is about 15A/m, hence, such applied field would not produce large variation in permeability as apparent in this result, as such; the effect of magnetic permeability variation in PEC sensing technique can be suppressed by normalisation technique as earlier predicted.

(a)   (b)
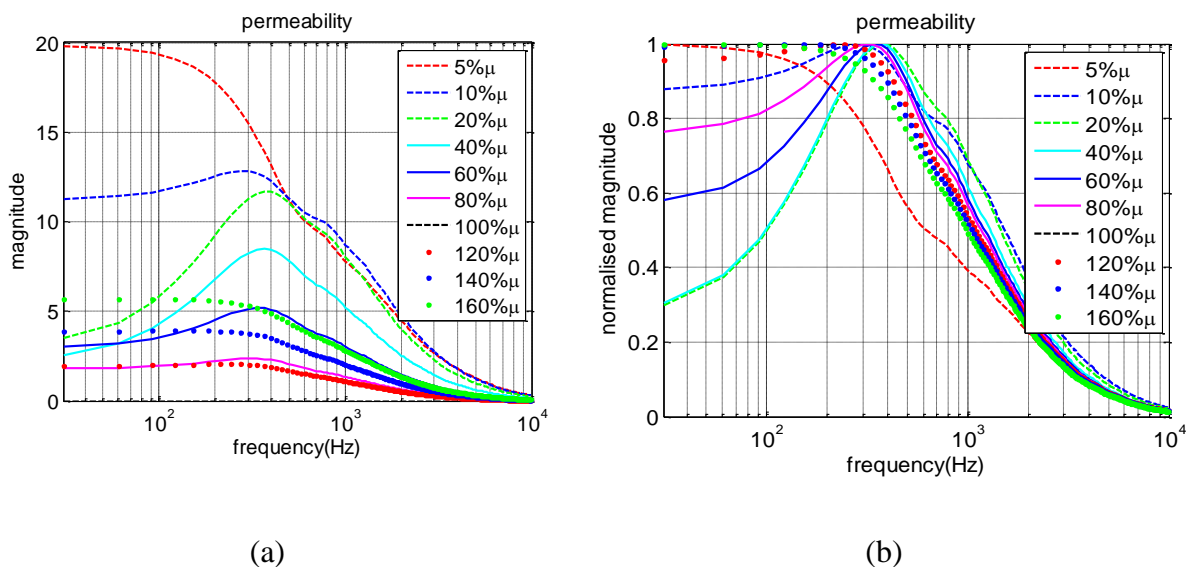
Figure 4.9: Magnitude spectrum pattern for high permeability variation: (a) non-normalised; and (b) normalised.

This claim is strengthened by looking at permeability more closely with the B-H relationship. If a magnetic field is applied to a material the atomic elements in the material begin to align with the magnetic field. This alignment causes an increase in magnetic flux density. But as applied field increases, the rate of alignment varies; hence, B varies in a hysteretic pattern with changing H [131, 132].

From this B-H relationship we could describe the magnetic permeability in one of three ways; initial permeability, differential permeability and recoil or incremental permeability. The

initial permeability is the magnetic permeability of a virgin material; that is of a completely demagnetised material prior to any applied field [133-135]. The differential permeability is the slope of the B-H curve at any point on the curve. However, if a small amount of ΔH is applied to H at any point on the B-H curve as illustrated in figure 4.10, a small but reversible change of permeability is apparent, the slope of which is defined as the recoil permeability Δμ. This does not vary remarkably with H for constant values of ΔH. However, as ΔH decreases, Δμ tends toward μ_o [134]. In this regime the reversible component of magnetisation dominates; which is the first term of the Rayleigh law of magnetisation that describes a quadratic dependence of magnetisation on the applied field ($M = \chi_0 H + \mu_0 \alpha H^2$, χ_0 is the initial susceptibility μ_0 is the permeability of free space, α is the Rayleigh constant and H is the applied field) Therefore, one can infer that the recoil permeability is the apparent permeability effect in pulsed eddy current testing [134, 135]. The reason being that as mentioned the typical PEC probe would only induce a magnetic field with low amplitude hysteresis within the material [119]. This field is very low compared to what is needed to magnetise the ferrous material. Figure 4.10 further describes mathematically the three identified magnetic permeability; that is, the inverse tangents of θ_1-θ_3 defines the initial, differential and recoil permeability respectively.
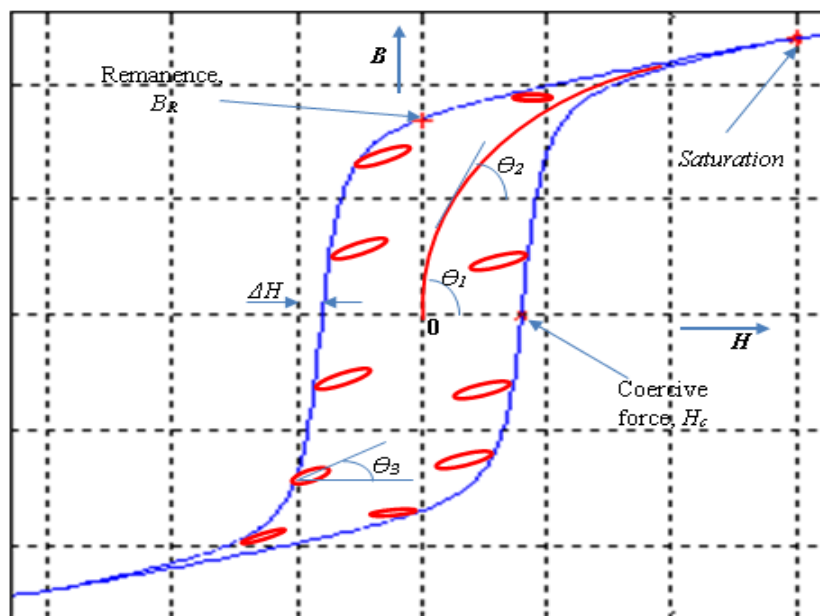
Figure 4.10: Typical Hysteresis Loop of a Ferromagnetic Material with reversible loops of recoil permeability

4.3. Experimental Validation

The experimental samples for the hitherto discussed numerical investigation of material property influence in PEC measurement are shown in figure 4.11. The experimental validation set-up follows the description of the experimental system of section 3.3. The PEC probe used consists of excitation coil with ferrite core and Hall sensor as the pick-up sensor. The PEC acquisition scheme uses the QinetiQ TRESCAN® system. A unit period of a digital excitation waveform is created in Matlab, which is then converted to an analog voltage signal by the analog output subsystem of the NI PCI-6255 DAQ board. This voltage signal is converted into excitation current by the signal conditioning TRESCAN box. This operates in current mode with an exponentially damped rectangular wave of 50% duty cycle, time constant, $T_c = 100\mu s$ and repetitive frequency of 200Hz. The excitation is fed into the probe's excitation coil and a hall sensor measures the PEC response which is low-pass filtered (10 kHz cut-off) and amplified by TRESCAN. This is then digitized by the DAQ board. The acquired digital waveform is post-processed in Matlab.

(a)   (b)

Figure 4.11: Experimental Validation Samples. (a) Photograph of Conductivity Samples. (b) Permeability Samples

4.3.1. Decoupled Influence of Conductivity

With the described experimental set up above, PEC responses were obtained for a range of electrical conductivities of reference standards whose values are shown in Table 4.1. Each of these standards has a circular geometry with a radial length of 40mm and thickness of 10mm.

(a)   (b)
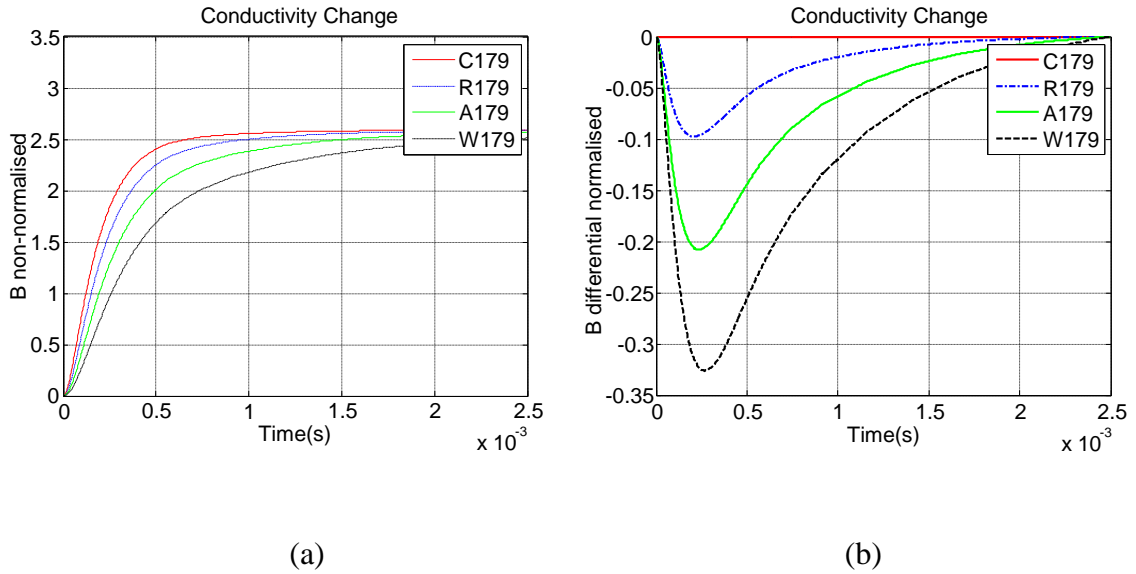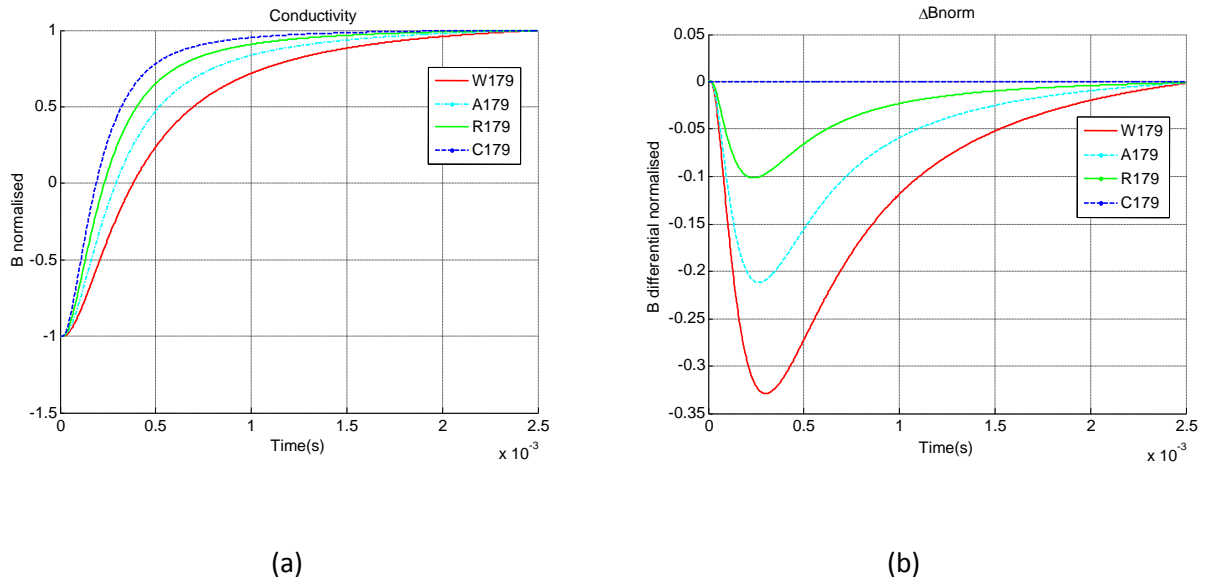
Figure 4.12: (a) Normalised PEC response. (b) Differential normalised PEC response.

(a)   (b)
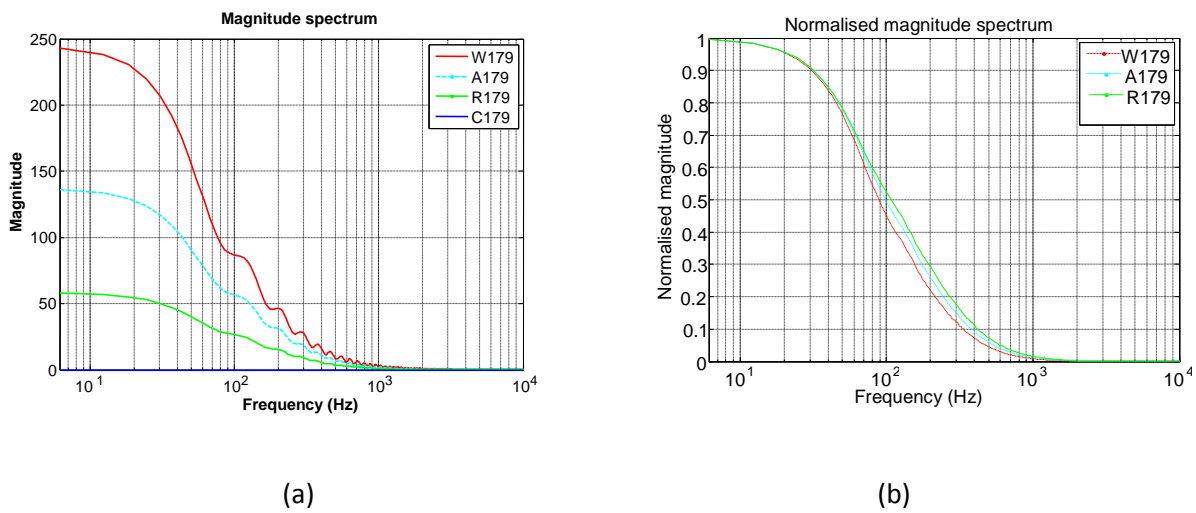
Figure 4.13: Magnitude spectrum pattern for conductivity: (a) non-normalised; and (b) normalised.

From the experimental result obtained and shown in figures 4.12(a) and (b), we observed the same trend as seen in the simulation results presented in figure 4.5(a) and (b) validating the theoretical ideas articulated in the numerical model. Similarly, figures 4.6(a) and 4.6(b) show a good agreement with experimental results shown in figures 13(a) and (b) as well showing that normalisation of the magnitude spectrum is not removing the effect of electrical conductivity.

TABLE 4.2: COMPARISON OF SIMULATED AND MEASURED PV(ΔBnorm)

Standard	σ(MS/m)	Measured	Simulation	Δ	ε(%)
R179	22.45	-0.1015	-0.0974	-0.0041	4.0394
A179	36.02	-0.2119	-0.2080	-0.0039	1.8405
W179	59.49	-0.3291	-0.3261	-0.0030	0.9116

Hence, it is imperative to compare the characterising features from numerical simulation and experimental studies. From [130] and [89] max(B) has been optimised to characterise magnetic permeability while PV(ΔBnorm) has been optimised to characterise electrical conductivity. Thus, using the latter optimised PEC feature, Table 4.2 above shows the relative deviation, Δ, between the measured and simulated result. Furthermore, figure 4.14 shows the fitting curves for the feature. A good match between the measured and the simulated results become obvious, thus validating the numerical model. Considering a cross-correlation analysis of the measured and simulated values of figure 4.14, according to [136], correlation coefficient of 1 show that the values are identical, 0 suggests there is no similarity between the measured and simulated results, while a negative 1 indicates a relationship with a phase shift of 180. Hence, computing the correlation coefficients using Matlab function corrcoef, we obtained [1 0.9999; 09999 1] which is a strong indication of significant correlation since all coefficients are close to 1. The error margin can be attributed to the intrinsic noise in the hall sensor used in the experimental studies. Again, in the finite element model, a lift-off of 0.5mm was considered whilst no lift-off was considered in the actual experiment.
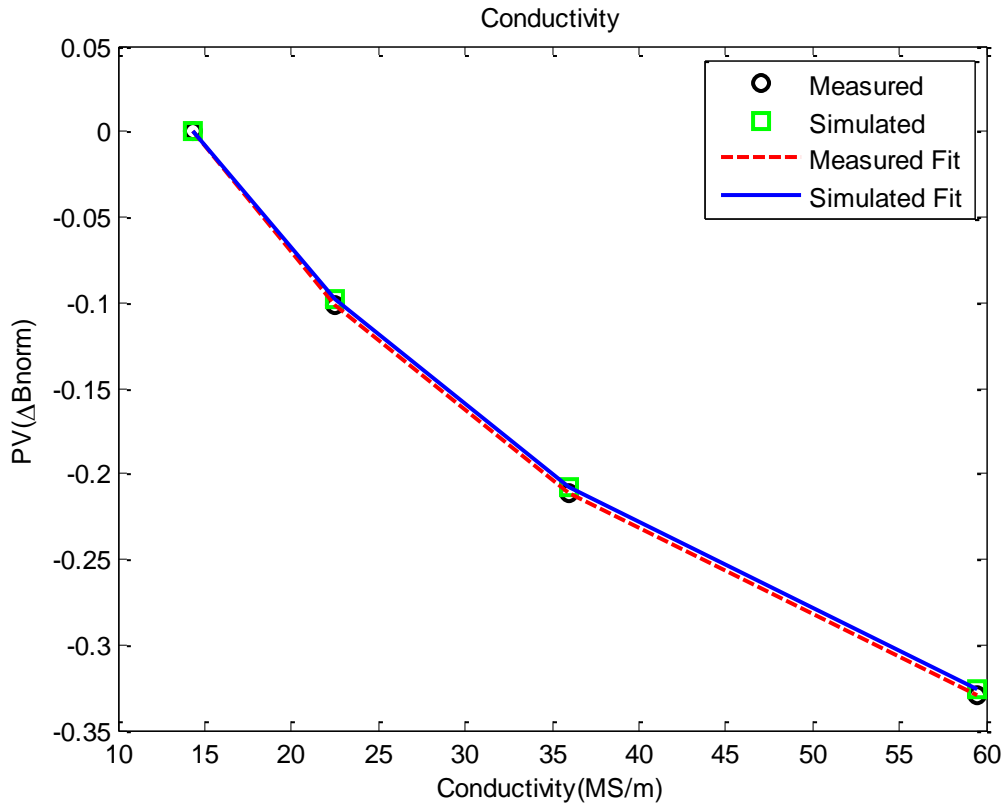
Figure 4.14: Comparison of Measured and Simulated Values for PV (ΔBnorm)

4.3.2. Decoupled Influence of Permeability

To investigate the influence of relative magnetic permeability experimentally, a set of low permeability reference standards calibrated at a magnetic field strength of 30KA/m with a circular geometry of dimension 40mm diameter × 30mm and bar shaped standards with dimensions 25mm × 25mm × 305mm, values 1.005, 1.123, 1.269 and 1.591 were used. The relative permeability of the standards was measured in accordance with BS 5884:1999. This standard employs three methods in determining the magnetic permeability of weakly magnetic materials and the reference method adopted is the solenoid method. Here, the relative magnetic permeability is derived from the magnetic polarization, J, and the corresponding magnetic field measured using a simple arrangement consisting of a d.c. supply, flux integrator, solenoid, search coil, variable resistor and ammeter [128]. Prior to the measurement, the standards were AC demagnetized and measurement made by inserting the bar into a search coil connected to a calibrated voltage integrator and measuring the induced volt second product corresponding to the magnetic polarization, J, when the bar was withdraw from the search coil. Demagnetizing corrections were applied to the measured J and

the corresponding relative permeability calculated at room temperature. And with the experimental set up of figure 3.5 (of section 3.3), PEC responses were obtained as shown in figure 4.15 below.

(a)   (b)
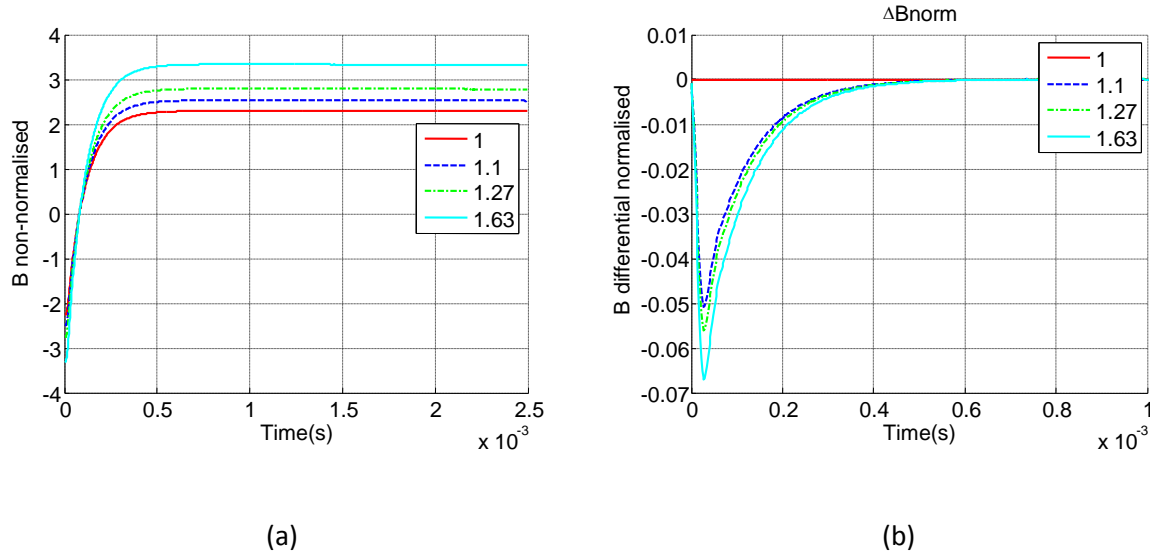
Figure 4.15: (a) Non-normalised PEC response. (b) Differential normalised PEC response.

The transient PEC response shown above corroborated the numerical result that relative permeability mainly affects the stable phase and the amplitude change increases with increased magnetic permeability.

Comparing the optimised characteristics feature of the magnetic permeability of the numerical model and the measured result, Table 4.3 shows the relative deviation, Δ, of the max (B). And the fitting curve is illustrated in figure 4.16 for this feature. Here the correlation coefficients show a great deal of confidence that there is a good match between the measured and simulated results as the coefficients are all close to 1 (i.e.[1 0.9986; 0.9986 1]) . The discrepancy observed can be attributed to the reasons stated earlier in section 4.1.1, the process history and surface condition of the sample as these affect the domain wall holding position and density [137] In addition, the probe-sample gap may give rise to the magnetic field varying spatially, thus, its amplitude at a given field point would largely depend on the probe and sample geometries [122]; moreover, phase lag in the motion of

magnetic domain wall relative to the excitation current is another source of frequency dependent variation [138].

TABLE 4.3: COMPARISON OF SIMULATED AND MEASURED Max (B)

Standard (μ)	Measured	Simulation	Δ	ε(%)
1	2.2960	2.2124	0.0836	3.6411
1.1	2.5333	2.3761	0.1572	6.2053
1.27	2.7824	2.6382	0.1442	5.1826
1.63	3.3366	3.1339	0.2027	6.0750
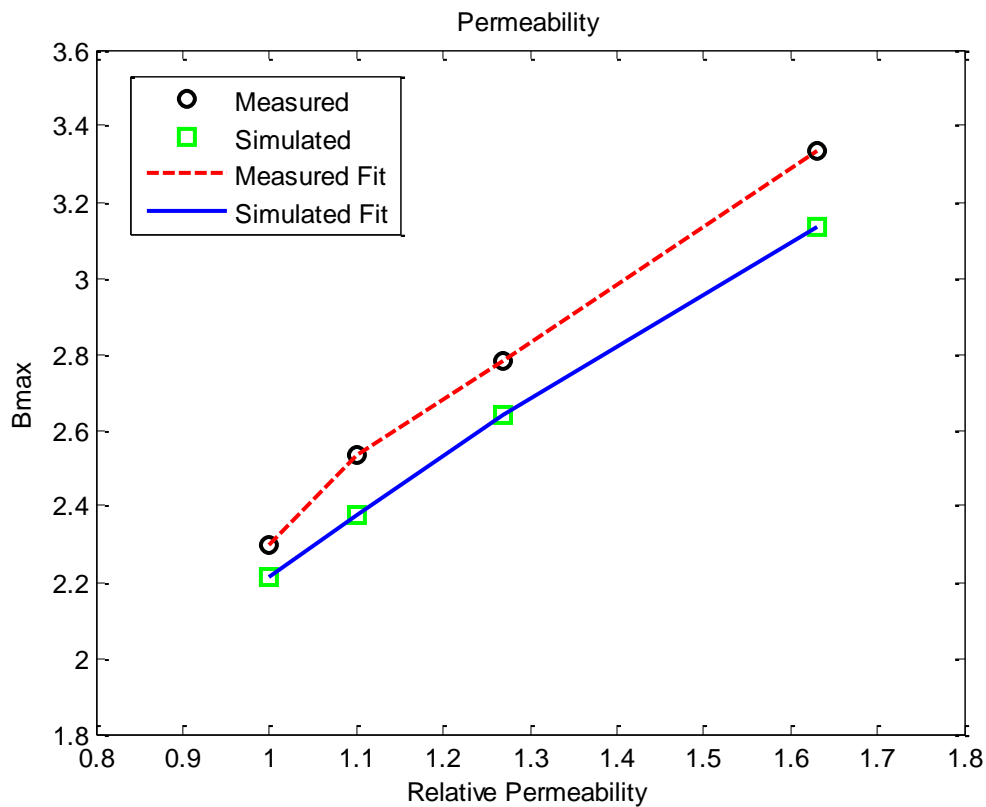
Figure 4.16: Comparison of Measured and Simulated Values for Max (B)

4.4. Chapter Summary

This chapter amongst other things has investigated the contributions of the EM properties of a test material to the in PEC measurements. It has been able to delineate the individual influences of these EM properties through numerical simulation which was validated by experimental studies. A good agreement within 6% error limit is observed in the numerical and experimental results. More importantly, we can infer from the results that conductivity effects are prominent in the rising edge of the transient response; hence, changing the spectral pattern in the frequency domain whilst permeability effects dominate in the stable phase of the transient response thus this effect can be suppressed or reduced by normalisation showing that it is only an amplitude change.

From these results, the design of novel PEC system which would potentially reduce the effect of changing permeability becomes feasible through normalisation. Furthermore, it becomes abundantly clear therefore, that the influence of conductivity is more than an amplitude change, thus to reduce the uncertainty in PEC measurements due to inhomogeneity, electrical conductivity must be mitigated. This finding becomes valuable in PEC applications for displacement measurement, stress, corrosion characterisation of ferrous materials and components in general and multiple parameter delineation and estimation in particular presented in chapter 5.

Chapter 5: Separation and Estimation of Lift-off and Defect Features in Magnetic Sensor based Pulsed Eddy Current Signals

This chapter focuses on defect characterisation independent of the lift-off effects using lift-off point of intersection (LOI) and the separation of these two parameters in pulsed eddy current (PEC) measurements for two material case studies: ferrous and non-ferrous materials. It reveals, amongst other things, that the first order derivative of the normalised PEC response maintains the LOI feature, which otherwise is not apparent in ferromagnetic materials using current methods; lift-off effects in ferrous materials vary strongly with the second order derivative of the normalised PEC response and the LOI can be used for defect estimation in a magnetic sensor-based PEC. These two characteristics provide a means of separating lift-off effects from the defect. Furthermore, a defect characterisation method using the slope of the normalised differential PEC signal (ΔBnorm) versus lift-off curve has been developed.

5.1. PEC Signal Characteristics

Typical signals measured using the Hall-effect sensor in the TRESCAN PEC systems are illustrated in figure 5.1. Here, time is normalised to the repetitive period T (referred to as normalised time). When the coil of the PEC probe is driven by an exponentially-damped square wave excitation current (I_{exc}), a periodic reversal of magnetic field is produced. This induces a pulse of eddy-currents that propagates down into the sample at each reversal. The Hall device located above the surface of the sample on the axis of the coil measures the perpendicular component of the magnetic flux density (B). With no sample in front of the probe, the measured magnetic flux density (B_{air}) is proportional to I_{exc}. As a result of the field induced by the eddy current opposing the incident field, the rise time of the magnetic flux density (B) is much longer than that of B_{air} as shown in figure 5.1. Usually, finding the difference between the reference signal (B_{air} or signal from a good part of the sample) and the detected signal (B) called balance or difference signal generates a relative signal ΔB which is nominally zero except the sample structure or its properties changes [121]. Also, normalising the detected (B) and the reference signal (B_{air}) to their respective maxima and finding the difference we obtain the differential normalised signal (ΔBnorm), which can be used to characterise the sample under test [89]. Thus, through a combination of the normalisation and differential process, the response as a result of the material properties or structural changes (defects) can be extracted [5].

(a)   (b)
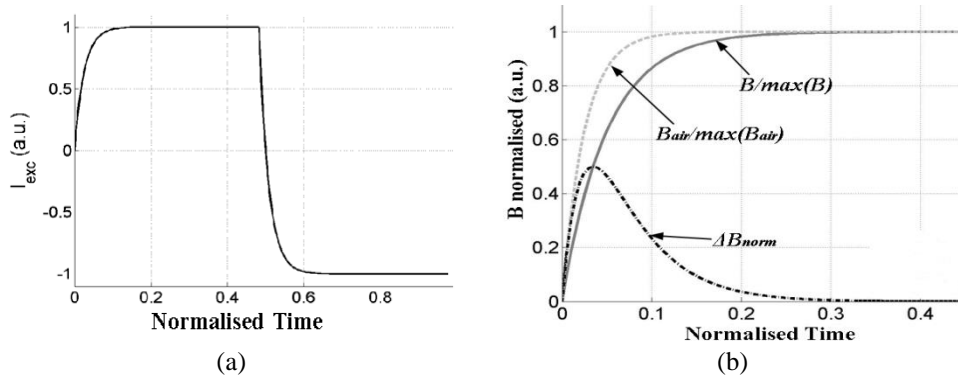
Figure 5.1: Typical PEC (a) excitation current and (b) transient response

Based on the pulsed eddy current operational principle and its signal characteristics, separation of defects and lift-offs is being proposed and investigated. Experimental studies of ferromagnetic and non-ferromagnetic material samples are presented.

5.2. Experimental Setup

The experimental setup for this investigation is shown in figure 3.5 of section 3.3. The QinetiQ probe used consist of a ferrite core, an excitation coil and a Hall sensor centred beneath the ferrite core, which is oriented to measure the perpendicular component of the magnetic field from the surface of the test piece. A description of the probe's parameters is summarised in Table 5.1. And figure 5.2 below gives the overall schematic structure and layout of the specimen used in the experimental investigation.

Table 5.1: Parameters for the QinetiQ Probe

Probe Parameter	Dimension
Inner Diameter of Excitation Coil	9.2mm
Outer Diameter of Excitation Coil	18.4mm
Number of Turns	260 turns of 0.19mm diameter copper wire
Coil Height	3.9mm
Outer Diameter of ferrite core	21.4mm
Height of ferrite core	6.7mm
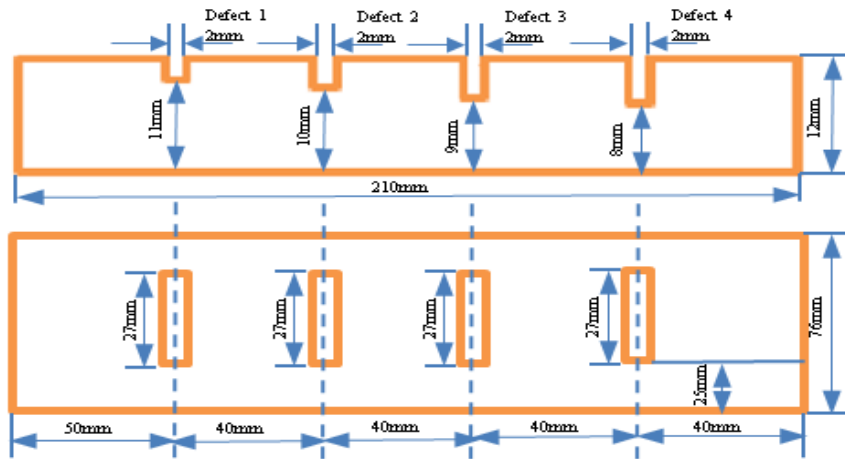
Figure 5.2: Schematic for the Specimen Structure

5.2.1. Separation and Estimation of Lift-off and Defect Depth using LOI Feature

In the experimental investigation of the lift-off effect on the PEC response carried out in this work, two cases were considered; ferrous and non-ferrous specimens. This is due to the fact that different materials have different LOI behaviour in PEC inspection. The methodology employed is graphically illustrated in figure 5.3. Essentially, this figure gives a novel LOI-based PEC defect characterisation of ferromagnetic materials in particular and a liftoff-defect delineation procedure for both ferromagnetic and non-ferromagnetic materials.
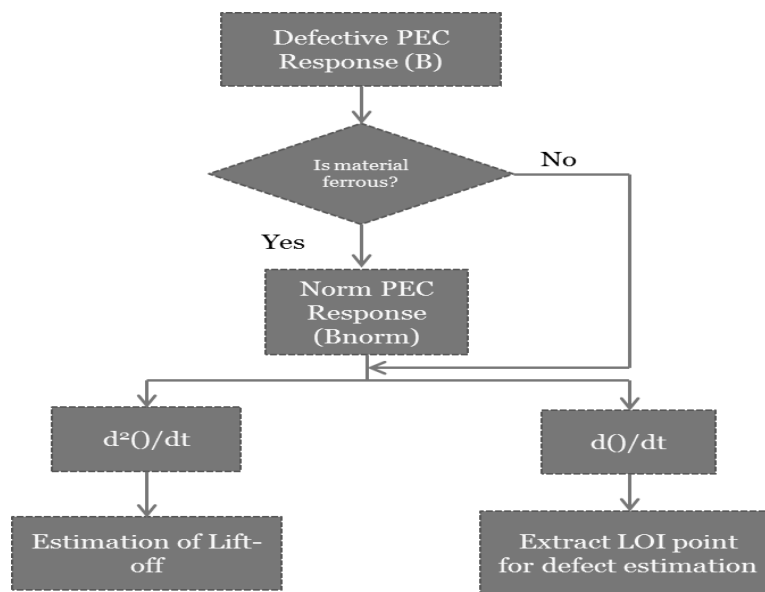
Figure 5.3: Liftoff-Defect Separation

5.2.1.1 Case 1: Ferrous Material

In this section, a brief description of the sample used, defect size and its LOI behaviour are presented.

5.2.1.1.1. Sample Description

In the first case, artificial slots of the same width (2mm) but with varying depths from 1-4mm were machined in a steel plate sample with dimensions 210mm X 76mm X 12mm to simulate surface flaws for investigation as shown in Figure 5.2. The steel plate is mild steel with electrical conductivity of 6.99 MS/m and a nominal relative permeability of 100 at an applied field of about 0.002 T. Plastic insulations of thickness $1 - 5mm$ in steps of 1mm were used to simulate varying lift-offs whilst the probe was centred on each defect in this experiment.

5.2.1.1.2. Lift-off point of Intersection (LOI) Behaviour

It is of interest to investigate the lift-off point of intersection (LOI) in the steel specimen for defect characterisation. This is important because if the PEC responses at the LOI points are known as a function of defect then it would be possible to characterise defect of a new plate of the same material through calibration. However from the non-normalised PEC response of figure 5.5(a), it is apparent that there is no LOI point. For aluminium samples Tian *et al.*[69] demonstrated that taking the first derivative of the non-normalised PEC response a LOI point also exist in magnetic sensor based PEC response.

Moreover, for steel sample, taking the first derivative of this response there exist no LOI point still. From [5] it has been established that the influence of magnetic permeability is prominent in the stable phase of the non-normalised transient response, hence, applying normalisation, we significantly minimise this effect and then we find the first order derivative of the response with respect to time. With this novel approach of taking the first order derivative of the normalised PEC response of figure 5.4(b), LOI points are preserved and observed for each defect as illustrated in figure 5.5.

(a) PEC Response   (b) Normalised PEC Response
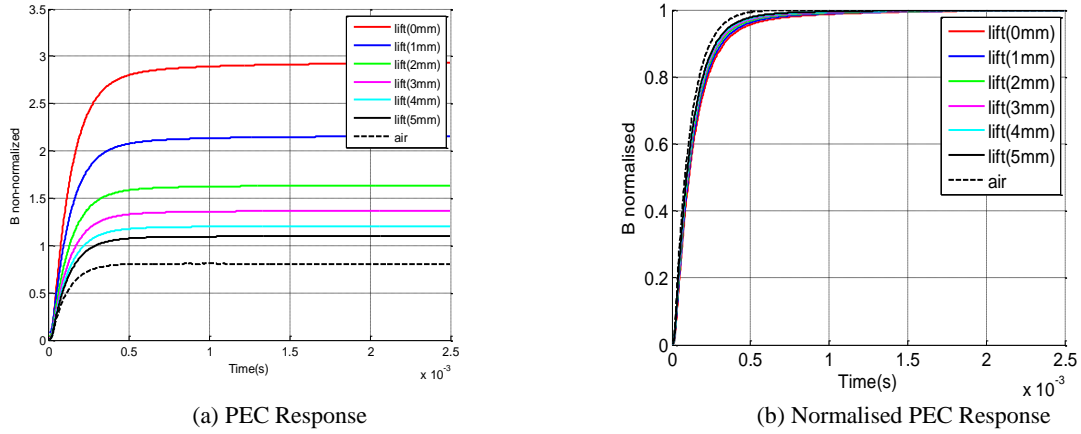
Figure 5.4: (a) Non-Normalised PEC Response and (b) Normalised PEC Response

(a) Defect 1   **(b) Defect 2**

(c) Defect 3   **(d) Defect 4**
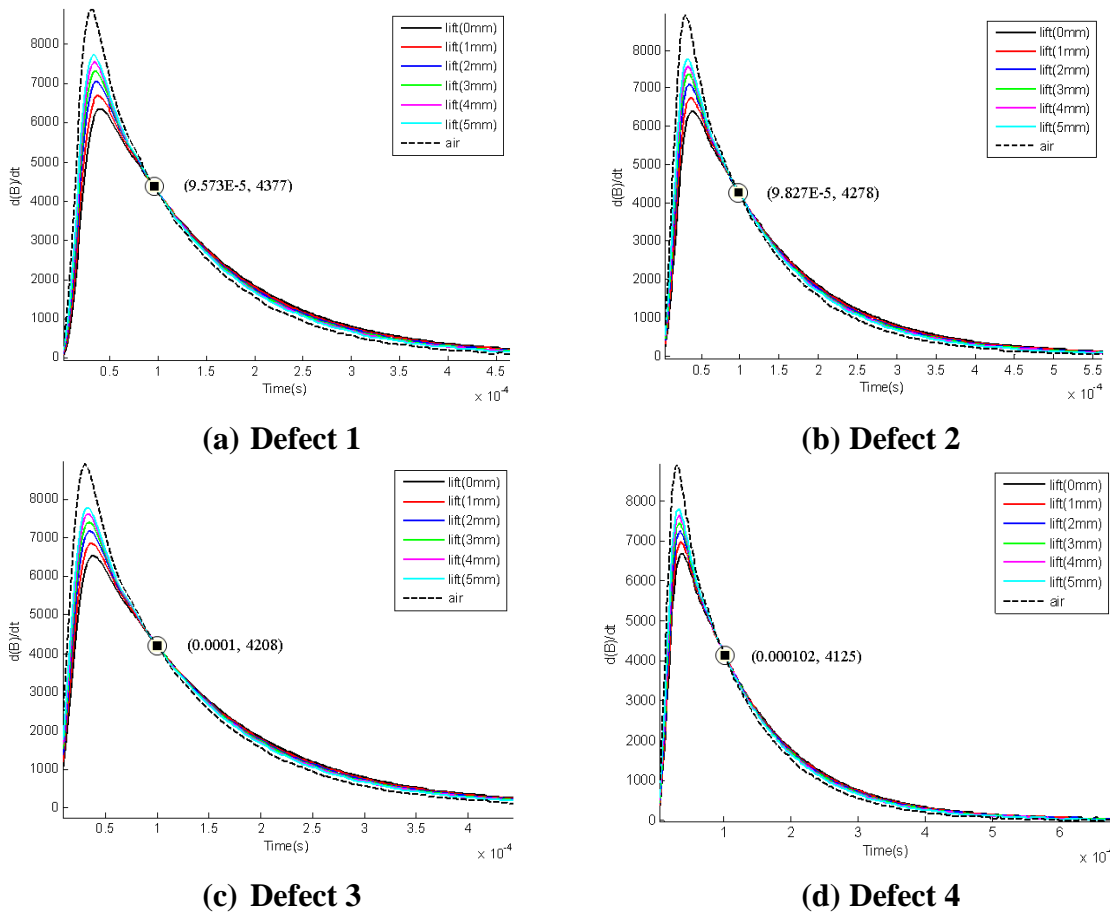
Figure 5.5: 1st Order derivatives of B normalised w.r.t. time for defects 1-4 with varying lift-offs

In figure 5.5, for each defect depth, six lift-off values were taken and the curve obtained in air is equally represented. From the LOI points for each of the defects we could represent the defect depths as a function of the time of intersection and as a function of the PEC output at that point in time. This is depicted in figure 5.6 where the asterisks represent the measured points and the continuous line is the fitted curve of these points. This graph shows the PEC output as a function of the time of intersection with defect depth as a parameter. To demonstrate repeatable results, three trials were conducted and the averaged outcome is illustrated in figure 5.6(b).

(a)   (b)
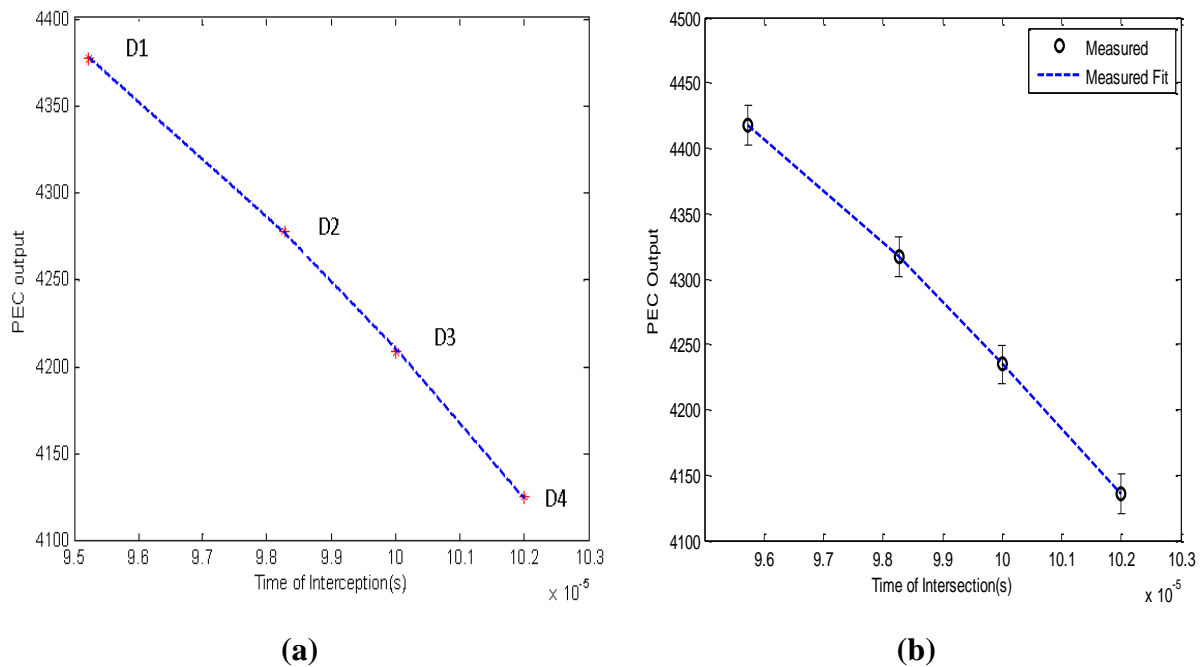
Figure 5.6: Determination of Defect depth from PEC output and LOI time of intersection (b) averaged over 3 trials

Furthermore, it is of interest to distinguish between the lift-off effect and defect, hence, the second derivative of the PEC response was taken as shown in figure 5.7. It is observed that this curve varied strongly with lift-off. This observation corroborate the findings of [92] though for a coil sensor where the impedance change is measured. For two distinct defects (defects 4 and 3), the second derivative of the B normalised PEC response matches well; meaning that this feature is a measure of the lift-off effect. Thus, whilst the LOI point is a

measure of the defect depth, the second derivative of PEC response is a measure of the lift-off effect.
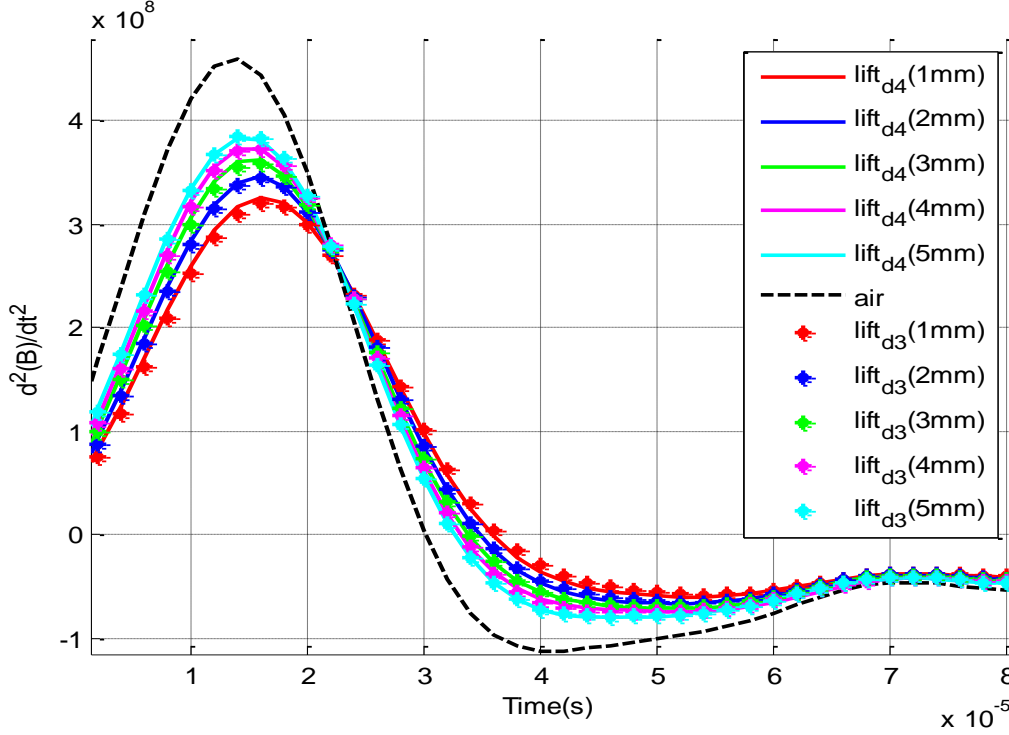
Figure 5.7: Determination of Lift-off Effect from 2nd derivative of B-normalised PEC response

From figure 5.7, we could develop a calibration graph for lift-off estimation by plotting its peak values against the applied lift-off values as depicted in figure 5.8. It is observed that the peak values of the second derivative of B-normalised PEC response with increasing lift-off defines a quadratic function which can be generalised by equation 5.1 whilst lift-off values can be estimated by equation 5.2 below. In addition, Table 5.2 shows the lift-off estimates derived from the generalised equation which demonstrates its usefulness in practice.

$$PV(\partial^2 B_{norm}/\partial t^2) = -1.813e6 LO^2 + 2.212e7 LO + 3.0611e8 \qquad (5.1)$$

and
$$LO = \frac{12.2041 \pm \sqrt{\Delta}}{2}, \qquad (5.2)$$

where the discriminant, $\Delta = 12.2041^2 - \left[4 \times (-168.89 + PV(\partial^2 B_{norm}/\partial t^2)/1.813e6)\right]$.
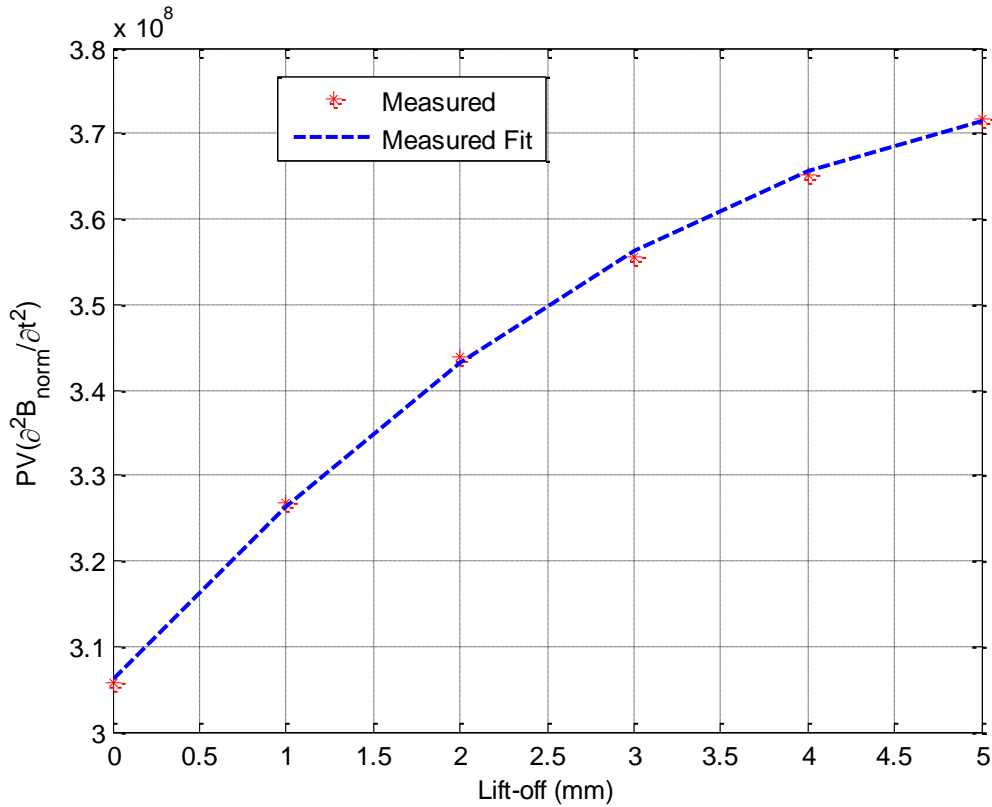
Figure 5.8: Steel - Lift-off Estimation Graph [$PV(\partial^2 B_{norm}/\partial t^2)$ **Vs *Lift-off*]**

Table 5.2: Lift-off Estimation Using LOI Feature (Steel)

Actual Lift-off (mm)	Estimated Lift-off (mm)	Relative Error (%)
0	0.0005	-
1	0.9991	0.09
2	2.0000	-
3	3.0038	0.13
4	4.0014	0.04
5	5.0007	0.01

5.2.1.2. Case 2: Non-Ferrous Material

A brief description of the test specimen used for this investigation, the defect characteristics and its LOI behaviour are presented here.

5.2.1.2.1. Sample Description

Using the same experimental setup described above an aluminium test calibration specimen with electrical conductivity of 25.8 MS/m (measured with the GE Sigma Conductivity meter)

92

was also investigated. A surface flaws investigation was carried out with artificial slots of the same width (2mm) but varying depths from 1-4mm were simulated in the aluminium plate sample of similar dimension to the steel described earlier. Plastic insulations with thickness 1~5mm in steps of 1mm were used to simulate varying lift-offs in this experiment as well. For this second case, the same methodology as described in the previous section is employed.

5.2.1.2.2. Lift-off point of Intersection (LOI) Behaviour

The LOI behaviour in the aluminium specimen was also investigated. Judging from its importance amongst which include defect identification and material property characterisation the following results were obtained from the first derivative of non-normalised PEC response are illustrated in figure 5.9.
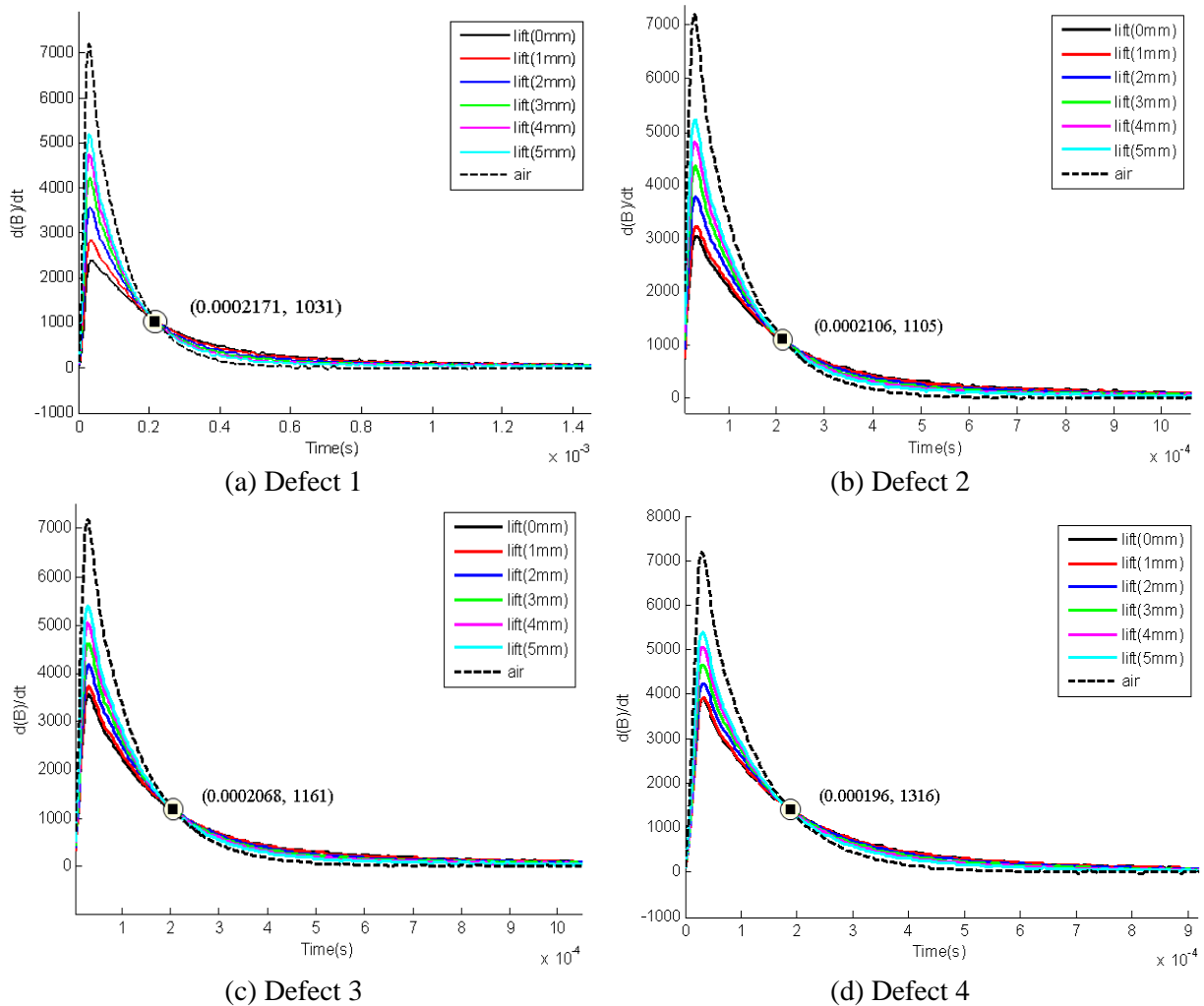
Figure 5.9: 1st Order derivatives of B non-normalised w.r.t. time for defects 1-4 with varying lift-offs

In figure 5.9, for each defect depth, six lift-off values were taken and the curve obtained in air is equally represented. From the LOI points for each of the defects we could represent the PEC output as a function of the time of intersection with defect depth as a parameter as shown in figure 5.10. The (b) part of figure 5.10 shows the results averaged over three trials demonstrating the repeatability and validity of the proposed.

(a) **(b)**
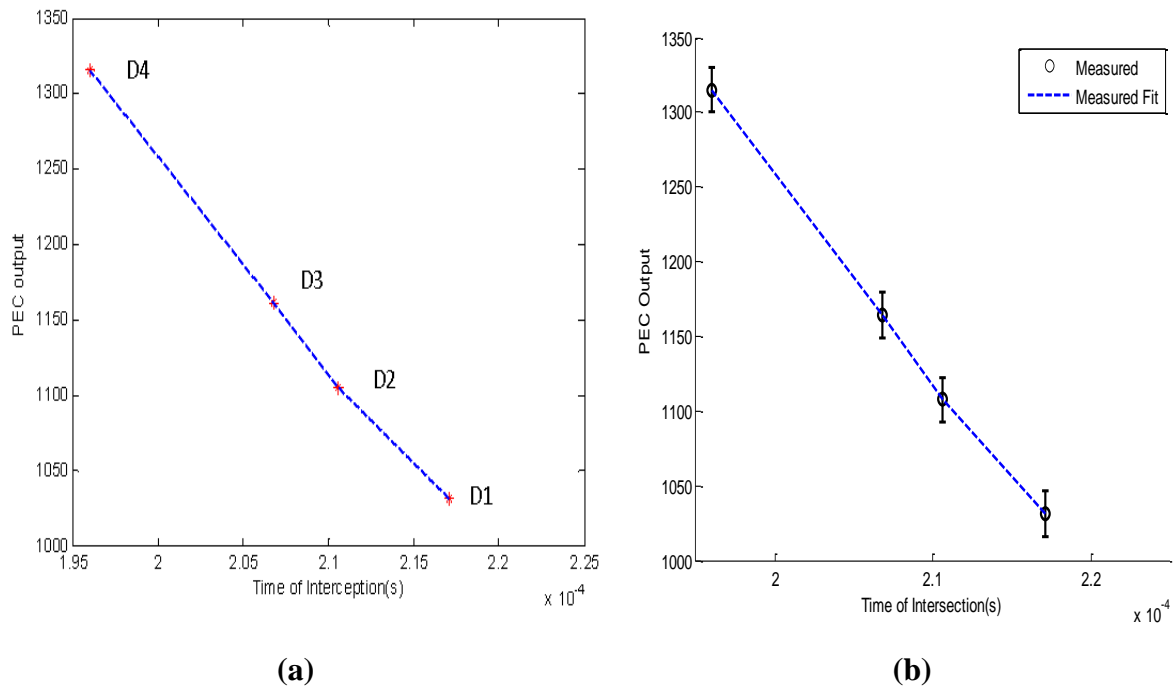
Figure 5.10: Determination of defect depth from PEC output and LOI time of intersection (b) averaged over 3 trials

In contrast to the LOI points obtained for the ferromagnetic material, these exhibit lower amplitude and later time of occurrence. In addition, for ferromagnetic materials as defect depth increases the amplitude of the LOI point reduces whilst its time of occurrence increases. The converse is true of non-ferrous material. This explains the contrast between figures 5.6 and 5.10, hence, each figure can be used to distinguish between the LOI behaviours on the two materials. Again, the second derivative of the PEC response was taken as shown in figure 5.11. It is observed that this curve varied strongly with lift-off. For two distinct defects (defect 4 and 3), the second derivative of the B non-normalised PEC response matches well; meaning that this feature is a measure of the lift-off effect. Thus, whilst the

LOI point is a measure of the defect depth, the second derivative of PEC response is a measure of the lift-off effect.
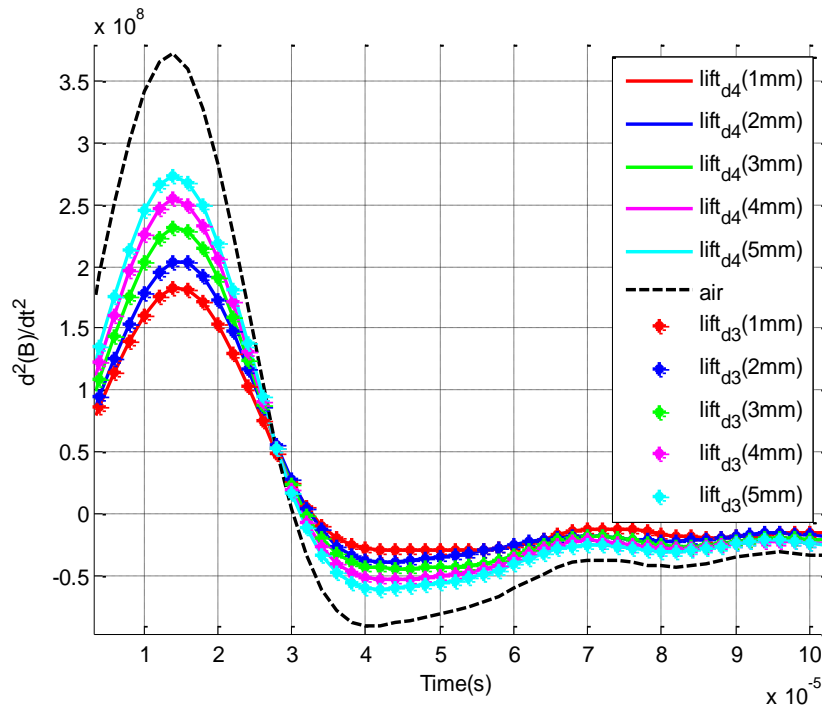
Figure 5.11: Determination of Lift-off Effect from 2nd derivative of PEC response
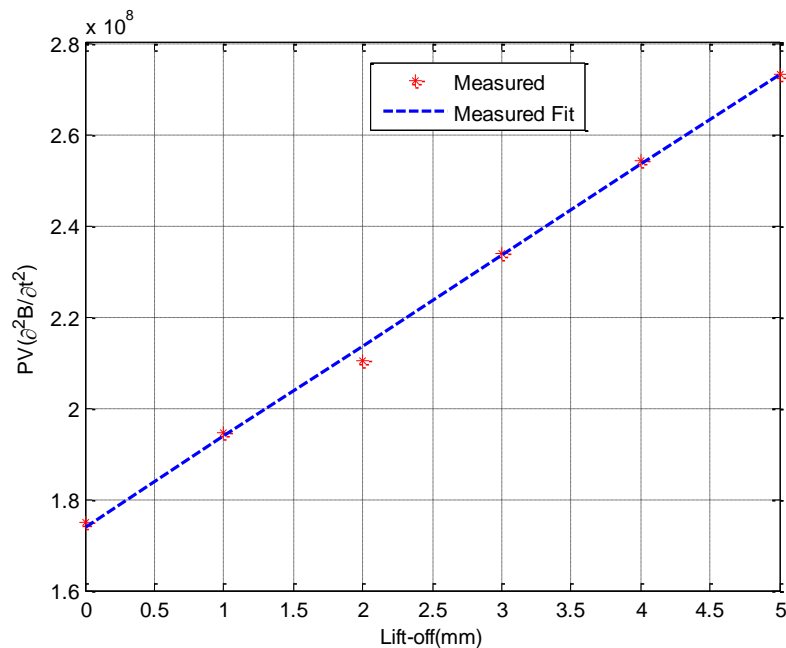
Figure 5.12: Aluminium - Lift-off Estimation Graph [$PV(\partial^2 B / \partial t^2)$ Vs *Lift-off*]

Figure 5.12 provides a means of developing a calibration graph for lift-off estimation as described in section *5.2.1.1.2*. However, it is observed in figure 5.12 that unlike the ferrous sample, the peak values of the second derivative of B non-normalised PEC response [$PV(\partial^2 B / \partial t^2)$] with increasing lift-off defines a linear function which can be generalised by equation 5.3 whilst lift-off values can be estimated with the second part of the equation. Table 5.3 shows the estimated lift-off values from this approach.

$$PV(\partial^2 B / \partial t^2) = 1.9854e7 LO + 1.739e8 \; ; \quad LO = \frac{PV(\partial^2 B / \partial t^2) - 1.739e8}{1.9854e7} \qquad (5.3)$$

Table 5.3: Lift-off Estimation Using LOI Feature (Aluminium)

Actual Lift-off (mm)	Estimated Lift-off (mm)	Relative Error (%)
0	0	-
1	1.0023	0.23
2	2.0046	0.23
3	3.0020	0.07
4	4.0042	0.11
5	5.0015	0.03

5.2.2. Defect Depth Estimation using Slope Feature

A number of researchers [94, 98] have extracted features to identify defects invariant of lift-off effects; here a non-LOI based novel approach to achieve this is illustrated in figure 5.13. At no lift-off, the PEC response is taken as the reference signal (Bref) and the response is also obtained at a given lift-off designated as (B). The differential (ΔB) and normalised differential (ΔBnorm) are then obtained as derivatives of the two responses. With this, a relationship between the peak values of the normalised differential (PV (ΔBnorm)), the lift-off (*X*) and defect depth (d) is obtained. The gradient (m) of this relationship can be correlated to a defect depth invariant of lift-off variation and by an inverse process; the relationship between *m* and *d* is obtained. In the inverse process depicted in the bottom half of Figure 5.13, a measurement at a known lift-off is obtained but without the knowledge of the defect depths, hence, we have defective PEC signals $B_1 \dots B_n$ without prior information about the defect. The peak values of the differential normalised PEC response are obtained for this and plotted against lift-off to determine the gradient. Once the gradient is obtained, the unknown defect depth information can be estimated by the calibrated relationship between

the gradient and defect depth in the forward process producing results that are largely independent of lift-off.
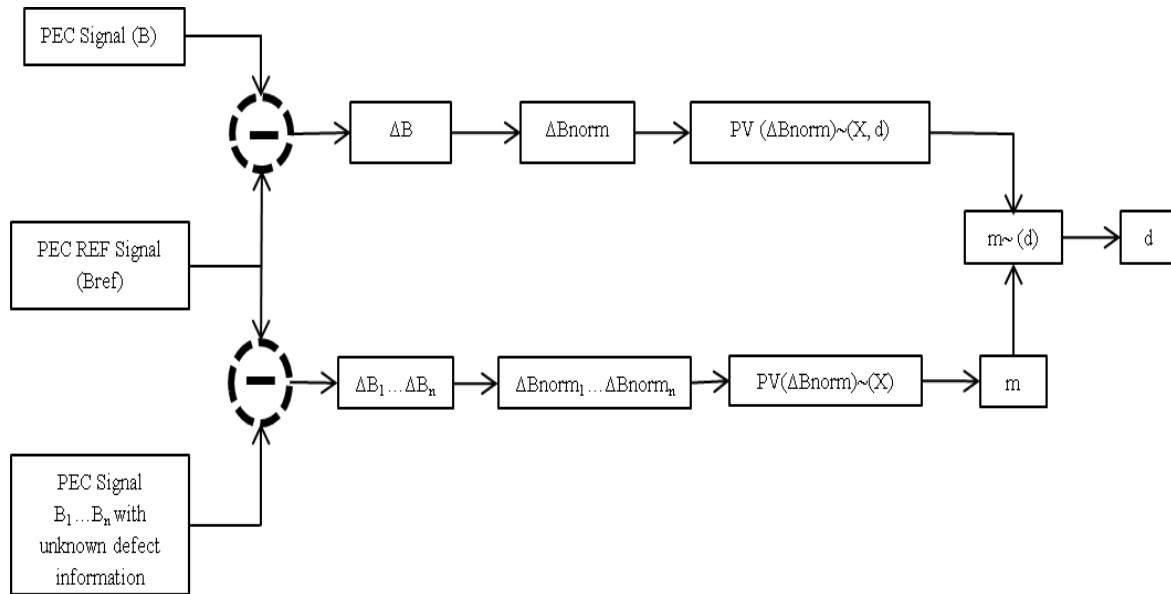
Figure 5.13: A Schematic of the Defect Depth Estimation using Slope Feature

5.2.2.1. Defect Depth Estimation for Ferrous Material

From figure 5.2, we observed that there are four different defects simulated in the calibration test piece. If the normalised differential PEC response (ΔBnorm) of each defect is obtained with varying lift-offs as shown in figure 5.14 for one of the defects, the peak values of the ΔBnorm show a monotonic relationship with lift-off; hence, the gradient of this monotonic relationship changes nonlinearly with the depth of the defects as depicted in figure 5.15. An equation for fitting the curve to extend this relationship is expressed in (5.4). The slope and defect depth satisfy the quadratic function well as the correlation coefficient is 0.99.

$$d = 4.7796E4 * m^2 - 1.8784E3 * m + 19.1728 \qquad (5.4)$$
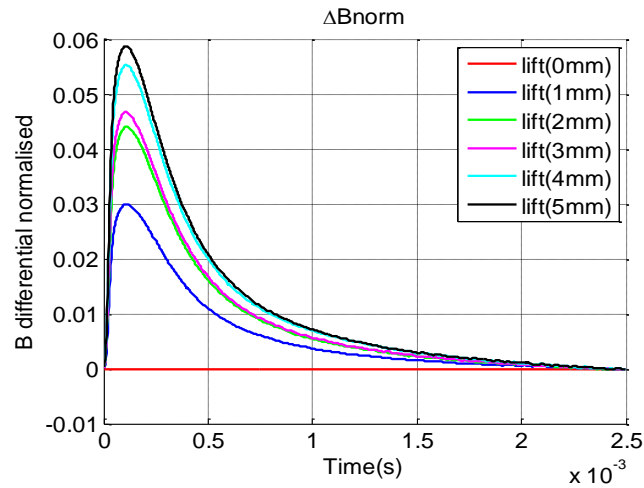
Figure 5.14: Differential Normalised PEC Response of Defects 1 with varying Lift-offs

(a) ΔBnorm Vs. Lift-off

(b) Defect Depth Vs. Slope
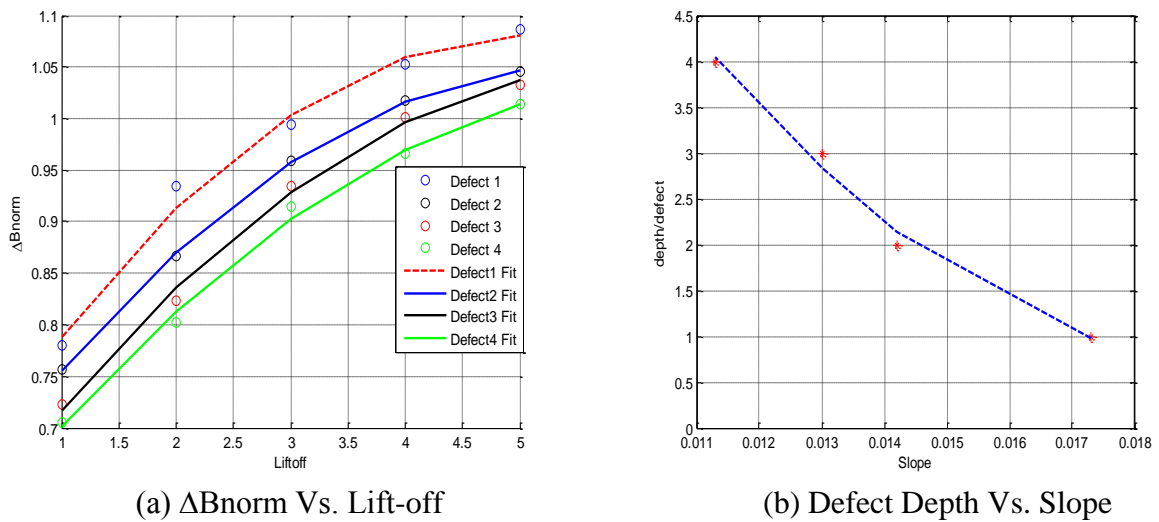
Figure 5.15: (a) Differential Normalised PEC Response of Defects 1-4 with varying Lift-offs (b) Defect Depth Vs. Slope of (a)

5.2.2.2. *Defect Depth Estimation for Non-Ferrous Material*

Using the same defect depth estimation approach described in section 5.2.2, defect depth is quantified without being dependent on the lift-off variations but in relation to the slope as expressed in (5.5). The slope (m) and defect depth (d) satisfy the cubic function well as the correlation coefficient is 0.9999.

$$d = -1.0216E7 * m^3 + 1.1501E6 * m^2 - 4.3194E4 * m + 543.2874 \qquad (5.5)$$

(a) ΔBnorm Vs. Lift-off

(b) Defect Depth Vs. Slope
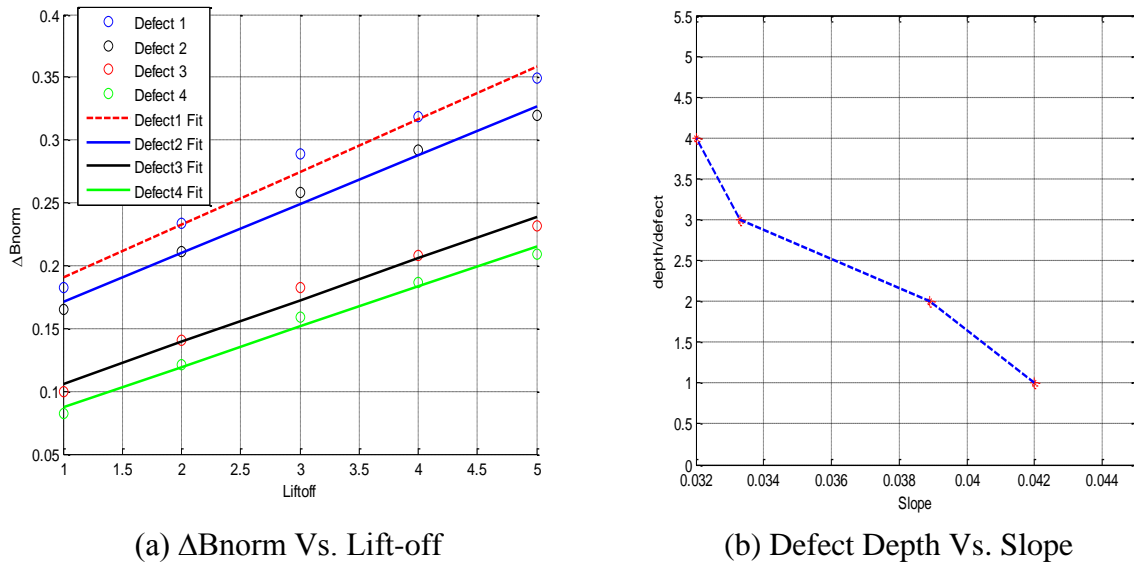
Figure 5.16: PV (ΔBnorm)-Liftoff Curve and Defect depth Vs. Slope

Figure 5.16(a) shows the PV (ΔBnorm)-liftoff curve depicting the monotonic relationship with lift-off; thus, the gradient of this relationship changes nonlinearly with the depth of the defects as shown in figure 5.16(b). In practical applications therefore, the calibration test piece can be tested with unknown defect depths but with known lift-off within the acceptable probe lift-off range. Once the gradient of the PV (ΔBnorm)-liftoff curve is calculated from a graph like figure 5.16(a), the defect depth (d) can be estimated from the cubic function relating *d* and *m* expressed in equation (5.5) and depicted in Figure 5.16(b). However, if the material is ferrous, equation (5.4) would be useful for such estimation. Hence, figures. 5.15(b) and 5.16(b) can be used as calibration charts for defect depth estimation.

5.2.3. LOI Feature Vs Slope Feature for Defect Estimation Approaches

A comparison of the defect estimation capabilities of the two methods developed is explored here by comparing their percentage relative error performance. A summary of this performance indicator for the two material type and methods is given in tables 5.4 and 5.5. It is observed that highest relative percentage error is approximately 4.35 % using the LOI feature and about 7.95% using the slope of (ΔBnorm Vs LO). The LOI feature approach demonstrates superior performance in defect estimation.

Table 5.4: Defect Estimation Using LOI time Feature

Steel Sample			Aluminium Sample		
Actual Defect Depth (mm)	Estimated Defect Depth (mm)	Relative Error (%)	Actual Defect Depth (mm)	Estimated Defect Depth (mm)	Relative Error (%)
1	1.011	1.10	1	1.021	2.10
2	2.010	0.51	2	2.087	4.35
3	3.098	3.27	3	3.010	0.33
4	3.982	0.45	4	4.011	0.28

Table 5.5: Defect Estimation Using Slope of (ΔBnorm *Vs LO*) Curve.

Steel Sample			Aluminium Sample		
Actual Defect Depth (mm)	Estimated Defect Depth (mm)	Relative Error (%)	Actual Defect Depth (mm)	Estimated Defect Depth (mm)	Relative Error (%)
1	0.972	2.80	1	1.033	3.30
2	2.159	7.95	2	2.021	1.05
3	3.098	3.27	3	3.212	7.07
4	3.760	6.00	4	4.024	0.60

5.3. Chapter Summary

This investigation presented a novel method for defect estimation using LOI and liftoff-defect separation in pulsed eddy current for ferromagnetic and non-ferromagnetic materials. Whereas the LOI point is not apparent in ferromagnetic materials, it has been demonstrated that with the first order derivative of the normalised PEC transient response, the LOI feature is preserved. The behaviour of the LOI coordinates with changing defect size provides a means for defect characterisation. Also, the characteristics of the LOI points have been used to delineate and measure varying defect sizes invariant of lift-off effects for both steel and aluminium specimens as those points provide unique coordinates for each defect. In contrast to the LOI point obtained for ferromagnetic materials, non-ferromagnetic materials exhibit lower amplitude and later time of occurrence. Ferromagnetic materials act as flux concentrators hence this explains this behaviour. Again, for non-magnetic samples LOI amplitude decreases with increasing defect size and the LOI time increases with defect size whilst the converse is true for ferromagnetic materials.

This novel approach distinguished the lift-off effect as a second order signal distortion factor and defects as a first order signal factor. This separation provides a means for multiple parameter measurement as coating thickness (lift-off) can be measured simultaneously with defect estimation. Among other things this method provides a direct and less laborious means of inspecting ferromagnetic critical components and structures without the rigour of covering the specimen with a thin layer of conductive, non-magnetic material.

Furthermore, the proposed slope feature extraction technique has demonstrated that defect depths can be estimated with relative lift-off effect independence. To this end, a quadratic curve fitting function defines the relationship between the slope and defect depth for ferrous materials whilst a cubic function defines the same for non-ferrous materials. However, defect estimation using the LOI feature has demonstrated superior performance exhibiting lesser defect sizing discrepancies from the investigation hence would be adopted in the subsequent chapter for defect mapping.

Chapter 6: Defect Mapping and Material Grade Discrimination with LOI Feature

Having investigated the LOI feature, lift-off effects and defect separation in the previous chapter, this chapter focuses on more practical applications of the LOI feature considering various lift-offs, different defects and material types: ferromagnetic and non-ferromagnetic in order to underscore and validate the significance of the LOI point. The first and second applications examined the case of surface breaking defects in a ferromagnetic sample and non-ferromagnetic sample respectively under different lift-offs and two probe configurations. The third study considered the case of natural crack (SCC) in a more complex geometry (cross-section of a steel pipe), which presents varying lift-off due to its curvature. Finally, the last application explored the potential of steel grade discrimination using the LOI feature.

6.1. Defect Mapping with LOI Feature

Since the pulsed eddy current inspection technique is non-contact and requires little or no surface preparation, it can be easily incorporated in an automated scanning system for imaging and defect mapping. It has been adopted for corrosion mapping, flaw detection, material characterisation amongst other things in the field of NDE [8, 77, 139]. With this NDE technique, it is possible to generate an image of localised electromagnetic property variations by mapping the amplitude of the magnetic field response obtained from the scanning of the target test sample. The spatial resolution of the pulsed eddy current images depends on the diameter of the coil and magnetic field broadening [140]. With recent advances, the use of magnetic sensor based PEC probes has become increasingly adopted, which are very sensitive to quasi-static magnetic fields; hence very useful for low frequency measurements and imaging. However, the problem of varying lift-off during the scanning process identified and treated in the previous chapter affects the intensity of the magnetic field. Such variations produce varying strength of induced (pulsed) eddy currents and by extension varying intensity of the secondary field produced by the induced eddy currents. The effect of this is that for small variation in the lift-off, significant changes may be observed in the pulsed eddy current responses leading to spurious signals or false alarm [141]. The LOI point which represents an invariant point less sensitive to lift-off but sensitive to defects and thickness of material samples offers the potential of evaluating the integrity of structures and

components invariant of lift-off effects. This feature is therefore used in PEC imaging as a proof of concept and to underscore its importance.

6.2. Experimental Procedure

To carry out this experimental work, a X-Y Matlab controlled scanning system illustrated in figure 6.1 is used to scan a pulsed eddy current probe over various material samples whose details (defect dimension, sample dimension and material properties) are given in sections 6.3 to 6.8
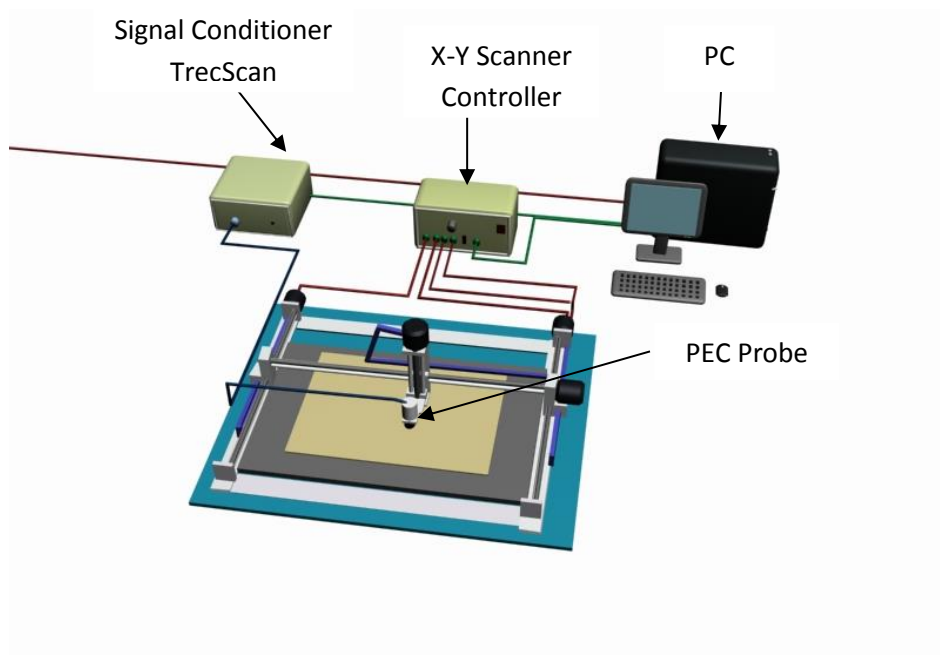
Figure 6.1: PEC Scanning System

The approach adopted for the experimental study is to carry out an initial investigation to determine the LOI points of the test sample thus: foremost, the LOI point of a non-defective part is determined and second the LOI points of the defective parts are determined. The LOI point with the greatest time is used as the time gating time in the experiment. Two pulsed eddy current probes (both of which consist of an excitation coil and a pickup Hall sensor to measure the magnetic field) are employed for these applications. The first is the ferrite core QinetiQ probe whose dimension and details are given in Table 5.1 of chapter 5 and the second is an air core probe previously developed in the Newcastle sensor group whose details are given in Table 6.1 below. Throughout the studies a scanning resolution of 1mm was maintained.

Table 6.1: Parameters for PEC Probe 2

Probe Parameter	Dimension
Inner Diameter of Excitation Coil	8.3mm
Outer Diameter of Excitation Coil	14.3mm
Number of Turns	500 turns
Coil Height	10mm

6.3. Ferromagnetic Sample Description

In this study, a mild steel sample block of dimension 253mm X 50mm X 10mm with machined slit defects to depict surface breaking crack were scan inspected using the LOI time feature and without the LOI time feature for the purpose of comparison. The engineered slits were of constant width (3mm) but with varying depth of 6 and 7 mm respectively as shown in figure 6.2. The steel sample has a conductivity of 6.99 MS/m and a nominal relative permeability of 100. As explained in section 6.2, before the scanning process the LOI points of interest in the steel sample under investigation are pre-determined. The C-scan results and their cross-profile are presented below.
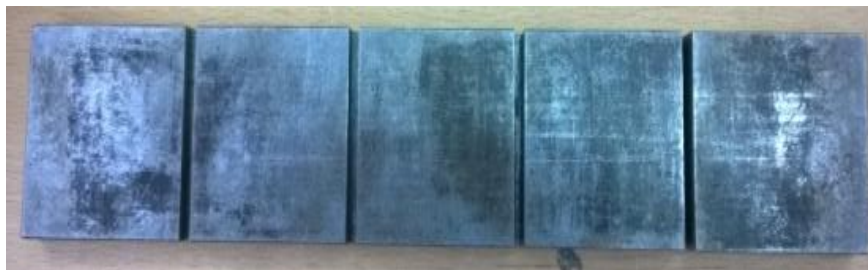
Figure 6.2: Photograph of mild steel sample

6.3.1. Improved Sensitivity to Defect using the LOI time feature

In this section the performance of the LOI time feature in contrast to when the LOI feature is not used is explored to demonstrate the improved sensitivity to surface breaking cracks of the former. C-scan images were acquired at three lift-offs; 0.5, 2.5 and 4.5mm. At each lift-off variation the sensitivity to defect of the acquired C-scans and their cross-profiles with and without the LOI feature are contrasted.

(a)   (b)

Figure 6.3: at Lift-off of 0.5mm (a) C-Scan with LOI time feature in the upper part and without in the Lower (b) Cross-profile of both

It is observed that the sensitivity to defect of the C-Scan when the PEC system is time gated at the LOI time is about 22 times more than when not (at a lift-off of 0.5mm). This significant contrast in the measured field intensity at the defective areas of the C-scan and its cross-profile of figure 6.3 shows that the lift-off effect is effectively compensated for using the LOI time feature.

For this material the LOI time used in time gating the system was obtained from prior investigation of the sample and determined as the LOI time of the thinnest part of the sample. This is so because this LOI time gave the highest sampling frequency (25 KHz) which contains the LOIs of all the defects simulated in the sample.

(a)   (b)

Figure 6.4: at Lift-off of 2.5mm (a) C-Scan with LOI time feature in the upper part and without in the Lower (b) Cross-profile of both

It is observed from figure 6.4 that the sensitivity to defect of the C-Scan when the PEC system is time gated at the LOI time is approximately 20 times better than when not at a lift-off of 2.5mm. This significant difference in defect sensitivity shows that the lift-off effect is well mitigated.

(a)   (b)

Figure 6.5: at Lift-off of 4.5mm (a) C-Scan with LOI time feature in the upper part and without in the Lower (b) Cross-profile of both

It is seen from figure 6.5 that the sensitivity to defect of the C-Scan when the PEC system is time gated at the LOI time is about 22 times better than when not at a lift-off of 4.5mm. This

significant difference in defect sensitivity shows that the LOI time feature is effective for lift-off effect compensation.

Overall, these experimental results show that the time rate of change of the normalised magnetic flux density is higher with the use of the LOI time feature than without this feature which is similar to results obtained in [6]. This means that the latter is less sensitivity to defect whilst the former demonstrates improved sensitivity over defective areas. In order to quantify this improved sensitivity to defects the amplitudes of $\frac{\partial B_{norm}}{\partial t}$ with and without the LOI time feature are calculated and presented in Table 6.2.

Table 6.2: Time rate of change of Normalised Magnetic flux amplitude with and without LOI time feature

Scan Description	Amplitude of $\frac{\partial B_{norm}}{\partial t}$ (au)		Ratio of the amplitudes of $\frac{\partial B_{norm}}{\partial t} LOI$ to $\frac{\partial B_{norm}}{\partial t} NonLOI$	
	Defect 1	Defect 2	Defect 1	Defect 2
Scan with LOI feature at LO=0.5mm*	0.1724	0.2762	21.63	22.73
Scan without LOI feature at LO=0.5mm	0.0080	0.0122		
Scan with LOI feature at LO=2.5mm	0.0312	0.0446	20.26	20.45
Scan without LOI feature at LO=2.5mm	0.0015	0.0022		
Scan with LOI feature at LO=4.5mm	0.0049	0.0056	23.33	20.74
Scan without LOI feature at LO=4.5mm	0.0002	0.0003		

* LO = Lift-off

6.3.2. Comparison of LOI performance for different probe configuration

For the two PEC probes employed in this study, it is of interest to compare their performance when the LOI time feature is used. To this end, C-scans of the same area for the steel sample are presented in figures 6.6 to 6.8.

(a)   **(b)**
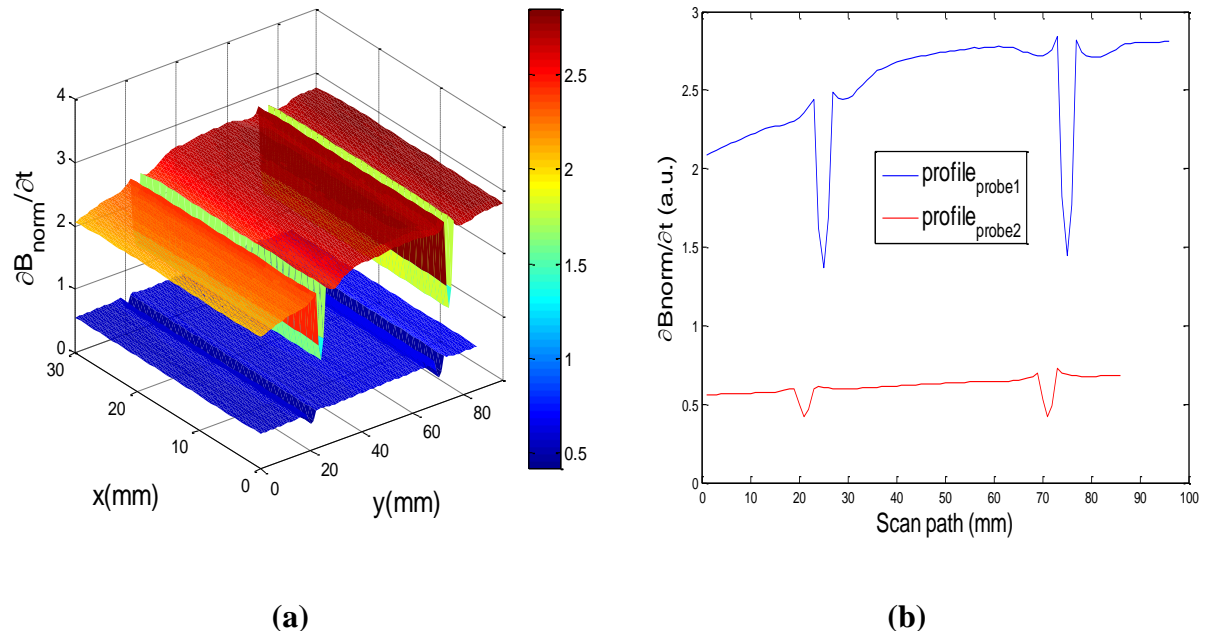
Figure 6.6: at LO=0.5mm (a) C-scan of probe 1 and probe 2 both time gated at the LOI time (b) cross-profile of (a)

(a)   **(b)**
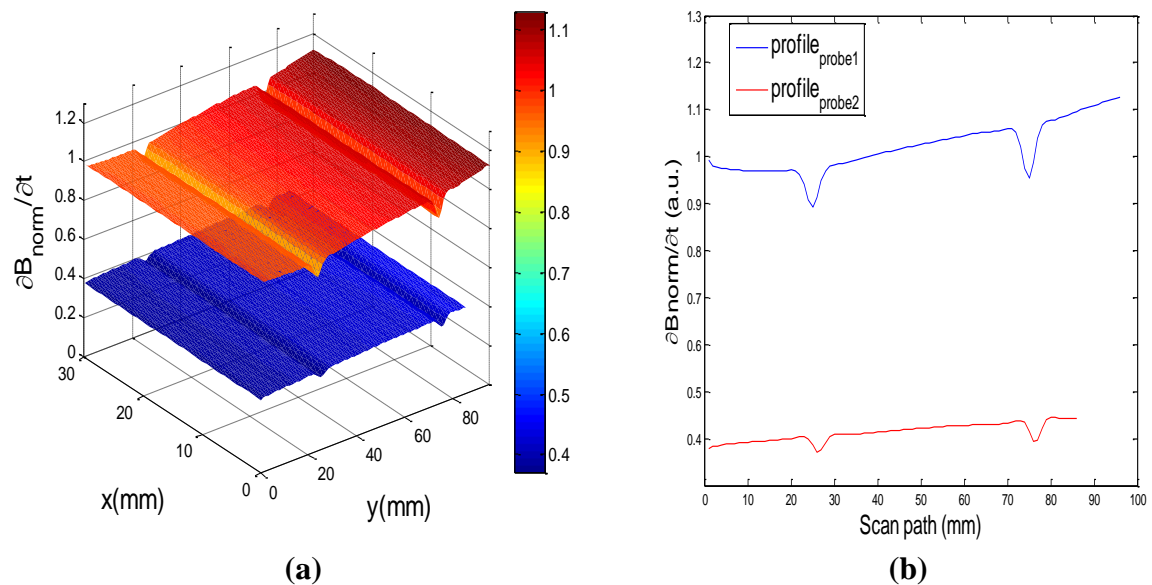
Figure 6.7: at LO=2.5mm (a) C-scan of probe 1 and probe 2 both time gated at the LOI time (b) cross-profile of (a)

(a)

(b)
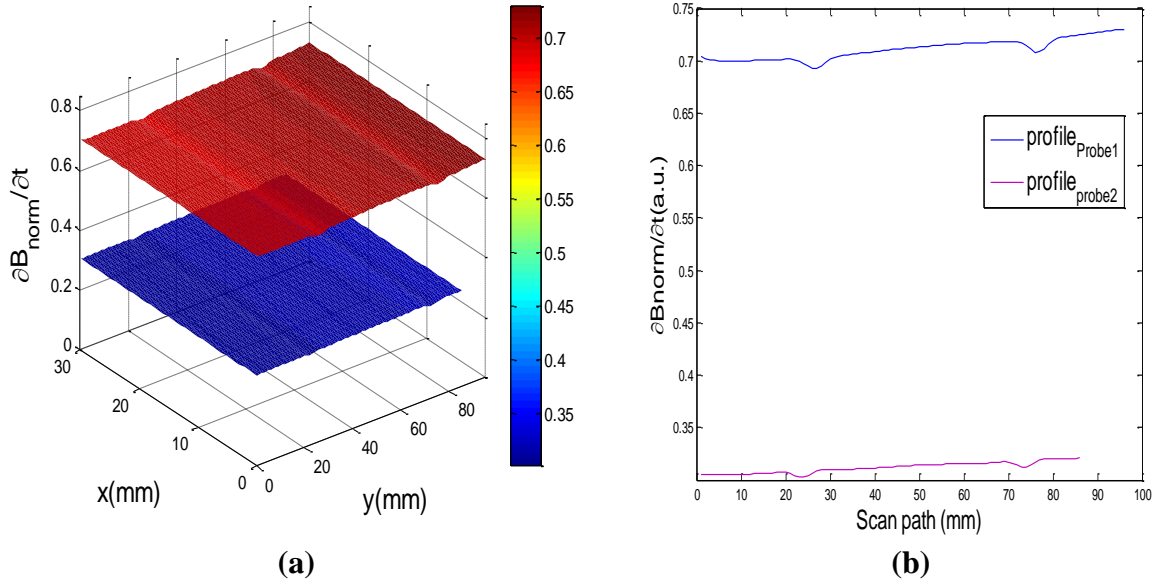
Figure 6.8: at LO=4.5mm (a) C-scan of probe 1 and probe 2 both time gated at the LOI time (b) cross-profile of (a)

From the results above, it can be observed that probe 1 exhibited improved sensitivity to defect than probe 2. One can therefore infer that though the LOI feature is useful in compensating for lift-off effects and provides improved sensitive to defect, however, its level of sensitivity to defect would differ based on probe configuration as well. It is believed that the ferrite core design of probe 1 has enhanced the intensity of the induced pulsed eddy current to the test material. Thus, probe design in conjunction with the LOI feature is a potential tool for lift-off effect compensation. To quantify this improved sensitivity to defects of probe 1 to 2, the amplitudes of $\frac{\partial B_{norm}}{\partial t}$ with the LOI time feature obtained for the two probes are calculated and presented in Table 6.3.

Table 6.3: LOI Performance of Probe 1 and Probe 2 for Steel Sample

Scan Description	Amplitude of $\frac{\partial B_{norm}}{\partial t}$ (au)		Ratio of the amplitudes of $\frac{\partial B_{norm}}{\partial t}\mathrm{Pr}obe_1$ to $\frac{\partial B_{norm}}{\partial t}\mathrm{Pr}obe_2$	
	Defect 1	**Defect 2**	**Defect 1**	**Defect 2**
Scan with Probe 1 at LO=0.5mm	1.0710	1.3730	6.21	4.97
Scan with Probe 2 at LO=0.5mm	0.1724	0.2762		
Scan with Probe 1 at LO=2.5mm	0.0770	0.1049	2.47	2.35
Scan with Probe 2 at LO=2.5mm	0.0312	0.0446		
Scan with Probe 1 at LO=4.5mm	0.0087	0.0104	1.78	1.86
Scan with Probe 2 at LO=4.5mm	0.0049	0.0056		

6.4. Non-Ferromagnetic Sample Description

For the second application, an aluminium sample with electrical conductivity of 25.8MS/m and geometrical dimension of 253mm X 50mm X 10mm was scanned. This had machined slit defects of constant width (3mm) and varying depth 7 and 9 mm to depict surface breaking crack similar to the steel sample. The same approach of inspection using (a) the LOI time feature and (b) without the use of the LOI time feature was followed. As explained in section 6.2, before the scanning process the LOI points of interest in the steel sample under investigation are pre-determined. For this material the LOI time used in time gating the system was determined as the LOI time of the thickest part of the sample. This is so because

this LOI time gave the highest sampling frequency (15 KHz), which contains the LOIs of all the defects simulated in the sample. The C-scans and their cross-profiles obtained from the experimental investigation are presented below.

6.4.1. Improved Sensitivity to Defect using the LOI time feature

In this section, the improved sensitivity to surface breaking cracks in the described aluminium sample with the LOI time feature employed is demonstrated. C-scan images were acquired at three lift-off values as with the steel sample of section 6.3. At each lift-off variation the sensitivity to defect of the acquired C-scans and their cross-profiles with and without the LOI feature are compared.

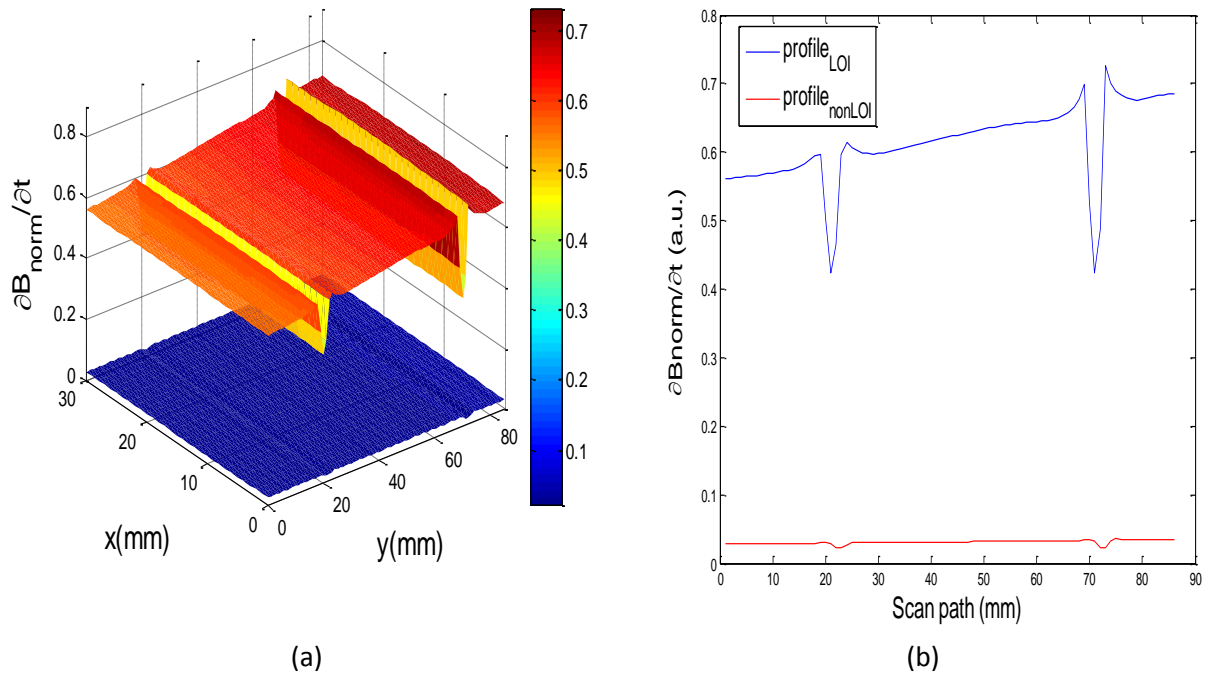(a)   (b)
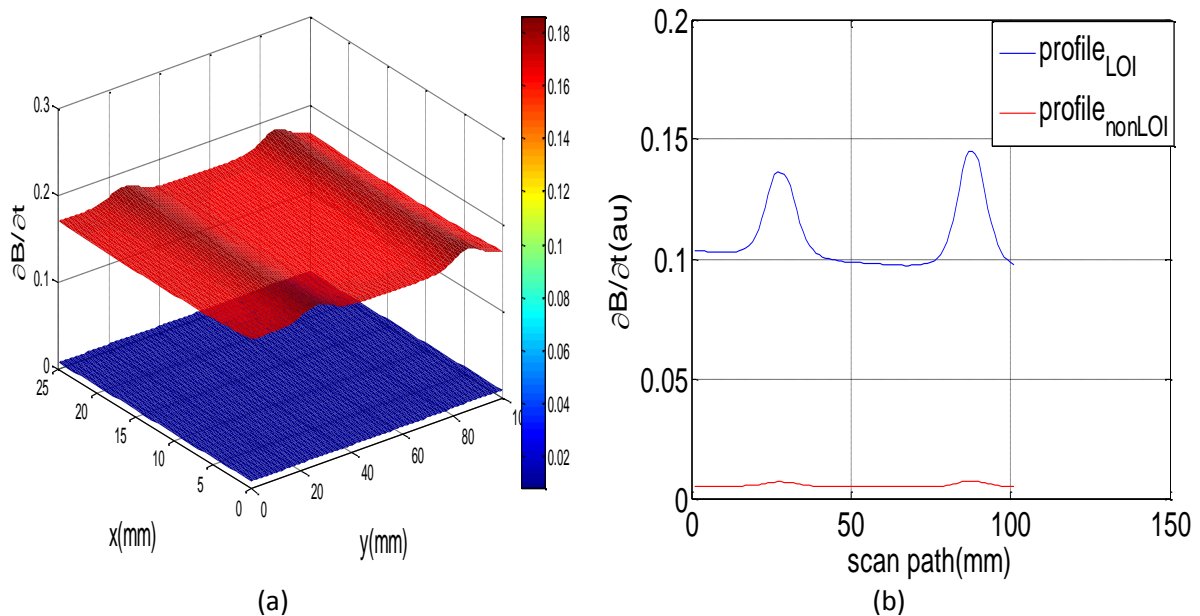
Figure 6.9: at Lift-off of 0.5mm (a) C-Scan with LOI time feature in the upper part and without in the Lower (b) Cross-profile of both

It is observed that at an applied lift-off of 0.5mm, the sensitivity to defect of figure 6.9 when the system is time gated at the LOI time is about 19 times in order of magnitude to the defect sensitivity when the PEC system is not time gated at the LOI point. This significant difference in sensitivity shows that the lift-off effect is well compensated for.

(a)   (b)
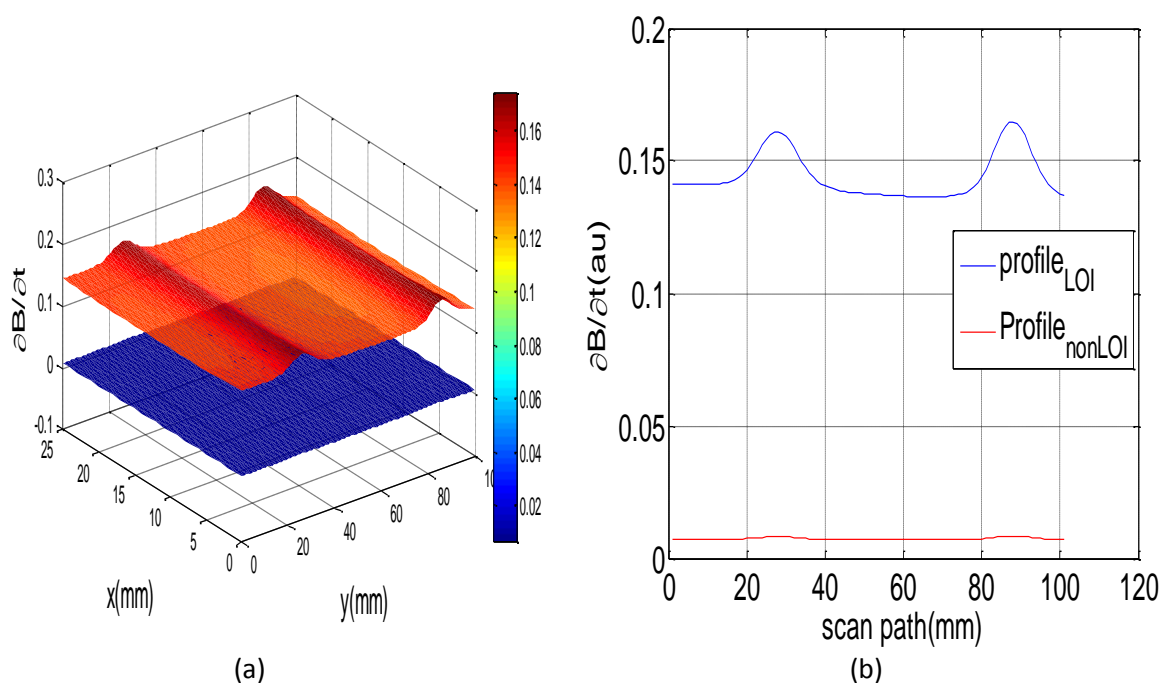
Figure 6.10: at Lift-off of 2.5mm (a) C-Scan with LOI time feature in the upper part and without in the Lower (b) Cross-profile of both

Also at a lift-off of 2.5mm a magnitude of the order of 20.5 (being the mean value of the two defects) is observed between the sensitivity to defect of the C-Scan when the PEC system is time gated at the LOI time and when not. This significant difference in defect sensitivity shows that the lift-off effect is minimised with the LOI time feature.
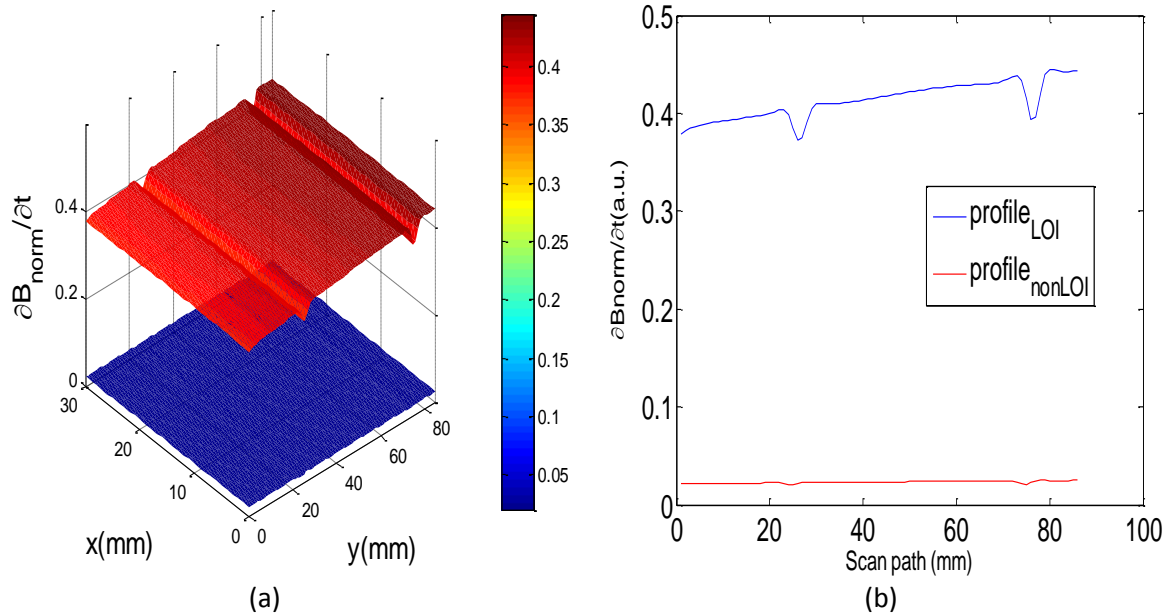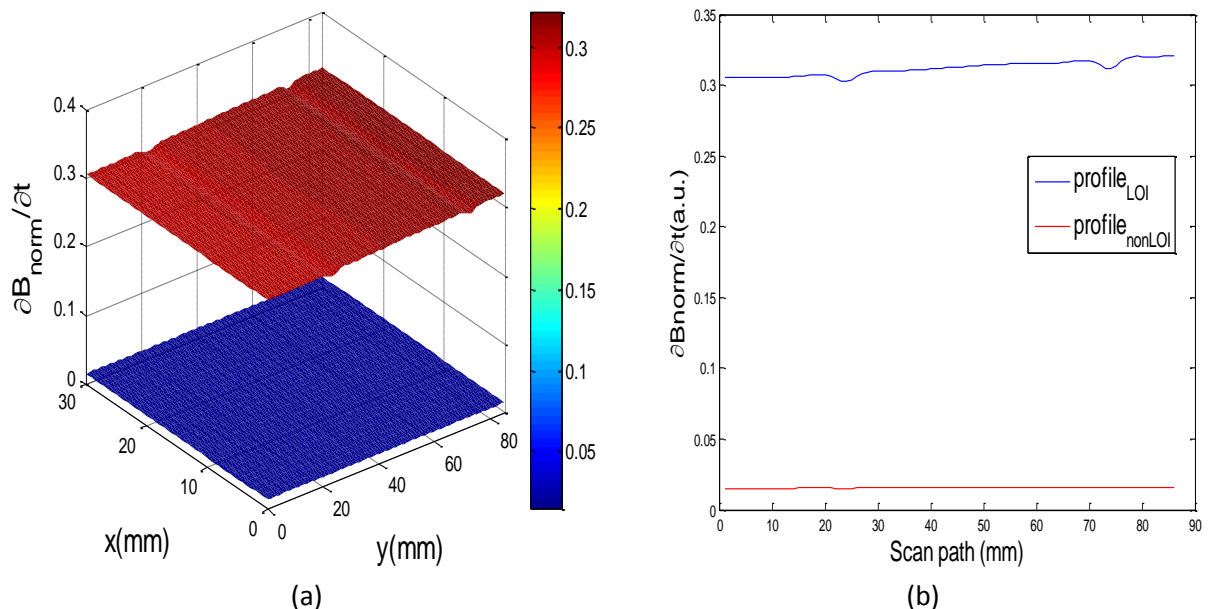

(a)   (b)
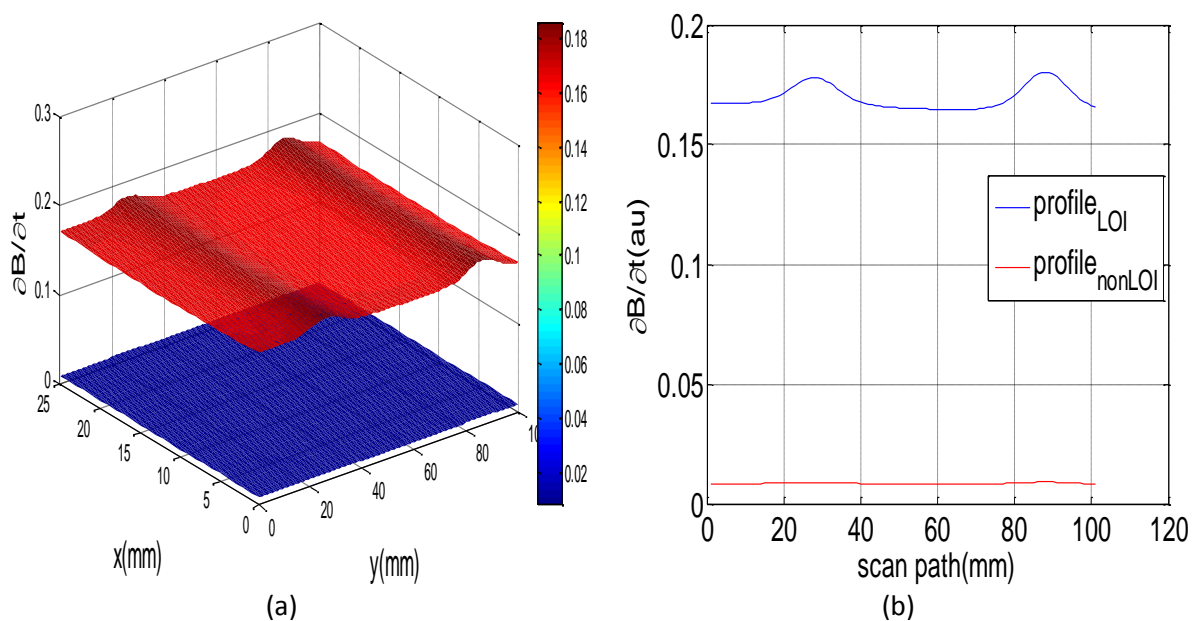
Figure 6.11: at Lift-off of 4.5mm (a) C-Scan with LOI time feature in the upper part and without in the Lower (b) Cross-profile of both

Furthermore, at a higher lift-off of 4.5mm without time gating at the LOI point, degradation in image is observed showing the effect of lift-off; however, one can observe a remarkable improvement in sensitivity to defect of the order of about 20 in comparison with the use of the LOI feature.

Overall, when the LOI feature is employed, the C-scans obtained demonstrated enhanced sensitivity to surface breaking crack than when LOI time feature has not been used, in effect validating the fact that the LOI time depicts a point in time where the lift-off effect is minimal. To quantify this enhanced sensitivity, the amplitudes of the $\frac{\partial B}{\partial t}$ with and without the LOI time feature are calculated and summarised in Table 6.4

Table 6.4: Time rate of change of Magnetic flux density amplitude with and without LOI time feature

Scan Description	Amplitude of $\frac{\partial B}{\partial t}$ (au)		Ratio of the amplitudes of $\frac{\partial B}{\partial t}LOI$ to $\frac{\partial B}{\partial t}NonLOI$	
	Defect 1	Defect 2	Defect 1	Defect 2
Scan with LOI feature at LO=0.5mm*	0.0326	0.2762	19.40	19.27
Scan without LOI feature at LO=0.5mm	0.0017	0.0122		
Scan with LOI feature at LO=2.5mm	0.0196	0.0271	20.52	20.41
Scan without LOI feature at LO=2.5mm	0.0010	0.0013		
Scan with LOI feature at LO=4.5mm	0.0105	0.0140	20.47	19.86
Scan without LOI feature at LO=4.5mm	0.0005	0.0007		

*LO=Lift-off

6.4.2. Comparison of LOI performance for different probe configuration

Here, a comparison of the cross-profile of the two PEC probes employed is carried out to underscore the LOI performance for the different probe designs. The results are presented in figures 6.12 to 6.14.
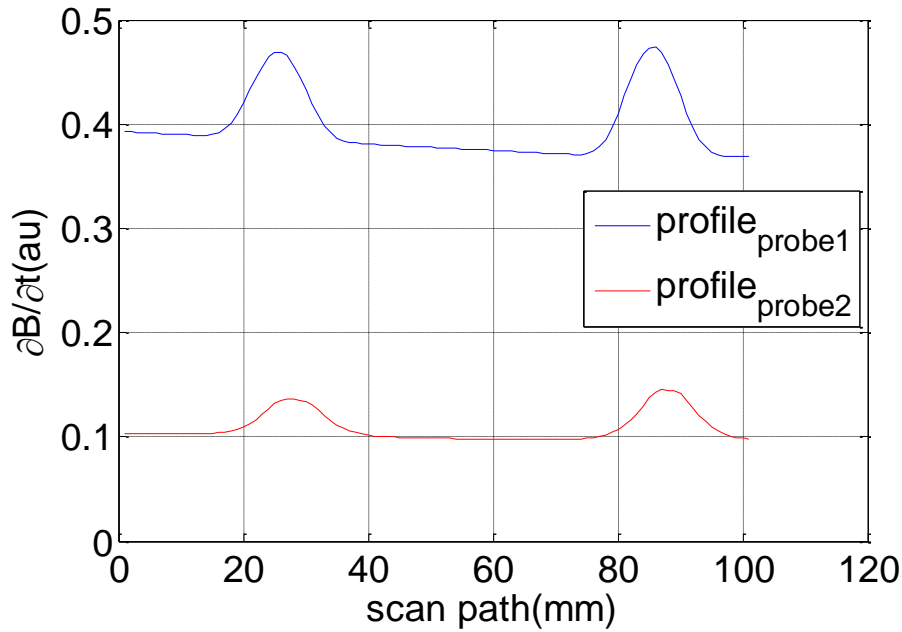
Figure 6.12: at LO=0.5, Cross-profile of probe 1 and probe 2 both time gated at the LOI time
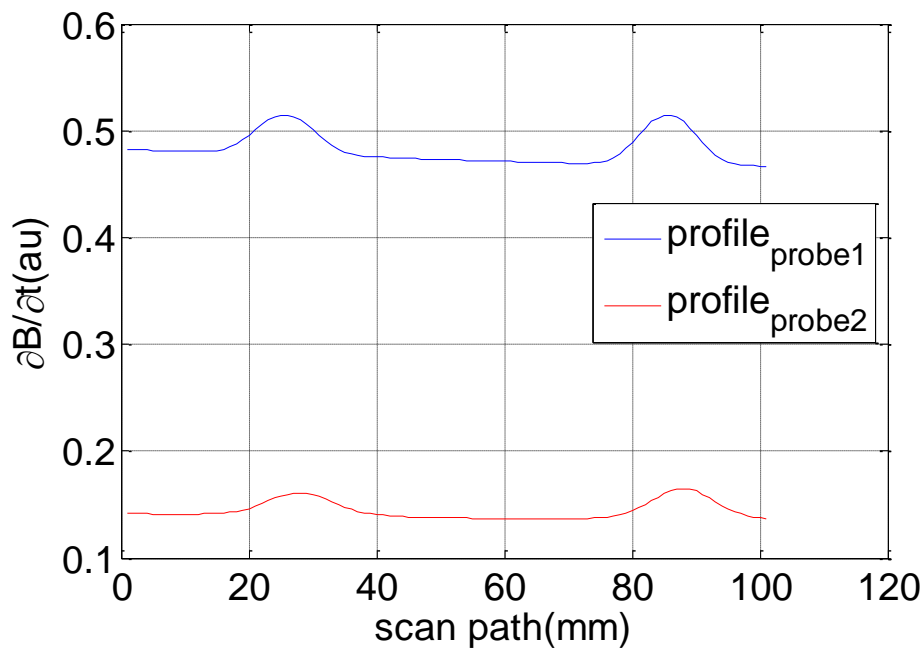
Figure 6.13: At LO=2.5, Cross-profile of probe 1 and probe 2 both time gated at the LOI time
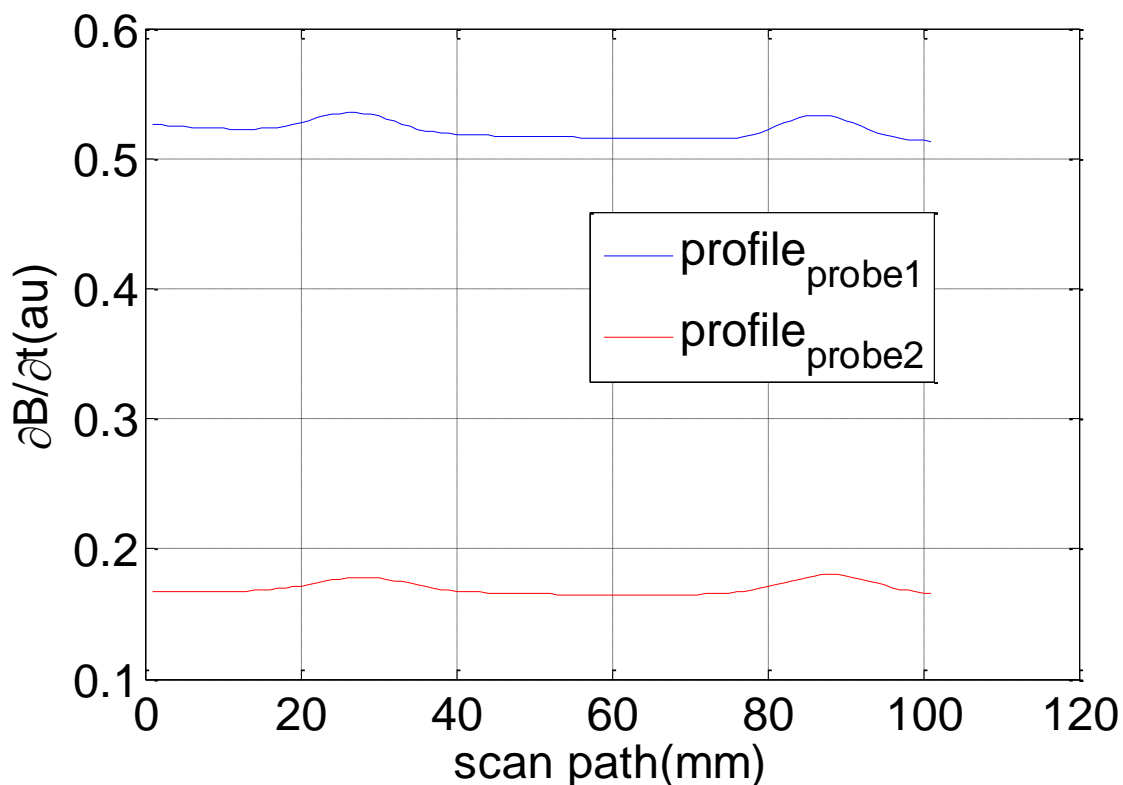
Figure 6.14: At LO=4.5, Cross-profile of probe 1 and probe 2 both time gated at the LOI time

From these results and as observed in the steel sample, probe 1 still demonstrated enhanced sensitivity to defect in comparison to probe 2. A summary of the quantified values for comparison is shown in Table 6.5.

Table 6.5: LOI Performance of Probe 1 and Probe 2 for Aluminium Sample

Scan Description	Amplitude of $\frac{\partial B}{\partial t}$ (au)		Ratio of the amplitudes of $\frac{\partial B}{\partial t}\mathrm{Pr}obe_1$ **to** $\frac{\partial B}{\partial t}\mathrm{Pr}obe_2$	
	Defect 1	Defect 2	Defect 1	Defect 2
Scan with Probe 1 at LO=0.5mm*	0.0797	0.1020	2.42	2.24
Scan with Probe 2 at LO=0.5mm	0.0330	0.0456		

Scan with Probe 1 at LO=2.5mm	0.0334	0.0444	1.72	1.62
Scan with Probe 2 at LO=2.5mm	0.0194	0.0274		
Scan with Probe 1 at LO=4.5mm	0.0124	0.0181	1.18	1.29
Scan with Probe 2 at LO=4.5mm	0.0105	0.0140		

*LO=Lift-off

6.5. Natural Crack: Stress Corrosion Crack Visualisation

The main objective here is to apply the proposed LOI time feature in stress corrosion crack defect visualisation demonstrating an enhanced sensitivity to defect in contrast to classical SCC visualisation. To carry out this investigation therefore, a steel sample with complex geometry (cross-section of a pipe) whose photograph is shown in figure 6.15 is scanned with the LOI time feature and without the LOI feature. With the concave curvature this geometry has, it presents varying lift-off as the probes moves over it. The B-Scan result of an area 100 by 110 mm^2 at a lift-off of 8mm (measured from the centre of the curvature) is shown below. Probe 1 has been used in this scanning process.

Figure 6.15: Photograph of Steel Sample with Stress Corrosion Crack
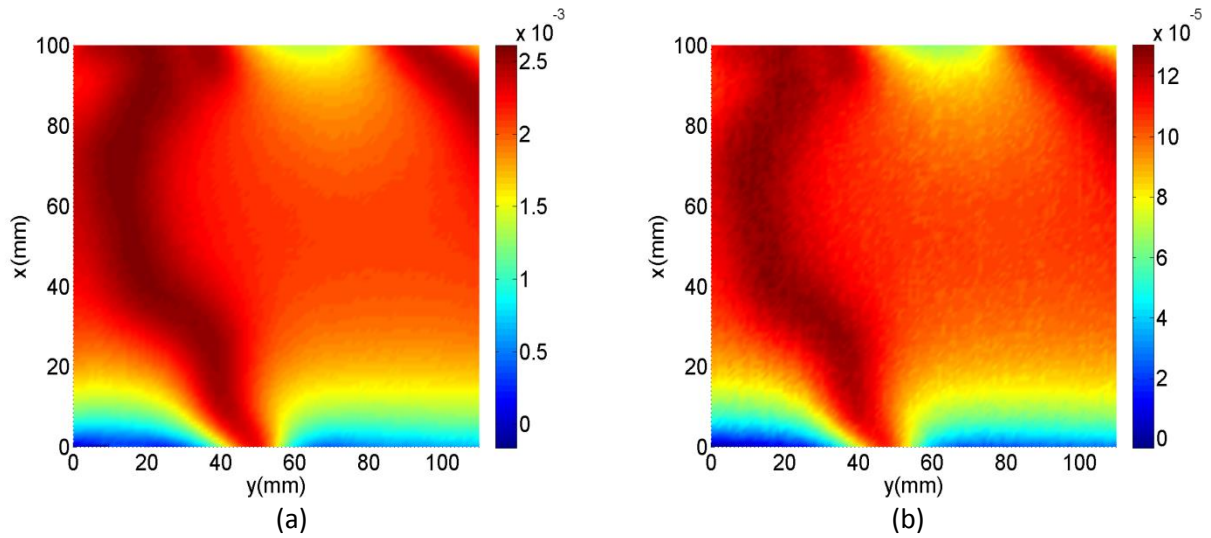
Figure 6.16: B-Scan Result at LO of 8mm (a) when time gated at the LOI time (b) without time gating at the LOI time

Due to the complex nature of the defect shown in figure 6.15, the range of $\frac{\partial B_{norm}}{\partial t}$ values of the defective area is calculated in order to quantify the enhanced sensitivity to defect of figure 6.16(a) in comparison to figure 6.16(b). This is summarised in Table 6.6 below.

Table 6.6: Time rate of change of normalised magnetic flux density with and without LOI feature

Scan Description	Local Range of $\frac{\partial B_{norm}}{\partial t}$	Ratio of the range of $\frac{\partial B_{norm}}{\partial t} LOI$ to $\frac{\partial B_{norm}}{\partial t} NonLOI$
Scan with LOI feature	1.10×10^{-3}	15.83
Scan without LOI feature	6.94×10^{-5}	

6.6. Steel Grade Discrimination Using LOI point

Since the LOI feature is sensitive to variation in the electromagnetic property of a material. One could exploit this variation to material properties (electrical conductivity and permeability) to discriminate between material grades. A demonstration of the potentials of the LOI feature to discriminate between two steel grades of different magnetic permeability is presented here. Steel 1 is 18CrNiMo5 (with 0.2% carbon content) and steel 2 is 42CrMo4 (with 0.4% Carbon content). From figure 6.17 there is a clear distinction between the LOI points of the two steel grades. The steel grade with the lower carbon content has higher amplitude and earlier LOI time while the other with the higher carbon content exhibited lower amplitude and later LOI time.

(a)   **(b)**
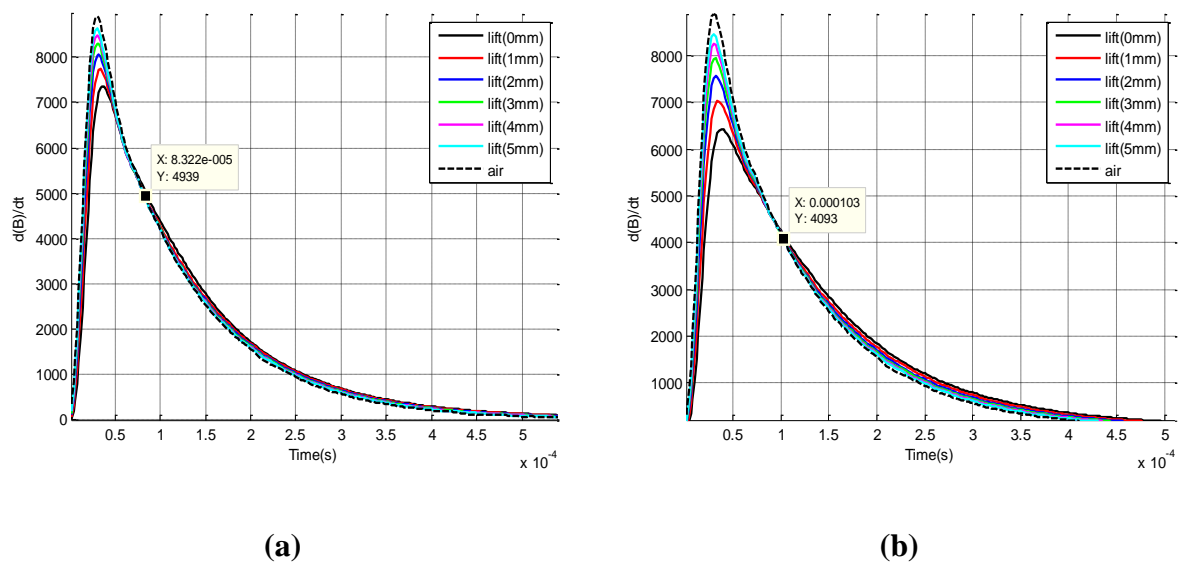
Figure 6.17: (a) Steel 1: 18CrNiMo5 (0.2% Carbon content) (b) Steel 2: 42CrMo4 (0.4% Carbon content)

6.7. Chapter Summary

This chapter presents some practical applications of the LOI time feature for different material types, defect sizes, and lift-offs to highlight the significance of the LOI point in PEC inspection technique. Specifically, a discussion on the experimental setup and approach, details of the probe configuration, material samples and defects were presented. For the first three experimental studies which dealt with PEC imaging for defect mapping, the LOI points

of interest are pre-determined prior to the scanning process. For the steel sample, the LOI of the thinnest part is used as the gating time, while that of the thickest part is used for the aluminium sample; reason being that in each case, these points gave the highest sampling frequency which contains all other LOI points of interest. By extension therefore, one can conclude that the LOI time feature of the thinnest part of ferromagnetic materials is to be used for PEC imaging whilst that of the thickest part should be used when the material is non-ferromagnetic in general.

Amongst other things the chapter brought to light the enhanced sensitivity to defect with the LOI time feature in contrast to when this feature is not used in the scanning process under varying lift-off conditions. In addition, further improvement in sensitivity to defect is achieved when a ferrite core PEC probe is used as against an air-core probe as the former acts as a flux concentrator.

Also, the potential of material grade discrimination is presented and discussed. The steel grade with the lower carbon content has higher amplitude and earlier LOI time while the other with the higher carbon content exhibited lower amplitude and later LOI time. However, the samples available for this particular study is limited, otherwise, it would have been possible to develop and calibration chart to trace this trend and compare it with the traditional PEC material grade discrimination method. It is therefore an area of future research interest.

Chapter 7: Conclusion and Future Works

This piece of research work is summarised and conclusions are drawn on the potentials of multiple parameter based pulsed eddy current technique for non-destructive testing and evaluation. Consequent upon the research outcome, the potential future outlooks are outlined.

7.1. Research Summary

The wide adoption of the (pulsed) eddy current sensing technique for non-destructive testing and evaluation in the oil and gas industry for asset management and structural integrity evaluation due to its attractive attributes such as low cost, broad bandwidth, tolerance to harsh environments, ease of incorporation into an automated system amongst other things is not without its associated challenges. Such challenges, which affect accurate detection and characterisation of defects in the main provides avenues for novel NDT & E approaches to mitigate such. Some notable contributory factors to these challenges has been identified through the search of extant literature; amongst which are the inhomogeneity of the materials, lift-off or coupling variation effect and relatively large lift-off effect due to coating or insulation layer.

The research work started by understanding the theoretical background to pulsed eddy current and electromagnetic NDE. In particular, the (pulsed) eddy current and magnetic diffusion behaviour in the presence of conductive substrate and their associated effects were considered and discussed in chapter 3.

Chapter 4 amongst other things investigated the influence of varying EM properties of a test material on PEC response signals due to inhomogeneity. This work has been able to separate the individual influences of the EM properties through numerical simulation which was validated by experimental studies. A good agreement within 6% error limit is observed in the numerical and experimental results. More importantly, we can infer from the results that conductivity effects are prominent in the rising edge of the transient response; hence, changing the spectral pattern in the frequency domain whilst permeability effects dominate in the stable phase of the transient response thus this effect can be suppressed or reduced by normalization showing that it is only an amplitude change.

From these results therefore, the design of a novel PEC probe which would potentially reduce the effect of changing permeability becomes feasible through normalization. Furthermore, it becomes abundantly clear therefore, that the influence of conductivity is more than an amplitude change, thus to reduce the uncertainty in PEC measurements due to inhomogeneity, electrical conductivity must be mitigated. This finding becomes valuable in PEC applications for displacement measurement, stress and corrosion characterisation of magnetic materials and components.

Again, another great challenge in pulsed eddy current NDE technique is that of lift-off which is as a result of many field realities identified in the literature survey of chapter 2.

A review of extant literature has shown that lift-off tend to mask useful information thereby affecting the accuracy and reliability of PEC measurements; hence, a number of approaches has been researched to solve this problem. An attractive approach to mitigate this problem is the use of the lift-off point of intersection (LOI) feature. However, this LOI feature is not apparent in ferromagnetic materials (which is widely used in the petro-chemical industry) except for a case where a non-magnetic but conductive layer of coating has been applied to the ferromagnetic material.

Fundamental to this approach of a thin-layer conductive non-magnetic material coating of a magnetic material is to drastically reduce the apparent magnetic permeability effects so that the LOI feature can be used for defect characterisation. This is a laborious approach and even less attractive when defective area to be probed is inaccessible say for example due to insulation. To circumvent this limitation therefore, the predicted behaviour of the effect of magnetic permeability in PEC response signal of chapter 4 becomes helpful. This understanding presents a means to mitigate this effect and in turn be able to characterise defect using the LOI feature in ferromagnetic materials without the use of conductive coating layers as demonstrated in chapter 5 of this thesis.

The investigation in chapter 5 presented a novel method for defect estimation using the LOI feature and a liftoff-defect separation in pulsed eddy current for ferromagnetic and non-ferromagnetic materials. Whereas the LOI point is not apparent in ferromagnetic materials, it has been demonstrated that with the first order derivative of the normalised PEC transient response, the LOI feature is preserved. The behaviour of the LOI coordinates with changing

defect size provides a means for defect characterisation. Also, the characteristics of the LOI points have been used to delineate and measure varying defect sizes invariant of lift-off effects for both steel and aluminium specimens as those points provide unique coordinates for each defect. In contrast to the LOI point obtained for ferromagnetic materials, non-ferromagnetic materials exhibit lower amplitude and later time of occurrence. Ferromagnetic materials act as flux concentrators hence this explains this behaviour. Again, for non-magnetic samples LOI amplitude decreases with increasing defect size and the LOI time increases with defect size whilst the converse is true for ferromagnetic materials.

This novel approach distinguished the lift-off effect as a second order signal distortion factor and defects as a first order signal factor. This separation provides a means for multiple parameter measurement as coating thickness (lift-off) can be measured simultaneously with defect estimation. Among other things this method provides a direct and less laborious means of inspecting ferromagnetic critical components and structures without the rigour of covering the specimen with a thin layer of conductive, non-magnetic material.

Furthermore, the proposed feature extraction technique has demonstrated that defect depths can be estimated with relative lift-off effect independence. To this end, a quadratic curve fitting function defines the relationship between the slope and defect depth for ferrous materials whilst a cubic function defines the same for non-ferrous materials.

To underscore the significance of the LOI time feature in PEC inspection technique the penultimate chapter presents some practical applications for different material types, defect sizes, and varying lift-offs. From this PEC imaging applications one can conclude that the LOI time feature of the thinnest part of ferromagnetic materials is to be employed as the sampling time for PEC imaging whilst that of the thickest part should be used when the material is non-ferromagnetic in general.

Amongst other things the research brought to light the enhanced sensitivity to defect with the LOI time feature in contrast to when this feature is not used in the scanning process under varying lift-off conditions. In addition, further improvement in sensitivity to defect is achieved when a ferrite core PEC probe is used as against an air-core probe as the former acts as a flux container.

7.2. Main Contributions

A thorough review of electromagnetic NDE techniques for defect detection and characterisation in petrochemical structures has been carried out. Major benefits and limitations of these techniques and the potential for simultaneous multiple parameter estimation have been assessed.

Delineation of the effects of permeability and conductivity in pulsed eddy current response signal has been investigated. The investigation revealed that electrical conductivity effect is largely associated with the rising edge and magnetic permeability dominates the stable phase of the transient response. In effect, the delineation of these two EM properties provides a laudable potential for multiple parameter measurement.

- This finding becomes valuable in PEC applications for displacement measurement, stress and corrosion characterisation of ferromagnetic materials and components with low and high relative permeability

- This study revealed that the apparent permeability effect in PEC signal response is the recoil or incremental permeability, which can be minimised through normalisation technique.

- Spectral response of PEC is investigated through numerical studies for samples with different magnetic permeability and electrical conductivity. The spectral response shows that high relative permeability affects the spectral magnitude pattern in a more complex manner than low relative permeability samples.

The characteristics and behaviour of lift-off point of intersection (LOI) under different test conditions: lift-off, defect and material properties were studied. A novel lift-off invariant method to estimate defects in ferromagnetic materials which preserves the LOI points has been developed. This approach provides a direct means of inspecting ferromagnetic materials without the rigour of covering it with a thin layer of conductive, non-magnetic material. Furthermore, the effect of lift-off and defect were separated. Whilst defect can be characterised by the LOI points, lift-off effects are seen as a second order PEC signal distortion factor.

- This result is useful for multiple parameter quantification; measurement of coating thickness, simultaneous estimation of lift-off and surface material

discontinuities/defects and for accurate (defect depth estimation for) profiling of the geometry of critical structures like internal pipeline walls.

A mathematical relationship between the peak values of the normalised differential PEC response [*PV* (ΔBnorm)], the lift-off (X) and defect depth (d) is developed for both ferromagnetic and non-ferromagnetic material samples. The gradient (m) of this relationship is correlated to defect depths invariant of lift-off variation in the forward process and by an inverse process defect information (d) can be estimated.

A comparison between the LOI approach and the non-LOI defect estimation approach above shows that the latter is a more involving approach and the relative percentage error (of which the highest value is 7.95%) of the estimated defect sizes is larger relative to those obtained with the LOI approach, which is less involving. Moreover, the LOI approach exhibited lesser defect sizing discrepancy within an approximate relative error value of 4.35% whilst providing the added advantage of estimating lift-off simultaneously.

The mapping of defects under varying lift-offs was investigated using the LOI time feature:

- The comparative analysis of the sensitivity to defect of PEC imaging when the LOI time feature were employed to the traditional PEC imaging demonstrated an enhance sensitivity

- Also, the study demonstrated more enhancements with improved probe configuration; that is, the use of the LOI feature with a ferrite core probe showed improved sensitivity to defect in comparison to the LOI feature in conjunction with an air core probe.

7.3. Suggestions for Future Works

In this work the effect of magnetic permeability and electrical conductivity were delineated in PEC signal response via computer simulation and experimental validation. However, the quantification of these parameters though not addressed in this work is worth considering and exploring with PEC measurements in order that the multiple parameter estimation (defect and lift-off estimates) achieved in this research work can be extended to permeability and conductivity estimation as well. This way, four parameters can be estimated from a single

scan of target areas. This may be realised through the correlation of PEC response to known conductivity and permeability standards and modelling.

In addition, it is believed that the C-scan images obtained in this study through the proposed LOI time feature can still be enhanced. One way of achieving this is by using the amplitude of the LOI point everywhere rather than at a fixed temporal location as employed in this study. This is an area of further investigation. Moreover, in this work, a single PEC inspection probe has been used. To improve on this, for adequate spatial information an array of sensors in contrast to the use of a single inspection probe will be considered.

Furthermore, future work will be channelled towards the extension and optimisation of the proposed multiple parameters separation and estimation of PEC response signal to deal with other challenges associated with inaccuracies in PEC response such as complex geometries and irregular defects formation in critical components and structures in the oil & gas industry to ensure a proactive management of material degradation.

Complex geometries such as varying pipe diameters due to multi-diameter pipeline structure are inevitable in practice. And these geometries are characterised with some ancillaries like flanges, weld joints, amongst others; it would be of interest to accurately delineate between these pipeline features and actual defects. To this end, forward models to understand and predict distinctive features of the aforementioned will form future research directions. Also, time-frequency distribution is a promising tool to unravel the intricacies of PEC response signals for a complete 3-D mapping of complex structures of critical importance. Therefore, linear and bilinear time-frequency analysis like short-term Fourier transform (STFT), wavelet decomposition and Wigner-Ville distribution will be explored.

A number of petrochemical pipelines are fraught with irregular shaped defects resulting from different corrosion mechanism and mechanical damage. Characterising and quantifying such defects is a major challenge. Although in this research, an attempt was geared towards characterising an irregular shaped defect, the bulk of the work concentrated on fairly controlled defect structures. Further research work in this direction would be of immense benefit.

In addition, the potentials of multiple parameter based PEC non-destructive testing and evaluation as against the current trend of multi-sensing modalities will be exploited in in-line inspection tools for pipeline geometric profiling and internal corrosion characterisation and mapping such as top-of-the-line corrosion (TOL) in wet gas lines, an area of further interest to the Petroleum Technology Development Fund.

References

[1]   D. S. Etkin, "Historical overview of oil spills from all sources (1960-1998)," in *Internation Oil Spill Conference Proceedings*, 1999, pp. 1097-1102.

[2]   K. A. Burns, S. D. Garrity, and S. C. Levings, "How Many Years until Mangrove Ecosystems Recover from Catastrophic Oil-Spills," *Marine Pollution Bulletin,* vol. 26, pp. 239-248, May 1993.

[3]   P.C. Nwilo and O. T. Badejo, "Impacts and management of oil spill pollution along the Nigerian coastal areas," *Adminitering Marine Spaces: International Issues - International Federation of Surveyors,* vol. 1, pp. 119-133, September 2006 2006.

[4]   D. S. Etkin, "Analysis of oil spill trends in the US and world wide," in *International Oil Spill Conference Proceedings*, 2001, pp. 1291-1300.

[5]   I. D. Adewale and G. Y. Tian, "Decoupling the Influence of Permeability and Conductivity in Pulsed Eddy-Current Measurements," *Ieee Transactions on Magnetics,* vol. 49, pp. 1119-1127, Mar 2013.

[6]   G. Y. Tian, Y. Z. He, I. Adewale, and A. Simm, "Research on spectral response of pulsed eddy current and NDE applications," *Sensors and Actuators a-Physical,* vol. 189, pp. 313-320, Jan 15 2013.

[7]   I.D. Adewale, G.Y. Tian, S. HuaDong, and G. Xiaoting, "Separation of lift-off effects and defect features in magnetic-sensor based pulsed eddy current signals," *Submitted article to Journal of Applied Physics D,* 2014.

[8]   I.D. Adewale, H. Zhang, G.Y. Tian, and T. Hope, "Defect mapping of steel substrate under fire protection layer using EM NDE methods," in *Nondestructive Evaluation/Testing: New Technology and Application (FENDT) Proceedings*, 2013, pp. 166-171.

[9]   G.Y. Tian, Y. He, I.D. Adewale, and A. Simm, "Spectral behaviour of pulsed eddy current NDE and applications," presented at the 18th World Conference on Nondestructive Testing, Durban, South Africa, 2012.

[10]   C. Argent, *Macaw's Pipeline Defects*. Basingstoke, Hampshire: Yellow Pencil Marketing Co., 2003.

[11]   T. Beuker, H. Lindner, and S. Brockhaus. (2010, June). *Review of Advanced In-Line Inspection: Solutions for Gas Pipelines* [Online]. Available: http://ppsa-online.com/papers/10-Aberdeen/2010-07-Rosen-slides.pdf [Accessed: May, 2014]

[12]   A. Cosham and P. Hopkins, "The effect of dents in pipelines - guidance in the pipeline defect assessment manual," in *ICPVT-10 Proceedings*, Vienna, Austria, 2003, pp. 1 - 9.

[13]   U. R. Evans, *An Introduction to Metallic Corrosion*, 3rd ed. London: Edward Arnold (Publishers) Ltd, 1981.

[14]   A. Handbook, *Corrosion* vol. 13: ASM Internation, 1987.

[15]   S. Caines, F. Khan, and J. Shirokoff, "Analysis of pitting corrosion on steel under insulation in marine environments," *Journal of Loss Prevention in the Process Industries,* vol. 26, pp. 1466-1483, Nov 2013.

[16]   V. A. Kanaikin, D. P. Varlamov, G. S. Korzunin, A. F. Matvienko, B. V. Patramanskii, and V. E. Shcherbinin, "Analysis of Stress-Corrosion Flaws in Main Gas Pipelines Based on the Results of In-Tube Nondestructive Testing," *Russian Journal of Nondestructive Testing,* vol. 45, pp. 317-324, May 2009.

[17]   J.C. Drury and A. Marino. (2000, October). *A comparison of the magnetic flux leakage and ultrasonic methods in the detection and measurement of corrosion pitting*

in ferrous plate and pipe [Online]. Available: www.ndt.net/article/wcndt00/papers/idn701.htm [Accessed: June, 2014]

[18] J.Wilson, M. Kaba, and G. Y. Tian, "New Techniques for the Quantification of Defects Through Pulsed Magnetic Flux Leakage " in *17th World Conference on Nondestructive Testing*, Shanghai, China, 2008.

[19] Z. Haixia and L. Hejun. (2000, June 2014). AAPI magnetic field sensor and its application in NDT. *15th WCNDT Proceedings*.

[20] Y. Lijian, L. Gang, Z. Guoguang, and G. Songwei, "Sensor development and application on the oil-gas pipeline magnetic flux leakage detection," in *Electronic Measurement & Instruments, 2009. ICEMI '09. 9th International Conference Proceedings* 2009, pp. 2-876-2-878.

[21] Y. H. Sun, Y. H. Kang, and C. Qiu, "A permanent magnetic perturbation testing sensor," *Sensors and Actuators a-Physical,* vol. 155, pp. 226-232, Oct 2009.

[22] Y. H. Sun and Y. H. Kang, "Magnetic compression effect in present MFL testing sensor," *Sensors and Actuators a-Physical,* vol. 160, pp. 54-59, May 2010.

[23] H. Dresp. *Magnetic flux leakage* [Online]. Available: http://wiki.iploca.com/display/rtswiki/10.3+The+NDT+toolbox[Accessed:June, 2014]

[24] TSC Inspection Systems. (June). *Alternating current field measurement* [Online]. Available: http://www.tscinspectionsystems.com/acfm [Accessed: May, 2014]

[25] M. P. Papaelias, C. Roberts, C. L. Davis, B. Blakeley, and M. Lugg, "Further developments in high-speed detection of rail rolling contact fatigue using ACFM techniques," *Insight,* vol. 52, pp. 358-360, Jul 2010.

[26] M. J. Knight, F. P. Brennan, and W. D. Dover, "Effect of residual stress on ACFM crack measurements in drill collar threaded connections," *NDT & E International,* vol. 37, pp. 337-343, Jul 2004.

[27] M. Smith and R. Sutherby, "The detection of pipeline SCC flaws using the ACFM technique," *Insight,* vol. 47, pp. 765-768, Dec 2005.

[28] C. K. Low and B. S. Wong, "Defect evaluation using the alternating current field measurement technique," *Insight,* vol. 46, pp. 598-605, Oct 2004.

[29] D. A. Topp. (2000, March). *Quantitative In-Service Inspection using the Alternating Current Field Measurement (ACFM) Method* [Online]. Available: http://www.ndt.net/article/v05n03/topp/topp.htm [Accessed: June, 2014]

[30] M. Smith and C. Laenen, "Inspection of nuclear storage tanks using remotely deployed ACFMT," *Insight,* vol. 49, pp. 598-605, 2004 2004.

[31] K. Krzywosz and F. Ammirato. (1999, June). Performance Based Remote-Field Eddy Current Examination of High-Pressure Feedwater Heaters. *The e-Journal of Nondestructive Testing & Ultrasonics 4(8).* Available: http://www.ndt.net/article/v04n08/krzywosz/krzywosz.htm [Accessed: May, 2014]

[32] H. Ostermeyer and D. Stegemann. (1999, August). *New Aspects for Remote Field Eddy Current Probe Development* [Online]. Available: http://www.ndt.net/article/ecndt98/et/393/393.htm [Accessed: June, 2014]

[33] D. E. Russell, D.D. Mackintosh, and A. A. Shatat, "Remote field testing," in *Electromagnetic Testing: Nondestructive Testing Handbook*. vol. 5, S.S. Udpa and P. O. Moore, Eds., 3rd ed Columbus, OH: American Society for Non-destructive Testing, 2004, pp. 207-226.

[34] Innospection. (December). *Remote Field Eddy Current Technique* [Online]. Available:http://www.innospection.com/pdfs/Remote%20Field%20Eddy%20Current.pdf [Accessed: Dec, 2014]

[35] F. Noorian and A. Sadr, "Computation of transient eddy currents in EMATs using discrete Picard method," in *18th Iranian Conference of Electrical Engrg. (ICEE) Proceedings* Isfahan, Iran, 2010, pp. 727 -731.

[36] W. Shujuan, X. Penghao, K. Lei, and Z. Guofu, "Research on influence of Lorentz force mechanism on EMAT's transduction efficiency in steel plate," in *5th IEEE Conference on Industrial Electronics and Applications (ICIEA 2010) Proceedings*, Taichung, Taiwan, 2010, pp. 196 - 201.

[37] S. Aliouane, M. Hassan, A. Badidi, and A. Benchaala, "Electromagnetic acoustic transducers (EMATs) design evaluation of their performances," in *15th World Conference on NDT (WCNDT 2000) Proceedings*, Rome, 2000.

[38] S. Starman. and V. Matz, "Separation of signals acquired with EMAT in dual coil configuration," in *17th World Conference on NDT (WCNDT) Proceedings*, Shanghai, China, 2008.

[39] R. S. Edwards, A. Sophian, S. Dixon, G. Y. Tian, and X. Jian, "Dual EMAT and PEC non-contact probe: applications to defect testing," *NDT & E International,* vol. 39, pp. 45-52, Jan 2006.

[40] H. Kwun and A. E. Holt, "Feasibility of under-lagging corrosion detection in steel pipe using the magnetostrictive sensor technique," *NDT & E International,* vol. 28, pp. 211 - 214, 1995.

[41] F. T. Calkins, A. B. Flatau, and M. J. Dapin, "Overview of magnetostrictive sensor technology," *Journal of Intelligent Material Systems and Structures,* vol. 18, pp. 1057-1066, Oct 2007.

[42] A. Vinogradov, "Method and system for generation of torsional guided waves using a ferromagnetic strip sensor," US 7573261 B1, 2009.

[43] Y. G. Kim, H. S. Moon, K. J. Park, and J. K. Lee, "Generating and detecting torsional guided waves using magnetostrictive sensors of crossed coils," *NDT & E International,* vol. 44, pp. 145-151, Mar 2011.

[44] P. Robert, *Electrical and Magnetic Properties of Materials*: Artech House Inc., 1988.

[45] S. Land. (May). *Magnetostrictive linear position sensor* [Online]. Available: http://www.sensorland.com/HowPage024.html [Accessed: June, 2014]

[46] P. Xu, S. Huang, and Z. Wei, "Differential eddy current testing sensor composed of double gradient winding coils for crack detection," in *Sensors Applications Symposium (SAS), 2010 IEEE*, Limerick, Ireland, 2010, pp. 59 - 63.

[47] L. Janousek, K. Capova, N. Yusa, and K. Miya, "Multiprobe inspection for enhancing sizing ability in eddy current nondestructive testing," *Ieee Transactions on Magnetics,* vol. 44, pp. 1618-1621, Jun 2008.

[48] Y. Cha, K. H. Kim, J. Shon, Y. H. Kim, and J. Kim, "Surface Flaws Detection Using AC Magnetic Field Sensing by a Thin Film Inductive Microsensor " *Ieee Transactions on Magnetics,* vol. 44, pp. 4022 - 4025, 2008.

[49] J. Garcia-Martin, J. Gomez-Gil, and E. Vazquez-Sanchez, "Non-Destructive Techniques Based on Eddy Current Testing," *Sensors,* vol. 11, pp. 2525-2565, Mar 2011.

[50] R. Ghoni, M. Dollah, A. Sulaiman, and F. M. Ibrahim. (2014, Defect characterisation based on eddy current techniques: technical review. *Advances in Mechanical Engineering 2014*.

[51] L. B. Pedersen, K. A. Magnusson, and Y. Zhengsheng, "Eddy current testing of thin layers using co-planar coils," *Research in Nondestructive Evaluation,* vol. 12, pp. 53-64, 2000.

[52]   D. Mercier, J. Lesage, X. Decoopman, and D. Chicot, "Eddy currents and hardness testing for evaluation of steel decarburizing," *NDT & E International,* vol. 39, pp. 652-660, Dec 2006.

[53]   D. F. He and M. Yoshizawa, "Saw-wave excitation eddy-current NDE based on HTS RF SQUID," *Ieee Transactions on Applied Superconductivity,* vol. 13, pp. 3803-3806, Sep 2003.

[54]   C. Lee, M. J. Johnson, and N. Nakagawa, "Development of a pulsed eddy current system and its characterization," *Review of Progress in Quantitative Nondestructive Evaluation, Vols 26A and 26B,* vol. 894, pp. 354-361, 2007.

[55]   C. P. Dolabdjian, L. Perez, V. O. De Haan, and P. A. De Jong, "Performance of magnetic pulsed-eddy-current system using high dynamic and high linearity improved giant magnetoresistance magnetometer," *Ieee Sensors Journal,* vol. 6, pp. 1511-1517, Dec 2006.

[56]   V. O. De Haan, P. A. De Jong, L. Perez, and C. Dolabdjian, "Towards material characterisation and thickness measurements using pulsed eddy currents implemented with an improved giant magneto resistance magnetometer," in *9th European NDT Conference (ECNDT 2006)*, Berlin, Germany, 2006, pp. 1 - 8.

[57]   V. O. De Haan and P. A. D. Jong, "Simultaneous measurement of material properties and thickness of carbon steel plates using pulsed eddy currents," in *16th World Conference on NDT (WCNDT 2004)*, Montreal, Canada, 2004.

[58]   J. M. Buckley. *An introduction to eddy current testing, theory and technology* [Online]. Available: http://joe.buckley.net/papers/eddyc.pdf [Accessed: May, 2014]

[59]   C. Murner and J. P. Hansen, "Buried corrosion detection in multi-layer airframe structures using pulsed eddy current," in *17th World Conference on NDT (WCNDT) Proceedings*, Shanghai, China, 2008.

[60]   G. Y. Tian, Z. X. Zhao, and R. W. Baines, "The research of inhomogeneity in eddy current sensors," *Sensors and Actuators a-Physical,* vol. 69, pp. 148-151, Aug 15 1998.

[61]   N. Karimian, J. W. Wilson, A. J. Peyton, W. Yin, J. Liu, and C. L. Davis, "Differential permeability behaviour of P9 and T22 power station Steels," *Journal of Magnetism and Magnetic Materials,* vol. 352, pp. 81-90, Feb 2014.

[62]   E. Uzal and J. H. Rose, "The Impedance of Eddy-Current Probes above Layered Metals Whose Conductivity and Permeability Vary Continuously," *Ieee Transactions on Magnetics,* vol. 29, pp. 1869-1873, Mar 1993.

[63]   S. Ghanei, M. Kashefi, and M. Mazinani, "Comparative study of eddy current and Barkhausen noise nondestructive testing methods in microstructural examination of ferrite-martensite dual-phase steel," *Journal of Magnetism and Magnetic Materials,* vol. 356, pp. 103-110, Apr 2014.

[64]   E. Uzal, I. Ozkol, and M. O. Kaya, "Impedance of a coil surrounding an infinite cylinder with an arbitrary radial conductivity profile," *Ieee Transactions on Magnetics,* vol. 34, pp. 213-217, Jan 1998.

[65]   K. R. Shao, Y. G. Guo, and J. D. Lavers, "Multiresolution analysis for reconstruction of conductivity profiles in eddy current nondestructive evaluation using probe impedance data," *Ieee Transactions on Magnetics,* vol. 40, pp. 2101-2103, Jul 2004.

[66]   N. Littrell, "Understanding and mitigating shaft runout," *Orbit,* vol. 25, pp. 5-17, 2005.

[67]   Y. T. Yu, G. Y. Tian, X. H. Li, and A. Simm, "An approach to ERO problem in displacement eddy current sensor," *Nondestructive Testing and Evaluation,* vol. 28, pp. 195-207, Sep 1 2013.

[68]   W. Yin, R. Binns, S. J. Dickinson, C. Davis, and A. J. Peyton, "Analysis of the lift-off effect of phase spectra for eddy current sensors," in *IEEE Instrumentation and Measurement Technology Conference (IMTC 2005) Proceedings*, Ottawa, Canada, 2005, pp. 1779 - 1784.

[69]   G. Y. Tian, Y. Li, and C. Mandache, "Study of Lift-Off Invariance for Pulsed Eddy-Current Signals," *Ieee Transactions on Magnetics,* vol. 45, pp. 184-191, Jan 2009.

[70]   A. Fahr, *Aeronautical Applications of Non-destructive Testing* vol. 1. Lancaster, Pennyslvania: DEstech Publications, Inc., 2013.

[71]   W. L. Yin, R. Binns, S. J. Dickinson, C. Davis, and A. J. Peyton, "Analysis of the liftoff effect of phase spectra for eddy current sensors," *Ieee Transactions on Instrumentation and Measurement,* vol. 56, pp. 2775-2781, Dec 2007.

[72]   L. Shu, H. Songling, and Z. Wei, "Development of differential probes in pulsed eddy current testing for noise suppression," *Sensor and Actuator A,* vol. 135, pp. 675 - 679, 2007.

[73]   L. A. N. M. Lopez, D. K. S. Ting, and B. R. Upadhyaya, "Removing Eddy-Current probe wobble noise from steam generator tubes testing using Wavelet Transform," *Progress in Nuclear Energy,* vol. 50, pp. 828-835, Sep 2008.

[74]   G. Y. Tian and A. Sophian, "Reduction of lift-off effects for pulsed eddy current NDT," *NDT & E International,* vol. 38, pp. 319-324, Jun 2005.

[75]   T. P. Theodoulidis, "Analytical modeling of wobble in eddy current tube testing with bobbin coils," *Research in Nondestructive Evaluation,* vol. 14, pp. 111-126, Jun 2002.

[76]   M. S. Safizadeh and M. Hasanian, "Gas pipeline corrosion mapping using pulsed eddy current technique," *International Journal of Advanced Design and Manufacturing,* vol. 5, pp. 11- 18, 2011.

[77]   R. A. Smith, G. R. Hugo, and D. J. Harrison, "Essential factors in improving the characterisation of cracks and corrosion using transient eddy current " in *6th Joint FAA/NASA/DoD Conference on Aging Aircraft Proceedings*, San Francisco, 2002, pp. 1-41.

[78]   T. Theodoulidis and J. R. Bowler, "Interaction of an Eddy-Current Coil With a Right-Angled Conductive Wedge," *Ieee Transactions on Magnetics,* vol. 46, pp. 1034-1042, Apr 2010.

[79]   T. P. Theodoulidis and J. R. Bowler, "Eddy current coil interaction with a right-angled conductive wedge," *Proceedings of the Royal Society a-Mathematical Physical and Engineering Sciences,* vol. 461, pp. 3123-3139, Oct 8 2005.

[80]   *Electromagnetic Testing: Non-destructive Testing Handbook*, 3rd ed. vol. 5. Columbus, OH: ASNT Press, 2004.

[81]   H. M. G. Ramos, O. Postolache, F. C. Alegria, and A. L. Ribeiro, "Using the Skin Effect to Estimate Cracks Depths in Mettalic Structures," *I2mtc: 2009 Ieee Instrumentation & Measurement Technology Conference, Vols 1-3,* pp. 1335-1340, 2009.

[82]   R.A. Smith and G.R. Hugo, "Transient eddy current NDE for ageing aircraft - capabilities and limitations," *Insight,* vol. 43, pp. 14-25, Jan 2001.

[83]   Y. Li, G. Y. Tian, and A. Simm, "Fast analytical modelling for pulsed eddy current evaluation," *NDT & E International,* vol. 41, pp. 477-483, Sep 2008.

[84]   G. Y. Tian and A. Sophian, "Study of magnetic sensors for pulsed eddy current techniques," *Insight,* vol. 47, pp. 277-279, May 2005.

[85]   P. P. L. Regtien, *Sensors for mechatronics*, 1st ed. Amsterdam ; New York: Elsevier, 2012.

[86]   C. Roumenin, S. Lozanova, and S. Noykov, "Experimental evidence of magnetically controlled surface current in hall devices," *Sensors and Actuators a-Physical,* vol. 175, pp. 47-52, Mar 2012.

[87]   L. B. Bai, G. Y. Tian, A. Simm, S. L. Tian, and Y. H. Cheng, "Fast crack profile reconstruction using pulsed eddy current signals," *NDT & E International,* vol. 54, pp. 37-44, Mar 2013.

[88]   Y. Z. He, F. L. Luo, M. C. Pan, F. B. Weng, X. C. Hu, J. Z. Gao, and B. Liu, "Pulsed eddy current technique for defect detection in aircraft riveted structures," *NDT & E International,* vol. 43, pp. 176-181, Mar 2010.

[89]   M Morozov, G.Y. Tian, and P.J. Withers, "The pulsed eddy current response to applied loading of various aluminum alloys," *NDT & E International,* vol. 43, pp. 493-500, Sep 2010.

[90]   B. Lebrun, Y. Jayet, and J. C. Baboux, "Pulsed eddy current signal analysis: Application to the experimental detection and characterization of deep flaws in highly conductive materials," *NDT & E International,* vol. 30, pp. 163-170, Jun 1997.

[91]   S. Hosseini and A. A. Lakis, "Application of time-frequency analysis for automatic hidden corrosion detection in a multilayer aluminum structure using pulsed eddy current," *NDT & E International,* vol. 47, pp. 70-79, Apr 2012.

[92]   J. H. V. Lefebvre and C. Mandache, "Pulsed eddy current measurement of lift-off," *Review of Progress in Quantitative Nondestructive Evaluation, Vols 25A and 25B,* vol. 820, pp. 669-676, 2006.

[93]   D. Kim, L. Udpa, and S. S. Udpa, "Lift-off invariance transformations for eddy current nondestructive evaluation signals," *Review of Progress in Quantitative Nondestructive Evaluation, Vols 21a & B,* vol. 615, pp. 615-622, 2002.

[94]   Y. Z. He, M. C. Pan, F. L. Luo, and G. Y. Tian, "Reduction of Lift-Off Effects in Pulsed Eddy Current for Defect Classification," *Ieee Transactions on Magnetics,* vol. 47, pp. 4753-4760, Dec 2011.

[95]   H. Hoshikawa, K. Koyama, and Y. Naruse, "Detecting weld zone over anticorrosion painting by rotating uniform eddy current probe," *Review of Progress in Quantitative Nondestructive Evaluation, Vols 24A and 24B,* vol. 760, pp. 502-508, 2005.

[96]   S. Giguere and S. J. M. Dubois, "Pulsed eddy current: Finding corrosion independently of transducer lift-off," *Review of Progress in Quantitative Nondestructive Evaluation, Vols 19a and 19b,* vol. 509, pp. 449-456, 2000.

[97]   C. Mandache and J. H. V. Lefebvre, "Transient and harmonic eddy currents: Lift-off point of intersection," *NDT & E International,* vol. 39, pp. 57-60, Jan 2006.

[98]   A. L. Ribeiro, H. G. Ramos, and J. C. Arez, "Liftoff insensitive thickness measurement of aluminum plates using harmonic eddy current excitation and a GMR sensor," *Measurement,* vol. 45, pp. 2246-2253, Nov 2012.

[99]   C. V. Mandache and J. H. V. Lefebvre, "Electromagnetic Enhancement of Pulsed Eddy Current Signals," *Review of Progress in Quantitative Nondestructive Evaluation,* vol. 26, pp. 318-324, 2007.

[100]   J. H. V. Lefebvre and C. Mandache, "Pulsed eddy current thickness measurement of conductive layers over ferromagnetic substrates," *International Journal of Applied Electromagnetics and Mechanics,* vol. 27, pp. 1-8, 2008.

[101]   P. B. Petrovic and Z. Jakovljevic, "Dynamic Compensation of Electrical Runout in Eddy Current Contactless Measurements of Non-Stationary Ferromagnetic Target," *Sensor Letters,* vol. 7, pp. 191-202, Apr 2009.

[102]   D. H. Biggs, "Method for removing electrical runout in machine shafts and apparatus for use with the same," U.S. Patent 3986380, 1975.

[103] Y. T. Yu, P. A. Du, and T. Yang, "Investigation on Contribution of Conductivity and Permeability on Electrical Runout Problem of Eddy Current Displacement Sensor," *2011 Ieee International Instrumentation and Measurement Technology Conference (I2mtc),* pp. 380-384, 2011.

[104] S. Giguere, B. A. Lepine, and J. M. S. Dubois, "Pulsed eddy current technology: Characterizing material loss with gap and lift-off variations," *Research in Nondestructive Evaluation,* vol. 13, pp. 119-129, Sep 2001.

[105] E. J. Rothwell and M. J. Cloud, *Electromagnetics*: CRC PRESS, 2001.

[106] F. C. Moon, *Magneto-solid mechanics*. New York: Wiley-Blackwell, 1984.

[107] M. V. K. Chari, *Numerical Methods in Electromagnetism*. San Diego, California: Academic Press, 2000.

[108] L. M. Vallese, "Diffusion of pulsed currents in conductors," *Journal of Applied Physics* vol. 25, pp. 225 -228, Feb 1954.

[109] S. Giguere, "Pulsed eddy-current for corrosion detection," Masters Thesis, Royal Military College of Canada, Ontario, 1999.

[110] Z. Qi, C. Tian-lu, Y. Guang, and L. Li, "Time and frequency domain features fusion for defect classification based on pulsed eddy current NDT," *Research in Nondestructive Testing,* vol. 23, pp. 171 - 182, 2012.

[111] G. Y. Tian and A. Sophian, "Defect classification using a new feature for pulsed eddy current sensors," *NDT & E International,* vol. 38, pp. 77-82, Jan 2005.

[112] T. L. Chen, G. Y. Tian, A. Sophian, and P. W. Que, "Feature extraction and selection for defect classification of pulsed eddy current NDT," *NDT & E International,* vol. 41, pp. 467-476, Sep 2008.

[113] T. Clauzon, F. Thollon, and A. Nicolas, "Flaws characterization with pulsed eddy currents NDT," *Ieee Transactions on Magnetics,* vol. 35, pp. 1873-1876, May 1999.

[114] J. H. V. Lefebvre and S. Dubois, "Lift-off point of intersection (LOI) behaviour," *Review of Progress in Quantitative Nondestructive Evaluation,* vol. 24, pp. 523 - 530, 2005.

[115] B. P. Lathi, *Linear systems and signals*. New York: Oxford University Press, 2002.

[116] Y. Li, T. Theodoulidis, and G. Y. Tian, "Magnetic field-based eddy-current Modeling for multilayered specimens," *Ieee Transactions on Magnetics,* vol. 43, pp. 4010-4015, Nov 2007.

[117] B. A. Auld and J. C. Moulder, "Review of advances in quantitative eddy current nondestructive evaluation," *Journal of Nondestructive Evaluation,* vol. 18, pp. 3-36, Mar 1999.

[118] J. Jin, *The finite element method in electromagnetics* New York: John Wiley & Sons Inc., 2002.

[119] Comsol Multiphysics. *Users' Handbook* [Online]. Available: http://www.comsol.com/comsol-multiphysics [Accessed: May, 2010]

[120] J. D. Kraus, *Electromagnetics*. New York: McGraw-Hill Inc., 1991.

[121] R. A. Smith, D. Edgar, J. Skramstad, and J. Buckley, "Enhanced transient eddy current detection of deep corrosion," *Insight,* vol. 46, pp. 88-91, Feb 2004.

[122] A. Simm and G. Y. Tian, "Investigation of directional eddy current complex measurements for defect mapping," *Insight,* vol. 52, pp. 320-325, Jun 2010.

[123] B. A. Lepine, J. S. R. Giguere, D. S. Forsyth, A. Chahbaz, and J. M. S. Dubois, "Interpretation of pulsed eddy current signals for locating and quantifying metal loss in thin skin lap splices," *Review of Progress in Quantitative Nondestructive Evaluation, Vols 21a & B,* vol. 615, pp. 415-422, 2002.

[124] O. F. Caltun, L. Spinu, A. Stancu, L. D. Thung, and W. Zhou, "Study of the microstructure and of the permeability spectra of Ni-Zn-Cu ferrites," *Journal of Magnetism and Magnetic Materials,* vol. 242, pp. 160-162, Apr 2002.

[125] T. Nakamura, "Snoek's limit in high-frequency permeability of polycrystalline Ni-Zn, Mg-Zn, and Ni-Zn-Cu spinel ferrites," *Journal of Applied Physics,* vol. 88, pp. 348-353, Jul 1 2000.

[126] M. Blodgett and P. B. Nagy, "Anisotropic grain noise in eddy current inspection of noncubic polycrystalline metals," *Applied Physics Letters,* vol. 72, pp. 1045-1047, Mar 2 1998.

[127] S. A. C. Harmon, M. J. Hall, L. C. A. Henderson, and P. P. Munday, "Calibration of commercial conductivity meters for measuring small items," *Iee Proceedings-Science Measurement and Technology,* vol. 151, pp. 376-380, Sep 2004.

[128] BSI, "Magnetic Materials - Methods for the determination of the relative permeability of feebly magnetic materials," ed. U.K. : BS5884:1999, 1999.

[129] M. J. Hall, A.E. Drake, S. A. C. Harmon, and C. I. Ager, "Low permeability reference standards with improved high magnetic field strength performance," *Inst. Electr. Eng. Proc. - Sci. Meas. Technol.,* vol. 145, pp. 181 - 183, 1988.

[130] Y. Z. He, G. Y. Tian, H. Zhang, M. Alamin, A. Simm, and P. Jackson, "Steel Corrosion Characterization Using Pulsed Eddy Current Systems," *Ieee Sensors Journal,* vol. 12, Jun 2012.

[131] F. Fiorillo, *Measurement and characterisation of magnetic materials*. London: Elsevier Academic Press, 2004.

[132] R. M. Bozorth, *Ferromagnetism*. New Jersey: D. Van Nostrand Co., 1951.

[133] J. W. Wilson, N. Karimian, J. Liu, W. Yin, C. L. Davis, and A. J. Peyton, "Measurement of the magnetic properties of P9 and T22 steel taken from service in power station," *Journal of Magnetism and Magnetic Materials,* vol. 360, pp. 52-58, Jun 2014.

[134] S. R. Oaten, "Assessment of defects in ferromagnetic metals with eddy currents," PhD Thesis, Brunel University, Middlesex, 1989.

[135] G. Bertotti, *Hysteresis in Magnetism: for physicists, material scientist and engineers*. San Diego: Academic Press, 1998.

[136] I Hughes and T. Hase, *Measurements and their uncertainties*. Oxford, U.K.: Oxford Uni. Press, 2010.

[137] N. Bowler, "Frequency-dependence of relative permeability in steel," *Review of Progress in Quantitative Nondestructive Evaluation, Vols 25A and 25B,* vol. 820, pp. 1269-1276, 2006.

[138] J. Slama, P. Krivosik, and V. Jancarik, "Modification of permeability components modelling," *Journal of Magnetism and Magnetic Materials,* vol. 215, pp. 641-643, Jun 2000.

[139] Y. Z. He, F. L. Luo, and M. C. Pan, "Defect characterisation based on pulsed eddy current imaging technique," *Sensors and Actuators a-Physical,* vol. 164, pp. 1-7, Nov-Dec 2010.

[140] M. R. Cherry, S. Sathish, J. Welter, R. Reibel, and M. P. Blodgett, "Development of High Resolution Eddy Current Imaging Using an Electro-Mechanical Sensor," *Review of Progress in Quantitative Nondestructive Evaluation, Vols 31a and 31b,* vol. 1430, pp. 324-331, 2012.

[141] TecScan Systems Inc. *Alleviating lift-off effects with the LOI for corrosion mapping of aircraft structures* [Online]. Available: http://www.pecscan.ca/PDFs/Technote_LOI.pdf [Accessed: July, 2014]

Appendix 1: Signal Processing Algorithms

1.1. 2D PEC Scanning Routine

Main Scanning Control Algorithm

```matlab
=================================================================================
%% MEASURE 2D PEC
close all, clear, clc

%% VARIABLES=====================================================================
% OUTPUT dir.
PATH = 'D:\ibk\scan1';
TEST_CASE = 'test2';

%% set Abs Zero position=========================================================

global ActualAbsCoord
ActualAbsCoord = [0 0 0];
global Bt_ref_NON Bt_ref time_OnePer f Ind_Freq b POL
POL = -1;

%% INPUT DATA====================================================================

% PEC
PEC_input_data
% CNC
CNC_input_data

%% Move to the REF position======================================================
 done = CNC_MoveRel([0,0,0]);
 done = CNC_MoveRel([0,0,0]);
 done = CNC_MoveRel([0,0,0]);

%% OBTAIN PEC REF================================================================
[Bt_ref_NON,Bt_ref,time_OnePer,f,Ind_Freq,b,aoCtrl,aiCtrl,MeasCtrl_out] =
get_PEC_ref(aoCtrl,aiCtrl,MeasCtrl);

%% Move back to ZERO POS=========================================================
 done = CNC_MoveRel([0,0,0]);
 done = CNC_MoveRel([0,0,0]);
 done = CNC_MoveRel([0,0,0]);

%% Move to the start position====================================================
[ActualAbsCoord,done] =
CNC_MoveAbs([CNC.start_from.X0,CNC.start_from.Y0,CNC.start_from.Z0]);

%% SCAN 2D=======================================================================
[X,Y,features] = CNC_Scan_2D(CNC,aoCtrl,aiCtrl,MeasCtrl);

%% Move to the Abs Zero==========================================================
[ActualAbsCoord,done] = CNC_MoveAbs([0,0,0]);

%% SAVE RESULT===================================================================
save([PATH '\' TEST_CASE ],'X','Y','features');

return
=================================================================================
```

Batch Code

```
=========================================================================
 clc, close all, clear ,
%% Path==================================================================
% PEC
addpath('H:\Program\control\PEC_scan2D\PEC_acquire',0)
% CNC Scanner Control
addpath('H:\Program\control\PEC_scan2D\CNC',0)
% PEC postprocessing
addpath('H:\Program\control\PEC_scan2D\PEC_postproc',0)

%% OPEN==================================================================
edit CNC_input_data.m
edit PEC_input_data.m
edit main2D.m

%% set Abs Zero pos======================================================
global ActualAbsCoord
ActualAbsCoord = [0 0 0];
=========================================================================
```

CNC Scanner Control input Code

```
=========================================================================
% Use this program to change scanner movement

%% CNC Scanner===========================================================
CNC.start_from.X0 = 0; % y0  (mm)
CNC.start_from.Y0 = 0; % x0  (mm)
CNC.start_from.Z0 = 0 ; % y0  (mm)

CNC.stop_at.Xs = 10; % ys  (mm)
CNC.stop_at.Ys = 10; % xs  (mm)
CNC.stop_at.Zs = 0; % ys  (mm)

CNC.step.dX = 1; % dx  (mm)
CNC.step.dY = 1; % dy  (mm)
CNC.step.dZ = 0; % dy  (mm)

CNC.scan_type = 1; % 1 == RASTER; 0 == MEANDER

CNC.speed.X = 10; % x'  (mm/sec)
CNC.speed.Y = 10; % y'  (mm/sec)
CNC.speed.Z = 10; % y'  (mm/sec)
=========================================================================
```

CNC Scanning Sub-Function: CNC_Scan_2D

```
=========================================================================
%% SCANNING 2D
% rows Y
% columns X

function [X,Y,features] = CNC_Scan_2D(CNC,aoCtrl,aiCtrl,MeasCtrl)
% BACK-UP
CNC0 = CNC;
global ActualAbsCoord
ind_y_max = (round((CNC.stop_at.Ys - CNC.start_from.Y0)/CNC.step.dY) + 1);

%%=====================================================================
for ind_y = 1:ind_y_max,
    ind_y
```

```matlab
    % get actual position
    ActualAbsCoord;
    % check for the end of scan
    fs = CNC_ScanOn(CNC,ActualAbsCoord); % scanflag
    % meas Z along the current line
    [X(ind_y,:),Y(ind_y,:),features(ind_y,:)] =
CNC_Scan_Line(CNC,aoCtrl,aiCtrl,MeasCtrl);

%% RETURN TYPE - RASTER=================================================
    if CNC.scan_type
        % return to the beginning of the current line
        if not(ind_y == ind_y_max)
            [ActualAbsCoord,done] =
CNC_MoveAbs([CNC.start_from.X0,ActualAbsCoord(2),ActualAbsCoord(3)]);
        end
        % move to the next line
        if not(ind_y == ind_y_max)
            [ActualAbsCoord,done] =
CNC_MoveAbs([ActualAbsCoord(1),CNC.start_from.Y0 +
ind_y*CNC.step.dY,ActualAbsCoord(3)]);
        end
    else
%% MEANDER==============================================================
    % CHECK IF IT IS EVEN or ODD Y LINE
        if mod(ind_y,2)
     % move to the next line
        if not(ind_y == ind_y_max)
[ActualAbsCoord,done] = CNC_MoveAbs([ActualAbsCoord(1),CNC.start_from.Y0 +
ind_y*CNC.step.dY,ActualAbsCoord(3)]);
            end
    % INVERT SCAN DIRECTION
            CNC.start_from.X0 = CNC0.stop_at.Xs;
            CNC.stop_at.Xs = CNC0.start_from.X0;
            CNC.step.dX = -1*CNC0.step.dX;
        else
            CNC = CNC0;
            % move to the next line
            if not(ind_y == ind_y_max)
                [ActualAbsCoord,done] =
CNC_MoveAbs([ActualAbsCoord(1),CNC.start_from.Y0 +
ind_y*CNC.step.dY,ActualAbsCoord(3)]);
            end
        end
    end

end
return
=======================================================================


PEC Input Data Code
=======================================================================
%% INPUT DATA
% clear, clc, close all,

%% GENERATION CONTROLS==================================================
aoCtrl.name = 'Dev1'; %
%  chan ao0 - excitation, chan ao1 - trigger
aoCtrl.chann.ind = [0 1];                              % indexes
aoCtrl.chann.range = [-10 10];[-10 10];         % Volt
aoCtrl.signal.ExcMode = 2;                          % 1 - single freq.
                                               % 2 - PEC square
```

```matlab
                                                    % 3 - PEC
exponentially damped
aoCtrl.signal.SampRate = .5e6;                      % Samp./sec.
aoCtrl.signal.freq =  [200];                        % excitation, Hz
aoCtrl.signal.ampl =  [2.52];                       % out voltage amplitude
aoCtrl.signal.phase = [0];                          % deg.
aoCtrl.signal.wfpts = 1e0;                          % number of waveform points
aoCtrl.signal.TimeConstR2L = 100E-6;                            % R/L
aoCtrl.signal.duty = 50;                            % duty cycle %
aoCtrl.signal.DCoffset = [0];                       % DC offset V
aoCtrl.signal.pretrig = 5E-6;                       % Sec
%==============================================================================

%% ACQUISITION CONTROLS==========================================================

%  chan ai0 - current, chan ai7 - Hall voltage

aiCtrl.name = 'Dev1'; %

aiCtrl.chann.ind = [0,7];                           % indexes
aiCtrl.chann.range = [-10 10]; [-10 10];            % RANGE
aiCtrl.chann.terminal   = 'Differential';          % CONNECTION
aiCtrl.chann.trigg      = 'PFI0';                   % RTSI0

aiCtrl.signal.freq      = aoCtrl.signal.freq;       % Hz
aiCtrl.signal.SampRate  = .5e6;                     % Samp./sec.
aiCtrl.signal.wfpts     = 1e0;                      % number of waveform points

aiCtrl0 = aiCtrl;

%% ACQUISITION TIME=============================================================

MeasCtrl.lockin.TimeConst = 200e-3;          % Sec.
MeasCtrl.filter.MovAv       = 40;            % moving average pts

%% SAVE
save input_data
%==============================================================================
```

PEC Acquisition Sub-function
```matlab
%==============================================================================
%% MEASURE INPUT SIGNAL
% uses: ao_start, acquire, lockin, gen_ramp

function [datai, time_ai, MeasCtrl_out, aiCtrl, aoCtrl] =
meas_pec(aoCtrl,aiCtrl,MeasCtrl);

daqreset

%% START AO of EXC. & COMP. WAVEFORMS=======================================
[AO, chan_ao, aoCtrl] = ao_start(aoCtrl);
pause(2)

%% ACQUIRE DATA 1===========================================================
[datai, time_ai, MeasCtrl_out, aiCtrl] = acquire(aiCtrl,MeasCtrl);

%% STOP CONTINUOUS OUTPUT and CLEAN UP======================================
stop(AO)
delete(AO)
```

138

```
delete(chan_ao)
return
===========================================================================
```

1.2. Lift-off-Defect Separation and Estimation Algorithm

```
%% PEC Post-processing =====================================================
clc, clear all, close all

%%
VARIABLES==================================================================
% INPUT directory

PATH = 'H:\Program\St_ibk\200hz\LOI';
TEST_CASE1 = 'L00';

name=['L00';'L10';'L20';'L30';'L40';'L50';'air'];

label=['L00';'L10';'L20';'L30';'L40';'L50';'air'];

pointsum =1:2500;   % total waveform point
pointsumr =1:1250;   % 1st half cycle waveform points
pointsumf =1251:2500; % latter half-cycle waveform points

%% PEC Reference Response extraction========================================
load([PATH '\' TEST_CASE1 ]);
Bt_NON(:,1) =    Ref.Bt_ref_NON(pointsum,1);
Bt(:,1) =         Ref.Bt_ref(pointsum,1);
time(:,1)   =     Ref.time_OnePer(pointsum,1);

Bt_NONr(:,1) =     Ref.Bt_ref_NON(pointsumr);
Btr(:,1) =        Ref.Bt_ref(pointsumr);
timer(:,1)   =     Ref.time_OnePer(pointsumr);

Bt_NONf(:,1) =     Ref.Bt_ref_NON(pointsumf);
Btf(:,1) =        Ref.Bt_ref(pointsumf);
timef(:,1)   =     Ref.time_OnePer(pointsumf);

%% Load all PEC Response ===================================================

for i=1:7
    load([PATH '\'  name(i,:) '.mat']);

    Bt_NON(:,i)=Ref.Bt_ref_NON(pointsum,1);
    Bt(:,i)= Ref.Bt_ref(pointsum,1);

    Bt_NONr(:,i)=Ref.Bt_ref_NON(pointsumr,1);
    Btr(:,i)= Ref.Bt_ref(pointsumr,1);

    Bt_NONf(:,i)=Ref.Bt_ref_NON(pointsumf,1);
    Btf(:,i)= Ref.Bt_ref(pointsumf,1);
end

%% transform ===============================================================
Bt_NON = Bt_NON';
Bt = Bt';
time=time';

Bt_NONr = Bt_NONr';
```

```matlab
Btr = Btr';
timer=timer';
diff_timer=diff(timer(:,1:1250));

Bt_NONf = Bt_NONf';
Btf = Btf';
timef=timef';
%% 1st half cycle PEC response ===========================================

for i=1:7
    h(i,:)= (Bt_NONr(i,:)+max(Bt_NONr(i,:))/2);
end



%% 1st Derivative before normalisation ==================================

pp1=spline(timer,h(1,:));
pp2=spline(timer,h(2,:));
pp3=spline(timer,h(3,:));
pp4=spline(timer,h(4,:));
pp5=spline(timer,h(5,:));
pp6=spline(timer,h(6,:));
pp7=spline(timer,h(7,:));
p_der1=fnder(pp1,1); p_der2=fnder(pp2,1); p_der3=fnder(pp3,1);
p_der4=fnder(pp4,1); p_der5=fnder(pp5,1); p_der6=fnder(pp6,1);
p_der7=fnder(pp7,1);
y_prime1=ppval(p_der1,timer);y_prime2=ppval(p_der2,timer);y_prime3=ppval(p_
der3,timer);
y_prime4=ppval(p_der4,timer);y_prime5=ppval(p_der5,timer);y_prime6=ppval(p_
der6,timer);y_prime7=ppval(p_der7,timer);
figure();hold on; grid on
plot(timer,y_prime1,'k-','linewidth',2)
plot(timer,y_prime2,'r-','linewidth',2)
plot(timer,y_prime3,'b-','linewidth',2)
plot(timer,y_prime4,'g-','linewidth',2)
plot(timer,y_prime5,'m-','linewidth',2)
plot(timer,y_prime6,'c-','linewidth',2)
plot(timer,y_prime7,'--k','linewidth',2)
legend(label(1,:),label(2,:),label(3,:),label(4,:),label(5,:),label(6,:),la
bel(7,:))
xlabel('Time(s)');ylabel('d(B)/dt');

%% Normalisation =========================================================

for i= 1:7
    n(i,:) = (Bt_NONr(i,:)/max(Bt_NONr(i,:))+1)/2;
end

%% 1st Derivative after normalisation (to obtain LOI) for Defect Estimation

pn1=spline(timer,n(1,:));
pn2=spline(timer,n(2,:));
pn3=spline(timer,n(3,:));
pn4=spline(timer,n(4,:));
pn5=spline(timer,n(5,:));
pn6=spline(timer,n(6,:));
pn7=spline(timer,n(7,:));
pn_der1=fnder(pn1,1); pn_der2=fnder(pn2,1); pn_der3=fnder(pn3,1);
pn_der4=fnder(pn4,1); pn_der5=fnder(pn5,1); pn_der6=fnder(pn6,1);
pn_der7=fnder(pn7,1);
```

```matlab
yn_prime1=ppval(pn_der1,timer);yn_prime2=ppval(pn_der2,timer);yn_prime3=ppv
al(pn_der3,timer);
yn_prime4=ppval(pn_der4,timer);yn_prime5=ppval(pn_der5,timer);yn_prime6=ppv
al(pn_der6,timer);yn_prime7=ppval(pn_der7,timer);

figure();hold on; grid on
plot(timer,yn_prime1,'k-','linewidth',2)
plot(timer,yn_prime2,'r-','linewidth',2)
plot(timer,yn_prime3,'b-','linewidth',2)
plot(timer,yn_prime4,'g-','linewidth',2)
plot(timer,yn_prime5,'m-','linewidth',2)
plot(timer,yn_prime6,'c-','linewidth',2)
plot(timer,yn_prime7,'--k','linewidth',2)
legend(label(1,:),label(2,:),label(3,:),label(4,:),label(5,:),label(6,:),la
bel(7,:))
xlabel('Time(s)');ylabel('d(B)/dt');

%% 2nd Derivative for Lift-off Estimation=================================
pqn1= spline(timer,yn_prime1);
pqn2= spline(timer,yn_prime2);
pqn3= spline(timer,yn_prime3);
pqn4= spline(timer,yn_prime4);
pqn5= spline(timer,yn_prime5);
pqn6= spline(timer,yn_prime6);
pqn7= spline(timer,yn_prime7);

pqn_der1=fnder(pqn1,1); pqn_der2=fnder(pqn2,1); pqn_der3=fnder(pqn3,1);
pqn_der4=fnder(pqn4,1); pqn_der5=fnder(pqn5,1); pqn_der6=fnder(pqn6,1);
pqn_der7=fnder(pqn7,1);
yyn4_prime1=ppval(pqn_der1,timer);yyn4_prime2=ppval(pqn_der2,timer);yyn4_pr
ime3=ppval(pqn_der3,timer);
yyn4_prime4=ppval(pqn_der4,timer);yyn4_prime5=ppval(pqn_der5,timer);yyn4_pr
ime6=ppval(pqn_der6,timer);yyn4_prime7=ppval(pqn_der7,timer);

figure();hold on; grid on
plot(timer,yyn4_prime1,'k-','linewidth',2)
plot(timer,yyn4_prime2,'r-','linewidth',2)
plot(timer,yyn4_prime3,'b-','linewidth',2)
plot(timer,yyn4_prime4,'g-','linewidth',2)
plot(timer,yyn4_prime5,'m-','linewidth',2)
plot(timer,yyn4_prime6,'c-','linewidth',2)
plot(timer,yyn4_prime7,'--k','linewidth',2)

legend(label(1,:),label(2,:),label(3,:),label(4,:),label(5,:),label(6,:),la
bel(7,:))
xlabel('Time(s)');ylabel('d^2(B)/dt^2');
```

Calibration Plots for Lift-off Estimation
```matlab
=========================================================================
clc, close all, clear all
%% Input Data===========================================================
cd ('D:\Fit\Peak_Value');
Load PV        %Peak Value of 2nd derivative of Bnorm PEC response
load PV1       % Peak Values of 2nd derivative of Bnon-norm PEC response
Load LO        % lift-off values

%% Calibration Plot for Lift-off Estimation (Steel)======================

figure();
plot(L0,PV,'r*')
hold on; grid on;
```

```matlab
n7=2;
p7=polyfit(L0,PV,n7);
PV_fitted1= polyval(p7,L0);
plot(L0,PV_fitted1,'b--','LineWidth',2)

xlabel('Lift-off (mm)');
ylabel('PV(\partial^2B_n_o_r_m/\partialt^2)');

PV_resid2 = PV - PV_fitted1; % residual value

SSresid7 = sum(PV_resid2.^2); %residual sum of squares

SStotal7 = (length(PV)-1) * var(PV); % total sum of sqaures

rsq7 = 1 - SSresid7/SStotal7 % Compute correlation coefficient (R2)

%% Calibration Plot for Lift-off Estimation (Aluminium)====================

figure();
plot(L0,PV1,'r*')
hold on; grid on;
n8=1;
p8=polyfit(L0,PV1,n8);
PV_fitted2= polyval(p8,L0);
plot(L0,PV_fitted2,'b--','LineWidth',2)

xlabel('Lift-off(mm)');
ylabel('PV(\partial^2B/\partialt^2)');

PV_resid3 = PV1 - PV_fitted2; % residual value

SSresid8 = sum(PV_resid3.^2); %residual sum of squares
SStotal8 = (length(PV1)-1) * var(PV1);  % total sum of sqaures

rsq8 = 1 - SSresid8/SStotal8 % Compute correlation coefficient
========================================================================
```

Calibration Plots for Defect Estimation

```matlab
========================================================================
clc, close all, clear all
%% Input Data===========================================================

cd ('D:\Fit\LOI_Points');
Load L_time          %LOI time points for steel
Load L_amp          %LOI amplitude points for steel
load LA_time          % LOI time points for aluminium
load LA_amp          % LOI amplitude points for aluminium
%% Calibration Plot for Defect Estimation (Steel)
```

```matlab
figure();
plot(L_time,L_amp,'r*')
hold on; grid on;
n7=2;
p7=polyfit(L_time,L_amp,n7);
defect_fitted1= polyval(p7,L_time);
plot(L_time,defect_fitted1,'b--','LineWidth',2)

xlabel('Time of Intersection (mm)');
ylabel('PEC output');

defect_resid2 = L_amp- defect_fitted1; % residual value

SSresid7 = sum(defect_resid2.^2); %residual sum of squares

SStotal7 = (length(L_amp)-1) * var(L_amp); % total sum of sqaures

rsq7 = 1 - SSresid7/SStotal7 % Compute correlation coefficient (R2)

%% Calibration Plot for Defect Estimation (Aluminium)======================

figure();
plot(LA_time,LA_amp,'r*')
hold on; grid on;
n8=3;
p8=polyfit(LA_time,LA_amp,n8);
defect_fitted2= polyval(p8,L0);
plot(LA_time,defect_fitted2,'b--','LineWidth',2)

xlabel('Lift-off(mm)');
ylabel('PV(\partial^2B/\partialt^2)');

defect_resid3 = LA_amp - defect_fitted2; % residual value

SSresid8 = sum(defect_resid3.^2); %residual sum of squares
SStotal8 = (length(LA_amp)-1) * var(LA_amp);  % total sum of sqaures

rsq8 = 1 - SSresid8/SStotal8 % Compute correlation coefficient
========================================================================
```

1.3. Defect Imaging Algorithm

```matlab
%% 3D Visualisation and Cross Profile=====================================

clear
close all
clc

PATH = 'H:\Program\ibk1\scan1';
dos(['mkdir ' PATH '\_print00'])
TEST_CASE = 'test29.mat';

%% LOAD Data=============================================================

load([PATH '\' TEST_CASE ]); % ,'X','Y','features','CNC'
YLIM = 1:size(features,1);
XLIM = 1:size(features,2);


if  not(exist('CNC','var')), CNC.scan_type = 1; end

if CNC.scan_type
    Xn = X(YLIM,XLIM);
else
    for i = YLIM,
        if  mod(i+1,2)
            Xn(i-YLIM(1)+1,:)  = fliplr(X(i,:));
        else
            Xn(i-YLIM(1)+1,:)  = X(i,:);
        end
    end
end
Yn = Y(YLIM,XLIM);

%% Feature Extraction====================================================

for i = YLIM,
    for j = XLIM,
        % PEAK VALUE

        dBdt_PV(i-YLIM(1)+1,j)   = features(i,j).dBdt_PV; % peak
value(derivative of Bnon-norm)
        dBndt_PV(i-YLIM(1)+1,j)     = features(i,j).dBndt_PV; % peak
value(derivative of Bnorm)
    end,
end


%% CORRECT DRIFT=========================================================

for i = 1:size(Xn,1),
% lin.reg. coeffs & regression
% dBdt_PV
p = polyfit(Xn(i,:),dBdt_PV(i,:),1);
dBdt_PV(i,:) = dBdt_PV(i,:) - Xn(i,:)*p(1);
% dBndt_PV
p = polyfit(Xn(i,:),dBndt_PV(i,:),1);
dBndt_PV(i,:) = dBndt_PV(i,:) - Xn(i,:)*p(1);

end
```

```matlab
%% PLOT=====================================================================

% PEAK VALUE OF TIME DERIVATIVE OF NON-NORMALISED PEC SIGNAL (Aluminium)

figure(1)
surf(Yn,Xn,dBdt_PV)
colormap jet
shading interp

%view(2)
%axis equal
 xlabel('y(mm)','FontSize',15)
 ylabel('x(mm)','FontSize',15)
 zlabel('\partialB/\partialt','FontSize',15)
 set(gca,'FontSize',20)
 set(gca,'XLim',[0 95],'YLim',[0 100],'ZLim',[0 0.8])
 h = colorbar; set(h,'FontSize',10)
 print('-dtiff',[PATH '\_print00' 'Bdt_PV'],'-f1') %save print to

%% PEAK VALUE OF TIME DERIVATIVE OF NON-NORMALISED PEC SIGNAL (Steel)======

figure(2)
surf(Yn,Xn,dBndt_PV)
colormap jet
shading interp
% view(2)
% axis equal
xlabel('y(mm)','FontSize',15)
ylabel('x(mm)','FontSize',15)
zlabel('\partialB_n_o_r_m/\partialt','FontSize',15)
set(gca,'FontSize',15)
set(gca,'XLim',[0 95],'YLim',[0 100],'ZLim',[0 0.4])
h = colorbar; set(h,'FontSize',10)
print('-dtiff',[PATH '\_print00' 'dBndt_PV'],'-f2')
%% CROSS-PROFILE
Yy = Yn(:,1);
profile_dBdt_PV = mean(dBdt_PV,2);
profile_dBndt_PV = mean(dBndt_PV,2);


=========================================================================
```

145